CONVECTIVE HEAT AND MASS TRANSFER IN BOUNDARY LAYER FLOW THROUGH POROUS MEDIA SATURATED WITH NANOFLUIDS

A THESIS SUBMITTED TO THE UNIVERSITY OF KWAZULU-NATAL
FOR THE DEGREE OF DOCTOR OF PHILOSOPHY
IN THE COLLEGE OF AGRICULTURE, ENGINEERING & SCIENCE

By
Nageeb Abdallah H. Haroun
School of Mathematics, Statistics & Computer Science
December 2016

Contents

Abstract

The thesis is devoted to the study of flow, heat and mass transfer processes, and cross-diffusion effects in convective boundary layer flows through porous media saturated with nanofluids. Of particular interest is how nanofluids perform as heat transfer fluids compared to traditional fluids such as oil and water. Flow in different geometries and subject to various source terms is investigated.

An important aspect of the study and understanding of transport processes is the solution of the highly non-linear coupled differential equations that model both the flow and the heat transportation. In the literature, various analytical and numerical methods are available for finding solutions to fluid flow equations. However, not all these methods give accurate solutions, are stable, or are computationally efficient. For these reasons, it is important to constantly devise numerical schemes that work more efficiently, including improving the performance of existing schemes, to achieve accuracy with less computational effort. In this thesis the systems of differential equations that describe the fluid flow and other transport processes were solved numerically using both established and recent numerical schemes such as the spectral relaxation method and the spectral quasilinearization method. These spectral methods have been used only in a limited number of studies. There is therefore the need to test and prove the accuracy and general application of the methods in a wider class of boundary value problems.

The accuracy, convergence, and validity of the solutions obtained using spectral methods, have been established by careful comparison with solutions for limiting cases in the published literature, or by use of a different solution method.

In terms of understanding the physically important variables that impact the flow, we have *inter alia*, investigated the significance of different fluid and physical parameters, and how changes in these parameters affect the skin friction coefficient, the heat and mass transfer rates and the fluid properties. Some system parameters of interest in this study include the nanoparticle volume fraction, the Hartmann number, thermal radiation, Brownian motion, the heat generation, the Soret and Dufour effects, and the Prandtl and Schmidt number. The dependency of the heat, mass transfer and skin friction coefficients on these parameters has been quantified and discussed.

In this thesis, we show that nanofluids have a significant impact on heat and mass transfer processes compared with traditional heat transfer fluids.

Declaration

The work described in this thesis was carried out under the supervision of Prof. P. Sibanda in the School of Mathematics, Statistics, & Computer Science, University of KwaZulu-Natal (PMB), from July 2014 to December 2016.

No portion of the work referred to in this dissertation has been submitted in any form to any university or institution of learning for any degree or qualification. The thesis represents my original work except where due reference and credit is given.

Sign: ....

Nageeb A.H Haroun Date

Sign: ....

Prof. P. Sibanda Date

Acknowledgments

I am deeply grateful to Prof. P. Sibanda for his constant support, guidance and inspiration throughout the research. I would like to extend my gratitude to Prof. S.S Motsa for his advice, invaluable help, explanations and comments on the use of spectral methods. I would like to thank Dr. Sabyasachi Mondal for his constant support, encouragement- and collaboration. I would like to thank my brother, Prof. Mahgoup A.H. Haroun, a true brother and friend, who taught me how to persist in difficult situations in order to be a successful man and helped me secure the financial aid to complete my studies. I would also like to thank my lovely wife Baliega Mohammed Essa and my beautiful daughter Lean Nageeb A.H Haroun for all their love, encouragement, and support in making the PhD project possible. My foremost sincere gratitude goes to my great mother, Khadiga Khallaha Iderise, who has always supported me in every thing that I have done so far, as well as to the Sudanese community in PMB for supporting me and my family. I would like to thank the Sudan government for their supporting this program. And last but not least I would like to acknowledge and thank my friends in SMSC for helping me with ideas and suggestions for my research and who generously supported me.

Publications

The following papers have been published:

1. NAH Haroun, Precious Sibanda, Sabyasachi Mondal and Sandile S Motsa, On unsteady MHD mixed convection in a nanofluid due to a stretching/shrinking surface with suction/injection using the spectral relaxation method: Boundary Value Problems (2015) 2015:24.

2. NAH Haroun, Precious Sibanda, Sabyasachi Mondal, Sandile S Motsa and Mohammad M Rashidi, Heat and Mass Transfer of Nanofluid through an Impulsively Vertical Stretching Surface using the Spectral Relaxation Method: Boundary Value Problems (2015) 2015:161.

3. Faiz Awad, NAH Haroun, Precious Sibanda, Melusi Khumalo, On couple stress effects on unsteady nanofluid flow over stretching surfaces with vanishing nanoparticle flux at the wall: Journal of Applied Fluid Mechanics, 9, 4, (2016) 1937-1944.

4. NAH Haroun, Sabyasachi Mondal, Precious Sibanda, Unsteady natural convective boundary-layer flow of MHD nanofluid over a stretching surfaces with chemical reaction using the spectralrelaxation method: Elsevier, International Conference on Computational Heat and Mass Transfer- Procedia Engineering 127 (2015) 18 - 24.

5. Sabyasachi Mondal, NAH Haroun, Precious Sibanda, The Effects of Thermal Radiation on an Unsteady MHD Axisymmetric Stagnation- Point Flow over a Shrinking Sheet in Presence of Temperature Dependent Thermal Conductivity with Navier Slip: PLOS ONE 10(9), (2015) 1 - 23.

Chapter 1

Introduction

1.1 Background and motivation

Fluid flow and heat transfer occur in both natural and man-made industrial situations. This is a longstanding subject that has been studied widely using different models of fluid flow. The transfer of heat and mass through porous media plays an important role in fluid mechanics and arises in many areas of natural and applied sciences. Nanofluids are recently developed heat transfer liquids that disperse solid nanoparticles. Recent research has shown that nanofluids enhance thermal conductivities and can improve the heat transport properties of fluids, thereby enhancing energy efficiency. There is thus significant potential for application of nanofluids in the field of enhanced heat transfer, including such areas as geophysics, petroleum engineering, geosciences, mechanics and biology, as suggested by Chen and Ewing [1]. Such flow, heat and mass transfer processes can be modelled mathematically by complex systems of partial differential equations, which are often non-linear due to both the complexity of the problem and the number of variables in the problem. There are several ways to solve these differential equations, such as analytical, semi-analytical and numerical methods. Each of these methods has both advantages and disadvantages. Analytical solutions, where they can be found, often provide the best insights into the effects of different parameters that have a bearing on the solution. This is not usually the case

with the other methods. Due to their complexity, most fluid flow models, including double-diffusive convection problems do not have exact solutions. To solve such problems various numerical methods and semi-analytical methods have been introduced and used successfully. The need for new methods, however, remains in order to mitigate the deficiencies of many current techniques such as slow convergence rates, computational inefficiency, etc. The main objective of the current study is to use two recent innovative numerical methods that have as yet not been used extensively to solve non-linear partial differential equations that arise in modelling fluid flows. A second objective is to investigate the influence of a plethora of physical parameters that characterise the problems.

Flows of practical significance, such as the spread of ground pollutants, take place in a porous medium. A porous medium is a material that consists of a solid matrix with interconnected voids (Bear and Bachmat [2]). The pores are saturated by a single fluid in single-phase flow, while the void space is often shared by a liquid and a gas in two-phase flow (Ingham and Pop [3]). Examples of natural porous media include beach sand, sandstone, limestone, wood and pulmonary tissue in the lungs (Corey [4] and Vazquez [5]). Porous media flows have been extensively studied on account of the important applications of such flows. For example, they offer a means of separating solid materials of different sizes (Strange and Webber [6], Nield and Bejan [7]). Porous media act as highly selective cages or screens that allow access only to particles below a certain size. A porous medium is generally characterized by two factors; namely, porosity and permeability, that generally control the storage and movement of fluids (Kaviany [8]).

The first factor, porosity, is the ratio of the void space of the porous medium to the total volume of the medium (Lethr and Lethr [9]). Mathematically, it is the ratio of the unit volume of void space denoted by φ and represents the total storage capacity of the medium. This is given by the ratio

$$\varphi = \frac{void\ volume}{total\ volume} = \frac{V_v}{V_T}, \tag{1.1}$$

where $0 < \varphi < 1$, V_v is the volume of void space and the total volume of the material is V_T. Porosity is a fraction between 0 and 1 so that the quantity $1 - \varphi$ defines the fraction

of the medium occupied by the solid (Bruschke and Advani [10]). By defining φ in this way, the implicit assumption is that all the void space is connected. If some pore space is disconnected from the remainder, then the concept of effective porosity is often introduced (Gupta and Gupta [11]). This is defined as the ratio of connected void to total volume. The porosity does not normally exceed 0.6 for natural porous media and can vary between 0.2595 and 0.4764 for synthetic beds of solid spheres of uniform diameter (Mondal and Pal [12]). The second property, the permeability of porous media, gives a sense of the ease with which a fluid can move freely through the pores. Permeability is determined as the proportionality constant in Darcy's law, see Darcy [13], that relates discharge and fluid physical properties to the pressure gradient in the porous media. For an anisotropic porous medium, Darcy's law can be expressed as

$$q_i = K_{ij} \frac{\partial h}{\partial x_i}, \tag{1.2}$$

where q_i $(i = 1,2,3)$ is the Darcy velocity, K_{ij}, the hydraulic conductivity of porous media and h is the water head at a point x_i which depends on the pressure P. This is a macroscopic quantity. For an isotropic porous medium, K_{ij} reduces to a scalar K and Darcy's law, given by Eq (1.2), becomes

$$q_i = -K \frac{\partial h}{\partial x_i}, \quad i = 1,2,3. \tag{1.3}$$

The hydraulic conductivity κ of the porous medium depends on the properties of both the solid and the fluid in the porous medium and is given by

$$\kappa = \frac{k\rho g}{\mu}, \tag{1.4}$$

where k is the permeability, μ is the viscosity, ρ density and g is the gravity term. In civil engineering, this type of flow is important in geothermal energy recovery, thermal energy storage, ground water pollution and crude oil extraction (Vafai [14]).

The significant topic investigated in this thesis is that of flow, mass and heat transfer in a nanofluid saturated porous medium. It is a topic of engineering interest, and an important field of study in itself. Several contributions have been made in modelling fluid flow,

heat and mass transfer in a nanofluid through a porous medium (Benzeghiba et al. [15]). Modelling fluid flow, heat and mass transfer in a porous medium saturated with a fluid has been undertaken in various ways. Firstly, the concept of non-Darcy effects on transport equations, for several geometrical configurations and boundary conditions has been used. The contributions in this regard include Zheng et al. [16]. Alternatively, research on porous media has applied the generalised Brinkman-Forcheimer extended Darcy model. Ranganatha and Viskanta [17] used this model to investigate convection in flow past a vertical flat plate, Nield and Kuznetsov [18] studied boundary layer flow in nanofluids while Kumari and Nath [19] studied non-Darcy natural convection in a Newtonian fluid flow in a porous medium. In this work we investigate convective transport of heat, momentum and mass in nanofluid boundary layer flows.

In heat transfer studies, the objective is often to determine energy transfer between bodies as a result of temperature differences, and the mechanisms of heat transfer. In the seventeenth and early nineteenth centuries, researchers postulated that all bodies contained an invisible substance called the caloric (Amin and Azarkish [20]). Heat transfer is now recognized as the flow of thermal energy due to a non-uniform temperature field. This is commonly measured as a heat flux, see Holman [21]. There are three types of heat transfer processes between differentially heated bodies namely, conduction, convection and radiation. Conduction is defined as the transport of energy from more energetic particles of a substance to the adjacent less energetic ones as a consequence of interactions among the particles. Heat conduction can occur in solids, liquids and gases (Burmeister [22]).

Convection is the transfer of energy through the adjacent liquid or gas and a solid surface that is in motion, and involves the combined impacts of fluid motion and conduction. Radiation is the transfer of energy through space in the form of electromagnetic waves or photons (Thirumale [23]).

Mass transfer occurs either via the bulk fluid motion or through the diffusion of a chemical species (Nield and Kuznetsov [24]). The primary focus in this thesis is on mass transfer through diffusion as a result of concentration gradients. An often mentioned example of

diffusive mass transfer is the humidification that occurs when a container of water is left open, leading to a mixture of air and water vapour in the atmosphere. A concentration gradient causes water to be transported from the liquid surface into the atmosphere (Welty et al. [25]). Mass transfer has several similarities to the process of heat transfer (Jaluria [26]). The mechanisms of heat and mass transfer may be considered in terms of conduction or convection. In this regard, heat conduction is due to temperature gradients normal to the interface between two materials, and mass diffusion is due to mass gradients normal to the surface (Kays and Crawford [27]), Moreover, if the fluid is moving, then its movement, as well as the two potential gradients, is responsible for transferring energy and mass. Hence the transport of mass or heat is via both molecular conduction processes and gross fluid motion (Gorla and Zinolabedini [28]).

The mechanism of heat transport, induced by buoyancy forces arising from a temperature gradient in the absence of other external sources, is called free or natural convection (Gorla and Tornabene [29], Gebhart et al. [30]) and Rathore and Kapuno [31]. It arises in situations such as cooling operations. In free convection, density variations in the fluid cause the hot fluid to move in an upward direction and the cold fluid to move in a downward direction. Numerous scholars have studied free convection flows, among them Jaluria and Gebhart [32], Cheng and Minkowycz [33] and Jaluria and Himasekhar [34]. Forced convection in a porous medium was investigated by Rudramoorthy and Mayilsamy [35]. A combination of natural and forced convection was studied by Wooding [36], Lai [37], and Lioyd and Sparrow [38]. Mixed convection with boundary layer stability and viscous dissipation over a horizontal surface was studied by, among others, Mureithi and Mason [39] whose findings showed that the boundary layer is dominated by internal regions of super velocities. They considered the simultaneous effects of inertial forces and viscous resistance on the flow in a porous medium. Their results showed that inertia and boundary friction effects have a significant bearing on heat transport and thus cannot be ignored.

1.2 Double-diffusive convection

There is a large number of analytical and numerical studies of heat and mass transfer in a porous medium. These studies assume different types of boundary conditions. Different methods have been used to solve the model equations. In this thesis, we give attention to processes of combined heat and mass transfer that are driven by buoyancy. Double-diffusive convection describes convection driven by two different density gradients with distinct diffusion rates (Siegmann and Rubenfeld [40], Hsia et al. [41]). Double-diffusive convection appears in many engineering and physical problems such as in contaminant transport in saturated soils, food processing, the mantle flow in the Earth's crust as well as in sea water (Bourich et al. [42]). Double-diffusive natural convection in fluid flow has been an active area of research for many years. Comprehensive reviews of the literature in this area can be found in articles by Mojtabi and Mojtabi [43], Beya and Lilia [44] and Mamou [45].

Motivation for the study of buoyancy driven heat and mass transfer is partly due to the natural occurance of this phenomenon in such diverse fields as the migration of moisture in insulation systems, the storage of grain in silos, the spread of soil contaminants including the disposal of nuclear wastes, and in crystal growth. It has also been claimed that double-diffusive convection occurs in magma chambers and in the modelling of solar ponds (Akbarzadeh and Manins [46], Narayana and Sibanda [47]). Nield [48] investigated double-diffusive convection in viscoelastic fluids in a porous medium. Numerous previous studies exist for the problem of a porous layer heated from below or the side, see among others, Baines and Gill [49], Gershuni et al. [50] and Khan and Zebib [51].

A number of studies are of particular relevance, such as Raptis et al. [52] who found similarity solutions for boundary layer flow about a vertical wall in a porous medium with a solute concentration and a constant temperature. Rudraiah et al. [53] gave a non-linear stability analysis of heat and mass transfer rates in a two-part fluid saturated porous boundary layer. They determined the transport processes in double-diffusive convection flow

for different Darcy-Rayleigh and Rayleigh numbers. Their results showed that a finite-amplitude instability may exist at subcritical Rayleigh numbers. Nield et al. [54] studied convection due to slanted solutal and applied thermal gradients in a shallow horizontal layer in porous media. Amahmid et al. [55] investigated double diffusive natural convection in a horizontal Brinkman porous layer with fixed mass and energy fluxes. Alloui et al. [56] studied the onset of heat and mass transfer rates in a rectangular porous layer between horizontal boundaries. They used the Galerkin finite element method to solve the problem equations and to investigate oscillatory and stationary instabilities. The impact of anisotropy on the onset of heat and mass transfer in a rotating frame in porous media was investigated by Patil et al. [57]. Nield et al. [54] extended their work to include the effects of inclined temperature and solutal gradients. They showed that both solutal Rayleigh numbers and inclined thermal, contribute significantly to the onset of convective instability. Malashetty and Basavaraja [58] studied the onset of heat and mass transfer in a horizontal fluid boundary layer subjected to thermal modulation. They observed that harmonic modulation advanced the onset of convection at low frequencies. The transition to chaos in double-diffusive Marangoni convection was investigated by Li et al. [59]. Magnetohydrodynamic (MHD) double-diffusive convective flow in a porous medium was investigated by Okedayo et al. [60].

The case of a non-Darcy porous medium saturated with a nanofluid with viscous dissipation was studied by RamReddy et al. [61]. A review of current literature shows the importance of combined heat and mass transfer in natural convection fluid flow. However, insufficient work has been carried out on double-diffusive convection in the case of nanofluids, such as enhancing thermal conductivity of the fluid to improve the heat transfer rate in various applications by suspensions of nanoparticles in the base fluid. Consequently, in this study we will investigate fluid flow and heat and mass transfer in nanofluids. The effect of significant physical parameters, like thermal radiation, heat generation/absorbtion, viscous dissipation, Navier slip, magnetic parameter, Soret and Dufour parameters on different types of nanofluids is studied using two spectral methods.

1.3 The study of nanofluids scope and motivation

Nanofluids are solid-liquid mixtures consisting of solid nanoparticles with size typically $(1-100)nm$ suspended in a liquid, see Xuan and Li [62]. The nanoparticles are usually made of metals (Al, Cu), oxides Al_2O_3 carbides (SiC), nitrides (AlN, SiN) or non-metals (e.g. graphite, carbon nanotubes). Common base fluids are water, oil and ethylene-glycol mixtures. The literature shows that the low thermal conductivity of these base fluids is a primary limitation in the performance of many devices. When nanoparticles are added to a base fluid, a drastic increase in thermal conductivity is observed, see Eastman et al. [63]. Hence, a nanofluid is not only of academic interest but also has industrial applications. Nanofluids are used to improve energy efficiency and heat transfer in many thermal control systems. A nanofluid has various advantages, for instance, smaller cooling systems, higher cooling rates, reduced inventory of heat transfer fluids, improved wear resistance, reduced friction coefficient, and decreased pumping-power needs (Kameswaran et al. [64]). It is highly desirable to achieve the highest possible thermal properties with the smallest possible concentration of nanoparticles. Among other uses, it is expected that a nanofluid can be used in cars, micro reactors and aeroplanes. The growth in the use of nanofluids is mirrored by the exponential increase in the number of research publications, see Zeinali Heris et al. [65]. Due to the growing importance of nanofluids, there is a large amount of literature on convective transport and nanofluid flow linked to a stretching surface. Choi et al. [66] showed that the addition of a small amount of copper nanoparticles, less than 1% by volume, could increase the fluid's thermal conductivity by as much as 40%. Other advantages include a three fold higher critical heat flux and thermal conductivity compared to the base fluid (Vassallo et al. [67]). Cooling by nanofluids has many potential applications. In this regard, You et al. [68] studied the feasibility of using nanofluids to enhance the cooling of nuclear reactors. Other studies indicate that nanofluids as cooling fluids have the potential to conserve over 1-trillion Btu of energy for industries in the USA alone. In

the literature it has been suggested that this may lead to possible emission reductions of nearly six million tonnes of carbon dioxide, 8600-tonnes of nitrogen oxides and 21000-tonnes of sulfur dioxide, see Routbort [69], Awad et al. [70], Kameswaran and Sibanda [71]. Nanofluids can be used to cool pipes exposed to high temperatures in geothermal power and energy extraction from the earth's crust (Wong and de Leon [72]). Nanofluids could be utilized as automatic transmission fluids, engine oils, lubricants and coolants, etc. Elsewhere, nanofluids have been used in biomedical applications such as in cancer therapeutics, nano-drug delivery systems, nano-cryosurgery and for cooling of microchips in computers (Boungiorno et al. [73]). The parameters which influence energy transfer characteristics of nanofluids are properties such as enhanced density, specific heat, viscosity and thermal conductivity. The thermo-physical properties of nanofluids also depend on the operating temperature of nanofluids.

The effect of a magnetic field on nanofluids has essential applications in engineering, physics and chemistry. These include thinning of copper wire, and the process of drawing, annealing and cooling of continuous filaments. Drawing such strips in an electrically conducting fluid through a magnetic field can control the rate of stretching and cooling, thereby improving the characteristics of the final product. Such an application for a linearly stretching sheet in an incompressible viscous MHD flow was investigated by Pavlov [74]. Jafar et al. [75] discussed the impact of MHD flow and energy transfer from a stretching/shrinking sheet with joule effects and viscous dissipation. In Chapter 2, Haroun et al. [76] investigated unsteady MHD nanofluid flow over a stretching/shrinking surface with injection or suction. They further assumed that the nanoparticle volume fraction at the wall could be actively controlled and that flow was subject to viscous dissipation. A model for MHD flow due to a uniformly stretched vertical permeable surface subject to a chemical reaction was implemented by Chamkha [77]. An analysis of the effects of chemical reactions on heat and mass transfer on MHD boundary layer flow due to a wedge with viscous dissipation and ohmic heating in a porous medium was presented by Kandasamy and Palanimani [78]. The effectiveness of a transverse magnetic field on fluid flow and heat transfer

due to a stretching surface was discussed by Anjali and Thiyagarajan [79]. The effect of a chemical reaction on heat and mass transfer from vertical surfaces in a porous medium subject to Dufour and Soret effects was studied by Postelnicu [80]. In general, nanofluids show great potential for enhancing heat transfer processes. The suspended nanoparticles significantly increase the thermal properties of nanofluids. The volume fraction, shape, dimensions and properties of the nanoparticles affect the thermal conductivity of nanofluids. The absence of good quality and consistent nanofluids limits the progress of future research and applications in this and related areas. Flow of nanofluids in thermal management, solar energy absorption, microelectronics, defense, nuclear systems (Vadasz [81]), space craft and the need for enhanced heat transfer and high-performance cooling is a vast area of still to be investigated research.

1.4 Numerical and empirical studies of double diffusive convection

There have been numerous experimental studies of mass and heat transfer processes. These include investigations by Griffiths [82], who studied convection experimentally using a Hele-Shaw cell in a porous medium. He measured energy salt fluxes via two layer convection techniques and compared the conclusions with predictions from numerical models. Through his investigations he found that there was agreement between laboratory and theoretical results. Murray and Chen [83] investigated the onset of mass and energy transfer in a porous medium. They performed experiments in a box consisting of glass beads and having rigid upper and lower walls. These allowed for a non-linear time-dependent profile for salinity. They showed that the beginning of convection was marked by a dramatic rise in heat flux at the critical temperature. The convection pattern was found to be predominantly three-dimensional.

Webb et al. [84] presented a numerical and experimental investigation of double-diffusive convection in a cylinder. They used a narrow tank heated from the sides and bottom with

a linearly stratified salt-water solution to form multiple mixed layers of fluid. Comparison between the laboratory and numerical results showed acceptable agreement. Heat and mass transfer in a multi-compound solution in a cylindrical cavity, when the bottom is cooled, was studied by Bai et al. [85]. They showed that heat and mass transfer rates occurred in the liquid because of the coupling of concentration and temperature gradients. Other experimental studies include those of Barman and Dutta [86] and Mergui et al. [87].

The equations for momentum, mass conservation and heat transfer are, in general, strongly non-linear with no analytical solutions. For this reason, numerical solutions are usually used to solve the complex systems of equations. Below we describe recent numerical studies which have considered, among other factors, the influences of hydromagnetics, chemical reaction, heat generation, heat radiation and Soret and Dufour effects.
Gebhart and Pera [88] investigated double-diffusive natural convection resulting from combined influences of mass and thermal transports. Minkowycz et al. [89] investigated the problem of free convection with suction/injection over permeable horizontal plates in a porous medium. The problem of modelling fluid flow has attracted many researchers, for instance see [90–93]. In some studies the interfacial velocities have been assumed to be small enough to be neglected. Studies have shown that the heat transfer rate at the surface grows with the Prandtl number, the unsteadiness parameter, the solid volume fraction of nanoparticles, and the buoyancy parameter, and that larger values of the Grashof number have substantial impact on the momentum boundary layer. Unsteady MHD of a nanofluid free convection boundary layer flow over a stretching sheet with viscous dissipation and thermal radiation was studied by Khan et al. [94]. A variety of methods have been used for these studies. Lai [91] obtained similar solutions, while implicit finite differences were used by Yih [92], Khan et al. [94] and Mahdy [95]. Mixed convection flow due to both inclined and vertical flat plates with combined mass and thermal diffusion was investigated by Chen et al. [96]. Unsteady heat and mass transfer due to an impulsively vertical surface with Soret, Dufour effects and chemical reaction was investigated by Chamkha

and El-Kabeir [90] to quantify the influences of the Dufour number, Soret number, mixed convection parameter, Hartmann number, suction/injection parameter and the chemical reaction parameter. For the case of uniform wall concentration and temperature gradients they showed that the heat and mass transfer rates outcomes may range from the asymptotic free convection limit to the forced convection limit.

A numerical study of the impacts of combined buoyancy forces from mass and thermal diffusion was examined by Hossain [97]. Yih [92] used the Keller-box method, a special type of implicit finite difference method, to study double-diffusive mixed convection near a wedge embedded in porous media. Mass transfer in steady two-dimensional flow of a viscous incompressible electrically conducting fluid through a porous medium was studied by Acharya et al. [98]. The study sought to determine the effect of physical parameters on heat and mass transfer. Transient heat and mass transfer from a vertical plate embedded in a power-law fluid was studied by Cheng [93]. He used a cubic spline collocation method to solve the conservation equations. Unsteady boundary layer fluid flow and heat transfer in nanofluids along a stretching sheet was investigated by Mahdy [95] utilizing an implicit finite difference method.

Characteristics of different models of nanofluids and physical parameters were discussed, and it was observed that with an increase in the buoyancy parameter, the heat transfer rate at the surface increases. Using an implicit finite difference technique, Khan et al. [94] found that larger values of the Grashof number had a significant impact on the momentum boundary layer for unsteady MHD boundary layer flow of a nanofluid subject to viscous dissipation and thermal radiation. In these and other studies it was shown that implicit finite differences are a useful method for solving non-linear partial differential equations. In this study we will investigate unsteady and steady MHD mixed convection in boundary layer flow, and heat and mass transfer in nanofluid flows in a porous medium.

Stretching surfaces have attracted significant research interest. One such example is by Ishak et al. [99] who investigated energy transfer through an unsteady stretching permeable surface with a prescribed wall temperature. They determined the influence of the

Prandtl number, suction/injection and the unsteadiness parameter on the heat transfer characteristics. Complementing this was a study by Joshi et al. [100] who used the fourth order Runge-Kutta method to solve the flow equations and determine how the physical parameters impact the fluid flow. Manjunatha et al. [101] used a fifth order Runge-Kutta Fehlberg method to investigate heat transfer and thermal radiation on boundary layer flow from a dusty fluid over unsteady stretching sheet. Bhattacharyya et al.[102] studied an unsteady MHD boundary layer flow with first order chemical reaction and diffusion along a permeable stretching sheet with blowing or suction using a quasi-linearization technique and the Keller-box method. From the literature, it can be seen that numerical methods, such as the Keller-box method, the fifth order Runge-Kutta Fehlberg method, the spectral relaxation and quasi-linearization methods can be useful for solving non-linear differential equations. Recently, Kameswaran et al. [103] studied hydromagnetic nanofluid flow due to a shrinking or stretching sheet with chemical reaction and viscous dissipation. They discussed two types of nanofluids, namely *Cu*- and *Ag*- water. The equations were solved numerically using the Matlab *bvp*4*c* solver. Hsiao and Lee [104] studied the problem of conjugate heat and mass transfer in MHD viscoelastic fluid past a stretching sheet. Double-diffusive convection was studied by Hayat et al. [105] who used the homotopy analysis method to solve the unsteady equations for MHD flow along a stretching surface. Joneidi et al. [106] studied the problem of convective heat and mass transfer due to a stretching surface using the homotopy analysis method. They assumed first order reaction kinematics in the flow. Cheng [107] studied double-diffusion convective through a horizontal cylinder of elliptic cross section with uniform wall heat and mass fluxes immersed in a porous medium. His results showed that the local surface concentration and local surface temperature on the elliptical cylinder tended to rise as the aspect ratio increased.

Double-diffusive convection through a rotating cylindrical annulus with conical caps was studied by Simitev [108], while Kuznetsov and Nield [109] investigated double-diffusive convection in nanofluid over boundary layer flow past a vertical plate using a revised boundary condition for the model. In the revised model, the nanofluid particle volume fraction

at the boundary was passively rather than actively controlled. The change in the boundary condition ensured that the model was physically more realistic than when other boundary conditions were used by previous researchers. In Chapter 5 we study double-diffusive convection in MHD nanofluid boundary layer flow past a stretching surface. The flow is subject to a chemical reaction. The spectral relaxation method is used to solve the flow equations. The classical model which involves the effects of thermophoresis and Brownian motion is revised in line with Kuznetsov and Nield [109].

1.5 The cross-diffusion effect

In recent years, the characteristics and mechanisms of fluid flow, with coupled heat and mass transfer through a porous medium saturated with nanofluids have attracted considerable attention, Narayana et al. [110]. The flux and driving potentials are complex with a complicated dynamical relationship. In general, an energy flux can be produced by concentration and temperature gradients. Thermal-diffusion, commonly known as the Soret effect, indicates mass flux generated by a temperature gradient, and the diffusion-thermo or the Dufour effect is to heat flux created by a concentration gradient, see Nield and Bejan [111]. Both processes have been comprehensively studied in gases, while the Soret effect has been studied both experimentally and theoretically in liquids. It is commonly accepted that Soret and Dufour effects are small when compared with phenomena described by other factors such as Fick and Fourier laws (Mojtabi and Charrier-Mojtabi [43]). Benamo-Mellya et al. [112] studied the effectiveness of using Soret coefficient measurement experiments in unsteady heat and mass transfer rates in a binary fluid mixture in a rectangular porous media. The vertical walls were set at a constant temperature whereas the horizontal walls were adiabatic. The semi-implicit and augmented Lagrangian method based on the Uzawa algorithm was used to solve the system equations (Vincent et al. [113]). The results demonstrated that, based on the Soret value, multiple convection-roll patterns can develop, while

thermal and solutal buoyancy forces oppose each other. When evaluating the optimum permeability for solute separation, a contradiction is observed in experimental and numerical results (Alam and Mollah [114]). Dufour and Soret effects are therefore commonly ignored in many heat and mass transfer processes. The effects of thermal-diffusion and diffusion-thermo are, however, important when density differences exist in the flow regime. For instance, when the density of a species does not exceed the density of the surrounding fluid, both diffusion-thermo and thermal-diffusion effects can be influential (Anjalidevi and Devi [115]).

Eckert and Drake [116] have also shown some cases where diffusion-thermo and thermal-diffusion effects may not be neglected. It has further been shown that there are a number of areas, such as in geosciences, where Soret and Dufour influences are significant. Kafoussias and Williams [117] examined mixed convection flow with Soret and Dufour effects, and temperature dependent viscosity. Mortimer and Eyring [118] used a transition state approach to derive a simple model for Dufour and Soret effects in thermodynamically ideal mixtures of substances with molecules of nearly equal size. In their model, the flow of heat and the diffusion-thermo effect was specified as the enthalpy change as molecules diffuse. The model was found to fit a reciprocal relationship earlier determined by Onsager [119]. Assuming a horizontal thermal gradient, Benano-Mellya et al. [112], investigated the problem of thermal-diffusion in binary fluid mixtures. Alam et al. [120] investigated thermal-diffusion and diffusion-thermo effects on free-forced convective flow along a semi-infinite vertical flat plate in hydrogen-air mixtures. They used the fourth order Runge-Kutta method to solve the conservation equations. Their investigation showed that thermal-diffusion and diffusion-thermo effects should not be ignored. Mansour et al. [121] studied the impact of thermal stratification and chemical reaction on heat and mass transfer, in flow past a vertical stretching surface, embedded in porous media, subject to Dufour and Soret effects. influences of the thermal-diffusion and diffusion-thermo parameters on free convection due to a vertical wavy surface in a Darcy porous medium have been investigated numerically by Narayana and Sibanda [122]. Narayana and Sibanda [47] investigated the problem of

micropolar fluid flow in a channel using the homotopy analysis method to solve the flow equations. Anjalidevi and Devi [115] investigated the influence of magnetic field and thermal radiation on a rotating disk subject to Dufour and Soret effects. Awad et al.[123] used the successive linearisation method in their study of Soret and Dufour influences in flow over inverted smooth and wavy cones.

In this Chapter 2 (see also Haroun et al. [124]) we use the spectral relaxation method in the study of heat and mass transfer in MHD nanofluid flow past an impulsively vertical stretching surface. The flow is subject to a chemical reaction and a thermophoretic force term. An earlier study by Awad et al. [70] investigated the problem of an unsteady nanofluid flow past a stretching sheet with couple stress effects.

1.6 Recent numerical solution techniques

Most problems in science and engineering are governed by non-linear differential equations. These equations are predominatingly strongly coupled and obtaining their exact solutions is not easy. This accounts for resorting to approximate numerical solutions. Through the years, a number of computational methods have been developed to solve non-linear coupled equations (Adomian [125]). These range from established numerical schemes like the Runge-Kutta schemes and finite difference techniques, to the finite element and finite volume methods. Many numerical methods unfortunately, converge slowly, are not sufficiently accurate or may not be computationally efficient. In such cases one may resort to perturbation methods to obtain approximate analytical solutions. Perturbation methods, however, require the presence of either a large or a small parameter in the problem, see Williams and Rhyne [126]. Additionally, these methods may have slow rates of convergence or may diverge for certain parameter values. In this study, we use at least two innovative numerical methods to solve highly non-linear systems of partial and ordinary differential equations that emerge in the study of fluid flow problems. The methods of particular interest are;

- the spectral relaxation method (SRM), and

- the spectral quasi-linearization method (SQLM).

These methods have been used in a limited sense by, for example, Motsa et al. [127], Motsa et al. [128], Shateyi and Marewo [129] and Motsa [130, 131].

In this study, the application of these methods is extended to systems of non-linear coupled partial differential equations that model complex fluid flow problems.

1.6.1 The spectral relaxation method

The spectral relaxation method is founded on simple iteration schemes formed by shrinking large systems of non-linear equations into smaller systems of linear equations, Sibanda et al. [132]. This method has been used to solve several non-linear problems and has been found to be efficient method, see Motsa [131]. The principal idea in the SRM is the rearrangement and decoupling of a system of non-linear differential equations in the Gauss-Seidel manner. The decoupled system of equations is integrated numerically using the Chebyshev spectral collocation method. In essence, any other numerical scheme, such as finite differences, many be used. It has been noted that the SRM gives good accuracy with only a few grid points (Motsa [131]). In Motsa and Makukula [133], the method was used to solve the problem of steady von Karman flow of a Reiner-Rivlin fluid with viscous dissipation and Joule heating. Accurate results were obtained and the speed of convergence of the method was significantly improved by using successive relaxation techniques. In Shateyi [134], the problem of steady MHD flow with a Maxwell fluid through a vertical stretching sheet in a Darcian porous medium was investigated. In Shateyi and Makinde [135], the SRM was applied to the problem of stagnation point steady flow and heat transfer of an electrically conducting incompressible viscous fluid. Shateyi and Marewo [129]

studied the magneto-dynamic and heat and mass transfer in boundary layer in incompressible upper-convected Maxwell fluid flow, due to a stretching sheet with viscous dissipation and thermal radiation. Motsa et al. [127], extended the method to a multistage technique to obtain better accuracy and computational efficiency. We applied the spectral relaxation method to solve the system of non-linear partial differential equations that describe double-diffusive convection and fluid flow problems.

1.6.2 The spectral quasi-linearization method

The spectral quasi-linearization method (SQLM) was originally introduced by Motsa and Shateyi [136]. In the SQLM, the non-linear equations are linearized using the Newton-Raphson based quasi-linearization method QLM of Bellman and Kalaba [137]. The method has been shown to be effective, easy to use and accurate compared to certain classical numerical methods such as finite elements and finite differences for some problems. For example, in Motsa and Shateyi [136], the SQLM scheme was used to solve the equations for unsteady free convective mass and energy transfer along a stretching surface in a porous medium. The method was compared with the local linearisation method and it was shown that the SQLM loses accuracy when the number of collocation points is large. The method has been used alongside other methods to determine its accuracy. In Dlamini et al. [138], the SQLM is compared with the compact finite difference quasi-linearization method for one and three dimensional systems of equations. The results showed that the SQLM had faster computational speed than the compact finite difference quasi-linearization mathod (CFD-QLM) but the SQLM was less accurate for the three dimensional problem. As another example, Motsa and Sibanda [139] used the method to develop a sequence of techniques with arbitrary higher order convergence. The techniques were used to determine solutions of Falknen-Skan type boundary layer equations. In this thesis we use the SQLM to solve systems of non-linear partial differential equations that describe fluid motion, and heat and mass transfer in nanofluids.

In the literature there is a wide range of techniques that may be described as spectral methods. In this thesis we are mostly interested in techniques that combine quasi-linearization with collocation such as Chebyshev collocation. The methods were first introduced by Motsa et al. [128], and Motsa and Makukula [133] for the solution of non-linear systems of equations that arise in the study of fluid flow problems.

Over the years, a number of computational methods have been developed to solve non-linear differential equations. Higher order systems have proven to be complicated to solve both analytically and numerically. As was described in Section 1.6, while methods such as the Runge-Kutta schemes, and the finite element method, are useful in terms of providing approximate solutions for systems of non-linear differential equations, because of slow accuracy, they may be inadequate for strongly non-linear systems of differential equations.

The spectral quasi-linearization method (SQLM) and the spectral relaxation method (SRM) are accurate, and have higher rates of convergence, with only a small number of grid points, and ease of implementation for complicated partial non-linear differential equations. Consequently, although the methods have not been applied extensively, we use them here for the following reasons:

1. Empirical evidence suggests that they are relatively easy to code in Matlab.

2. They have been used in a relatively small number of studies of different degrees of complexity, although the suggestion is that they are applicable to all non-linear ordinary differential and partial differential equations. We therefore seek to show, through solving various systems of coupled non-linear equations, that the quasi-linearization based spectral methods are accurate, robust and provide alternative solutions to finite element based techniques.

The methods are described in Motsa et al. [128], Motsa and Sibanda [140] and in various chapters, specifically in Chapter 4 in this thesis. In this chapter we give a brief review of various fluid flow models, and studies on heat and mass transfer. We present an overview

of two methods that can be used in the numerical solution of highly non-linear ordinary and partial differential equations, which arise in fluid mechanics and other engineering applications, (see Motsa [130], Dlamini et al. [138], Motsa and Sibanda [140]). The goal is to highlight the advantages of these methods over traditional methods of solving problems in fluid mechanics and to construct and analyse various fluid models, including factors that impact on heat and mass transfer processes.

1.7 Thesis objectives

The objectives of this thesis are to construct and analyse fluid flow models in different areas configurations and subject to various source terms and boundary conditions. We investigate how the fluid properties are influenced by changes in fluid and physical parameters and determine the impact and significance, if any, that these parameter changes have on heat and mass transfer processes.

A further objective is to test the accuracy, robustness and general validity of the SRM and SQLM techniques when solving systems of highly non-linear equations that describe and model fluid flow problems. The findings were validated against results from the literature such as the finite element and finite difference methods and the Matlab bvp4c solver.

1.8 Structure of the thesis

The main body of this thesis consists of six chapters and the conclusion. In each chapter a particular problem is investigated. The chapters focus firstly on the central theme and on the effects of nanofluids and cross-diffusion on fluid flow within a porous medium, and secondly on the application of the spectral linearization method and the spectral quasi-linearization method to the solution of a series of non-linear differential equations. The chapters are as follows;

In Chapter 2 we study double-diffusive convection in nanofluid flow along a stretching or

shrinking surface, subject to suction or injection velocity, viscous dissipation, and a chemical reaction.

In Chapter 3 we extend the study in Chapter 2 to consider heat and mass transfer when the flow is subject to a homogeneous chemical reaction, and heat generation with the assumption that thermal-diffusion effects are significant. The coupled non-linear equations are solved numerically using SRM and SQLM. A significant departure from earlier studies is the use of a recent boundary condition (Kuznetsov and Nield [109]), namely that the nanoparticle volume fraction at the wall may not be actively controlled.

In Chapter 4 we extend the work presented in Chapter 3 to the case of a couple stress nanofluid with vanishing nanoparticle flux at the wall. The conservation equations are solved numerically using both the spectral relaxation and quasi-linearization methods. The qualitative and quantitative influence of the physical parameters such as the Lewis number, the couple stress, thermophoresis parameters and the Prandtl number on the fluid behavior are determined.

In Chapter 5 we investigate heat and mass transfer in unsteady MHD nanofluids boundary layer flow past a stretching surface. We seek to provide both a quantitative and qualitative solutions as to how the thermophoresis and Brownian parameters influence the flow behaviour. This problem is modelled using sets of nonlinear partial differential equations which are solved numerically using SRM.

In Chapter 6 we study the problem of axisymmetric MHD stagnation point flow due to a shrinking sheet, subject to Navier slip condition and temperature dependent thermal conductivity. The SRM is used to solve the flow equations. Heat transfer processes are discussed for two types of wall heating, namely, a prescribed surface heat flux and a prescribed surface temperature.

In Chapter 7 we present the main findings from this study. We also highlight some significant points for future extension of this study, and also its limitations.

Chapter 2

On unsteady MHD mixed convection in a nanofluid due to a stretching/shrinking surface with suction/injection using the spectral relaxation method

In this chapter, we investigate heat and mass transfer in flow through a stretching/shrinking sheet with suction/injection. We consider copper-water and silver-water nanofluids and assume that the nanoparticle volume fraction can be actively controlled at the boundary surface. For these reasons, we use copper-water and silver-water nanofluids because they have great potential for enhancing heat transfer processes, and thermal properties of nanofluids. The flow is subject to a heat source, viscous dissipation and Soret and Dufour effects. The coupled non-linear partial differential equations that describe the fluid flow are solved numerically using SRM.

Haroun et al. *Boundary Value Problems* (2015) 2015:24
DOI 10.1186/s13661-015-0289-5

Boundary Value Problems
a SpringerOpen Journal

RESEARCH Open Access

On unsteady MHD mixed convection in a nanofluid due to a stretching/shrinking surface with suction/injection using the spectral relaxation method

Nageeb A Haroun, Precious Sibanda*, Sabyasachi Mondal and Sandile S Motsa

*Correspondence:
sibandap@ukzn.ac.za
School of Mathematics, Statistics and Computer Science, University of KwaZulu-Natal, Private Bag X01, Scottsville, Pietermaritzburg, 3209, South Africa

Abstract

In this study we investigate heat and mass transfer in magnetohydrodynamic mixed convection flow of a nanofluid over an unsteady stretching/shrinking sheet. The flow is subject to a heat source, viscous dissipation and Soret and Dufour effects are assumed to be significant. We have further assumed that the nanoparticle volume fraction at the wall may be actively controlled. The physical problem is modeled using systems of nonlinear differential equations which we have solved numerically using the recent spectral relaxation method. In addition to the discussion on physical heat and mass transfer processes, we also show that the spectral relaxation technique is an accurate technique for solving nonlinear boundary value problems.

Keywords: nanofluids; dimensionless suction/injection; magnetohydrodynamic; Soret and Dufour effects; heat generation parameter

1 Introduction

Nanofluids are suspensions of metallic, non-metallic or polymeric nano-sized powders in a base liquid which are used to increase the heat transfer rate in various applications. In recent years, the concept of nanofluid has been proposed as a route for increasing the performance of heat transfer liquids. Due to the increasing importance of nanofluids, there is a large amount of literature on convective heat transport in nanofluids and problems linked to a stretching surface. An excellent collection of articles on this topic can be found in [1–4]. The majority of the previous studies have been restricted to boundary layer flow and heat transfer in nanofluids. Following the early work by Crane [5], Khan and Pop [6] were among the first researchers to study nanofluid flow due to a stretching sheet. Other researchers studied various aspects of flow and heat transfer in a fluid of infinite extent; see, for instance, Chen [7] and Abo-Eldahab and Abd El-Aziz [8]. A mathematical analysis of momentum and heat transfer characteristics of the boundary layer flow of an incompressible and electrically conducting viscoelastic fluid over a linear stretching sheet was carried out by Abd El-Aziz [9]. In addition, radiation effects on viscous flow of a nanofluid and heat transfer over a nonlinearly stretching sheet were studied by Hady *et al.* [10]. Theoretical studies include, for example, modeling unsteady boundary layer flow of a nanofluid over a permeable stretching/shrinking sheet by Bachok *et al.* [11]. Rohni *et al.* [12] devel-

oped a numerical solution for the unsteady flow over a continuously shrinking surface with wall mass suction using the nanofluid model proposed by Buongiorno [13].

The effect of an applied magnetic field on nanofluids has substantial applications in chemistry, physics and engineering. These include cooling of continuous filaments, in the process of drawing, annealing and thinning of copper wire. Drawing such strips through an electrically conducting fluid subject to a magnetic field can control the rate of cooling and stretching, thereby furthering the desired characteristics of the final product. Such an application of a linearly stretching sheet of incompressible viscous flow of MHD was discussed by Pavlov [14]. In other work, Jafar *et al.* [15] studied the effects of magnetohydrodynamic (MHD) flow and heat transfer due to a stretching/shrinking sheet with an external magnetic field, viscous dissipation and Joule effects.

A model for magnetohydrodynamic flow over a uniformly stretched vertical permeable surface subject to a chemical reaction was suggested by Chamkha [16]. An analysis of the effects of a chemical reaction on heat and mass transfer on a magnetohydrodynamic boundary layer flow over a wedge with ohmic heating and viscous dissipation in a porous medium was done by Kandasamy and Palanimani [17]. Rashidi and Erfani [18] studied the steady MHD convective and slip flow due to a rotating disk with viscous dissipation and ohmic heating. Rashidi *et al.* [19] found approximate analytic solutions for an MHD boundary-layer viscoelastic fluid flow over a continuously moving stretching surface using the homotopy analysis method. Rashidi and Keimanesh [20] used the differential transform method and Padé approximants to solve the equations that model MHD flow in a laminar liquid film from a horizontal stretching surface. The effect of a transverse magnetic field on the flow and heat transfer over a stretching surface were examined by Anjali-Devi and Thiyagarajan [21]. The influence of a chemical reaction on heat and mass transfer due to natural convection from vertical surfaces in porous media subject to Soret and Dufour effects was also studied by Postelnicu [22].

Despite all this previous work, there is still a lot that is unknown about the flow and heat and mass transfer properties of different nanofluids. For instance, the composition and make of the nanoparticles may have an impact on the performance of the nanofluid as a heat transfer medium. In this paper we investigate unsteady MHD mixed convection boundary layer with suction/injection subject to a number of source terms including Dufour and Soret effects, heat generation, an applied magnetic field and viscous dissipation. Various numerical and or semi-numerical methods can and have been used to solve the equations that model this type of boundary layer flow. These equations are non-similar and coupled. In this paper we use the spectral relaxation method (SRM) that was recently proposed by Motsa [23]. This spectral relaxation method promises fast convergence with good accuracy, has been successfully used in a limited number of boundary layer flow and heat transfer problems (see [24, 25]). In this paper we discuss the fluid flow and heat transfer as well as highlight the strengths of the solution method.

2 Governing equations

Consider the two-dimensional unsteady laminar MHD mixed convective flow of a nanofluid due to a stretching sheet situated at $y = 0$ with stretching velocity $u = ax$, where a is a constant. The temperature and nanoparticle volume fraction at the stretching surface are T_w and C_w, respectively, and those of the ambient nanofluid are T_∞ and C_∞,

respectively. The x and y directions are in the plane of and perpendicular to the sheet, respectively. The continuity, momentum, energy and concentration equations of unsteady, incompressible nanofluid boundary layer flow are as follows (see Yang [26]):

$$\frac{\partial u}{\partial x} + \frac{\partial v}{\partial y} = 0, \tag{2.1}$$

$$\frac{\partial u}{\partial t} + u\frac{\partial u}{\partial x} + v\frac{\partial u}{\partial y} = -\frac{1}{\rho_{nf}}\frac{\partial p}{\partial x} + \frac{\mu_{nf}}{\rho_{nf}}\frac{\partial^2 u}{\partial y^2} + g\beta_T(T - T_\infty) + g\beta_C(C - C_\infty) - \frac{\sigma B_0^2}{\rho_{nf}}u, \tag{2.2}$$

$$\frac{\partial T}{\partial t} + u\frac{\partial T}{\partial x} + v\frac{\partial T}{\partial y} = \alpha_{nf}\frac{\partial^2 T}{\partial y^2} + \frac{Q}{(\rho c_p)_{nf}}(T - T_\infty) + \frac{\rho_f D_m K_T}{C_s(\rho c_p)_{nf}}\frac{\partial^2 C}{\partial^2 y}, \tag{2.3}$$

$$\frac{\partial C}{\partial t} + u\frac{\partial C}{\partial x} + v\frac{\partial C}{\partial y} = D_m\frac{\partial^2 C}{\partial y^2} + \frac{D_m K_m}{T_m}\frac{\partial^2 T}{\partial y^2} - R(C - C_\infty), \tag{2.4}$$

where t, u and v are the time, the fluid velocity and the normal velocity components in the x and y orientations, respectively; ν_{nf}, p, ρ_{nf}, σ, B_0, μ_{nf}, g are the nanofluid kinematic viscosity, the pressure, nanofluid density, electrical conductivity, the uniform magnetic field in the y direction, the effective dynamic viscosity of the nanofluid and gravitational acceleration, respectively; β_T, β_C, T, C, α_{nf}, $(\rho cp)_{nf}$, Q are the volumetric thermal expansion coefficient, the solutal expansion coefficient, the temperature of the fluid in the boundary layer, fluid solutal concentration, the thermal diffusivity of the nanofluid, the nanofluid heat capacitance and the volumetric rate of heat generation, respectively; ρ_f, D_m, K_T, C_s, $(cp)_{nf}$, T_m, R are the density of the base fluid, the mass diffusivity of concentration, thermal diffusion ratio, concentration susceptibility, specific heat of the fluid at constant pressure, mean fluid temperature and the chemical reaction parameter, respectively.

The boundary conditions are as follows:

$$\begin{aligned} &t \geq 0: \quad u = U_w(x) = ax, \qquad v = v_w, \qquad T = T_w, \qquad C = C_w \quad \text{at } y = 0, \\ &t \geq 0: \quad u = U_\infty(x) = a_\infty x, \qquad v = 0, \qquad T = T_\infty, \qquad C = C_\infty \quad \text{as } y \to \infty, \end{aligned} \tag{2.5}$$

and the initial conditions are

$$\begin{aligned} &t < 0: \quad u(x,y,t) = 0, \qquad v(x,y,t) = 0, \\ &\qquad T(x,y,t) = T_w, \qquad C(x,y,t) = C_w, \quad \forall x, y, \end{aligned} \tag{2.6}$$

where a_∞ (> 0) is the stagnation flow rate parameter, $a < 0$ for a shrinking surface and $a > 0$ for a stretching surface. Here v_w is prescribed suction velocity ($v_w < 0$) or blowing velocity ($v_w > 0$).

In the free stream the momentum equation (2.2) becomes

$$U_\infty\frac{dU_\infty}{dx} = -\frac{1}{\rho_{nf}}\frac{\partial p}{\partial x} - \frac{\sigma B_0^2}{\rho_{nf}}U_\infty. \tag{2.7}$$

Substituting (2.7) in (2.2) the momentum equation is written as

$$\begin{aligned} \frac{\partial u}{\partial t} + u\frac{\partial u}{\partial x} + v\frac{\partial u}{\partial y} = \nu_{nf}\frac{\partial^2 u}{\partial y^2} + U_\infty\frac{dU_\infty}{dx} + (U_\infty - u)\frac{\sigma B_0^2}{\rho_{nf}} \\ + g\beta_T(T - T\infty) + g\beta_C(C - C\infty). \end{aligned} \tag{2.8}$$

The effective dynamic viscosity of the nanofluid was given by Brinkman [27] as

$$\mu_{nf} = \frac{\mu_f}{(1-\phi)^{2.5}}, \tag{2.9}$$

where ϕ is the solid volume fraction of nanoparticles, μ_f is the dynamic viscosity of the base fluid. In equations (2.1)-(2.4),

$$\begin{aligned}
&(\rho c_p)_{nf} = (1-\phi)(\rho c_p)_f + \phi(\rho c_p)_s,\\
&\rho_{nf} = (1-\phi)\rho_f + \phi\rho_s, \qquad \nu_{nf} = \frac{\mu_{nf}}{\rho_{nf}},\\
&\alpha_{nf} = \frac{k_{nf}}{(\rho c_p)_{nf}}, \qquad \frac{k_{nf}}{k_f} = \frac{(k_s+k_f)-2\phi(k_f-k_s)}{(k_s+k_f)+\phi(k_f-k_s)},
\end{aligned} \tag{2.10}$$

where k_{nf} is the thermal conductivity of the nanofluid, k_f and k_s are the thermal conductivities of the fluid and of solid fractions, respectively, and ρ_s is the density of solid fractions, $(\rho c_p)_f$ and $(\rho c_p)_s$ are the heat capacity of the base fluid and the effective heat capacity of a nanoparticle, respectively, k_{nf} is the thermal conductivity of the nanofluid.

The continuity equation (2.1) is satisfied by introducing a stream function $\psi(x,y)$ such that

$$u = \frac{\partial\psi}{\partial y}, \qquad v = -\frac{\partial\psi}{\partial x}. \tag{2.11}$$

We introduce the following non-dimensional variables (see Liao [28]):

$$\begin{aligned}
&\eta = \left[\frac{a_\infty}{\nu_f\xi}\right]^{\frac{1}{2}} y, \quad \xi = 1-\exp(-\tau), \tau = a_\infty t, \qquad \psi = [a_\infty \nu_f \xi]^{\frac{1}{2}} x f(\xi,\eta),\\
&\theta(\xi,\eta) = \frac{T-T_\infty}{T_w-T_\infty}, \qquad \Phi(\xi,\eta) = \frac{C-C_\infty}{C_w-C_\infty},
\end{aligned} \tag{2.12}$$

where $f(\xi,\eta)$ is a dimensionless stream function, $\theta(\xi,\eta)$ is the dimensionless temperature and $\phi(\xi,\eta)$ is the dimensionless solute concentration. By using (2.11) and (2.12), the governing equations (2.3), (2.4) and (2.8) along with the boundary conditions (2.5) are reduced to the following two-point boundary value problem:

$$\begin{aligned}
&f''' + \phi_1\left[\frac{\eta}{2}(1-\xi)f'' + \xi\left(ff'' - f'^2 + 1 + Ha^2\left(1-f'\right) + Gr_t\theta + Gr_c\Phi\right)\right]\\
&\quad = \phi_1\xi(1-\xi)\frac{\partial f'}{\partial\xi},
\end{aligned} \tag{2.13}$$

$$\theta'' + \frac{k_f}{k_{nf}}Pr\phi_2\left[\frac{\eta}{2}(1-\xi)\theta' + \xi\left(f\theta' + \delta\theta\right) + \frac{D_f}{\phi_2}\Phi''\right] = \frac{k_f}{k_{nf}}Pr\phi_2\xi(1-\xi)\frac{\partial\theta}{\partial\xi}, \tag{2.14}$$

$$\Phi'' + Sc\left[\frac{\eta}{2}(1-\xi)\Phi' + \xi\left(f\Phi' - \gamma\Phi\right) + Sr\theta''\right] = Sc\xi(1-\xi)\frac{\partial\Phi}{\partial\xi}. \tag{2.15}$$

The boundary conditions are as follows:

$$\begin{aligned}
&f(\xi,0) = f_w, \qquad f'(\xi,0) = \lambda, \qquad \theta(\xi,0) = 1, \qquad \Phi(\xi,0) = 1 \quad \text{at } \eta = 0, \xi \geq 0,\\
&f'(\xi,\infty) = 1, \qquad \theta(\xi,\infty) = 0, \qquad \Phi(\xi,\infty) = 0 \quad \text{as } \eta \to \infty, \xi \geq 0,
\end{aligned} \tag{2.16}$$

where primes denote differentiation with respect to η, $\alpha_f = k_f/(\rho c_p)_f$ and $\nu_f = \mu_f/\rho_f$ are the thermal diffusivity and kinetic viscosity of the base fluid, respectively. Other non-dimensional parameters appearing in equations (2.13) to (2.15) are Ha, Gr_t, Gr_c, Gr_c, Pr, δ, D_f, Sc, γ and Sr, and they denote the Hartmann number, the local temperature Grashof number, the local concentration Grashof number, the Prandtl number, the dimensionless heat generation parameter, the Dufour number, the Schmidt number, the scaled chemical reaction parameter and the Soret number, respectively. These parameters are defined mathematically as

$$\begin{aligned}
&Ha^2 = \frac{\sigma B_0^2}{a_\infty \rho_{nf}}, \qquad Gr_t = \frac{g\beta_T(T_w - T_\infty)}{a_\infty^2 x},\\
&Gr_c = \frac{g\beta_C(C_w - C_\infty)}{a_\infty^2 x}, \qquad Pr = \frac{\nu_f}{\alpha_f}, \qquad \delta = \frac{Q}{a_\infty(\rho c_p)_{nf}},\\
&D_f = \frac{D_m K_T(C_w - C_\infty)}{C_s(C_p)_f \nu_f(T_w - T_\infty)}, \qquad Sc = \frac{\nu_f}{D_m},\\
&\gamma = \frac{R}{a_\infty}, \qquad Sr = \frac{D_m K_T}{T_m}\frac{(T_w - T_\infty)}{\nu_f(C_w - C_\infty)}.
\end{aligned} \tag{2.17}$$

The boundary conditions are as follows:

$$\begin{aligned}
&f(\xi,0) = f_w, \qquad f'(\xi,0) = \lambda, \qquad \theta(\xi,0) = 1, \qquad \Phi(\xi,0) = 1 \quad \text{at } \eta = 0, \xi \geq 0,\\
&f'(\xi,\infty) = 1, \qquad \theta(\xi,\infty) = 0, \qquad \Phi(\xi,\infty) = 0 \quad \text{as } \eta \to \infty, \xi \geq 0.
\end{aligned} \tag{2.18}$$

The nanoparticle volume fractions ϕ_1 and ϕ_2 are defined as

$$\phi_1 = (1-\phi)^{2.5}\left[1 - \phi + \phi\left(\frac{\rho_s}{\rho_f}\right)\right], \qquad \phi_2 = \left[1 - \phi + \phi\frac{(\rho c)_s}{(\rho c)_f}\right]. \tag{2.19}$$

In equations (2.18), $f_w = -v_w/\sqrt{a_\infty \nu_f \xi}$ represents suction ($f_w > 0$) or injection ($f_w < 0$) and λ ($= a/a_\infty$) is the stretching/shrinking parameter.

3 Skin friction, heat and mass transfer coefficients

The skin friction coefficient C_f, the local Nusselt number Nu_x and the local Sherwood number Sh_x characterize the surface drag, wall heat and mass transfer rates, respectively.

The shearing stress at the surface of the wall τ_w is defined as

$$\tau_w = -\mu_{nf}\left(\frac{\partial u}{\partial y}\right)_{y=0} = -\frac{U_\infty \mu_f}{(1-\phi)^{2.5} x}\sqrt{\frac{U_\infty x}{\nu_f \xi}} f''(0,\xi), \tag{3.1}$$

where μ_{nf} is the coefficient of viscosity.

The skin friction coefficient is obtained as

$$C_{fx} = \frac{2\tau_w}{\rho_f U_\infty^2}, \tag{3.2}$$

and using equation (3.1) in (3.2) we obtain

$$\frac{1}{2}(1-\phi)^{2.5} C_{fx} = -\xi^{-\frac{1}{2}} Re_x^{-\frac{1}{2}} f''(0,\xi). \tag{3.3}$$

The heat transfer rate at the surface flux at the wall is defined as

$$q_w = -k_{nf}\left(\frac{\partial T}{\partial y}\right)_{y=0} = -k_{nf}\frac{(T_w - T_\infty)}{x}\sqrt{\frac{U_\infty x}{\nu_f \xi}}\theta'(0,\xi), \tag{3.4}$$

where k_{nf} is the thermal conductivity of the nanofluid. The local Nusselt number is defined as

$$Nu_x = \frac{xq_w}{k_f(T_w - T_\infty)}. \tag{3.5}$$

Using equation (3.4) in equation (3.5), the dimensionless wall heat transfer rate is obtained as

$$\left(\frac{k_f}{k_{nf}}\right)Nu_x = -\xi^{-\frac{1}{2}}Re_x^{\frac{1}{2}}\theta'(0,\xi). \tag{3.6}$$

The mass flux at the wall surface is defined as

$$q_m = -D\left(\frac{\partial C}{\partial y}\right)_{y=0} = -D\frac{(C_w - C_\infty)}{x}\sqrt{\frac{U_\infty x}{\nu_f \xi}}\Phi'(0,\xi), \tag{3.7}$$

and the local Sherwood number (mass transfer coefficient) is obtained as

$$Sh_x = \frac{xq_m}{D(C_w - C_\infty)}. \tag{3.8}$$

The dimensionless wall mass transfer rate is obtained as

$$Sh_x = -\xi^{-\frac{1}{2}}Re_x^{\frac{1}{2}}\Phi'(0,\xi), \tag{3.9}$$

where Re_x represents the local Reynolds number and is defined as

$$Re_x = \frac{xu_\infty}{\nu_f}. \tag{3.10}$$

4 Cases of special interest

In this section we highlight two particular cases where equations (2.12) to (2.14) reduce to ordinary differential equations.

4.1 Initial steady flow

For steady flow and a regular fluid, if we assume that $\xi \to 0$, where $0 < \xi \leq 1$, then $t \approx 0$. Thus $f(\eta,\xi) \approx f(\eta)$, $\theta(\eta,\xi) \approx \theta(\eta)$ and $\Phi(\eta,\xi) \approx \Phi(\eta)$. In this case equations (2.12) to (2.14) reduce to

$$f''' + \frac{1}{2}\phi_1 \eta f'' = 0, \tag{4.1}$$

$$\theta'' + \frac{1}{2}\frac{k_f}{k_{nf}}Pr\phi_2 \eta\theta' + \frac{k_f}{k_{nf}}PrD_f\Phi'' = 0, \tag{4.2}$$

$$\Phi'' + \frac{1}{2}Sc\eta\Phi' + ScSr\theta'' = 0, \tag{4.3}$$

subject to the appropriately modified boundary conditions (2.18). The exact solutions of these equations cannot be easily obtained. The numerical solutions were obtained using the spectral relaxation method (SRM).

4.2 Final steady state flow

In this case, we have $\xi = 1$ when $t \to \infty$, corresponding to $f(\eta,1) = f(\eta)$, $\theta(\eta,1) = \theta(\eta)$ and $\Phi(\eta,1) = \Phi(\eta)$. Equations (2.12) to (2.14) reduce to the following forms:

$$f''' + ff'' - f'^2 + 1 + Ha^2\left(1 - f'\right) + GR_t\theta + Gr_c\Phi = 0, \tag{4.4}$$

$$\theta'' + \frac{k_f}{k_{nf}}Pr\phi_2\left(f\theta' + \delta\theta\right) + \frac{k_f}{k_{nf}}PrD_f\Phi'' = 0, \tag{4.5}$$

$$\Phi'' + Sc\left(f\Phi' - \gamma\Phi + Sr\theta''\right) = 0, \tag{4.6}$$

subject to the boundary conditions (2.18). Equations (4.1) to (4.6) were solved using the SRM, Motsa [23].

The spectral relaxation method (SRM) is an iterative procedure that employs the Gauss-Seidel type of relaxation approach to linearize and decouple the system of differential equations. Further details of the rules of the SRM can be found in [24, 25]. The linear terms in each equation are evaluated at the current iteration level (denoted by $r+1$) and the non-linear terms are assumed to be known from the previous iteration level (denoted by r). The linearized form of (2.13)-(2.15) is

$$f'''_{r+1} + a_{1,r}f''_{r+1} + a_{2,r}f'_{r+1} - \phi_1\xi(1-\xi)\frac{\partial f'}{\partial\xi} = R_{1,r}, \tag{4.7}$$

$$\theta''_{r+1} + b_{1,r}\theta'_{r+1} + b_{2,r}\theta_{r+1} - \frac{k_f}{k_{nf}}Pr\phi_2\xi(1-\xi)\frac{\partial\theta}{\partial\xi} = R_{2,r}, \tag{4.8}$$

$$\phi''_{r+1} + c_{r,1}\phi'_{r+1} + c_{2,r}\phi_{r+1} - Sc\xi(1-\xi)\frac{\partial\phi}{\partial\xi} = R_{3,r}, \tag{4.9}$$

where

$$a_{1,r} = \phi_1\left[\frac{\eta}{2}(1-\xi) + \xi f_r\right], \qquad a_2 = -\phi_1\xi Ha^2,$$

$$R_{1,r} = -\phi_1\left[\xi\left(1 - f_r'^2\right) + Ha^2 + Gr_t\theta_r + Gr_c\phi_r\right],$$

$$b_{1,r} = \frac{k_f}{k_{nf}}Pr\phi_2\left[\frac{\eta}{2}(1-\xi) + \xi f_{r+1}\right], \qquad b_{2,r} = \frac{k_f}{k_{nf}}Pr\phi_2\xi,$$

$$R_{2,r} = -\frac{k_f}{k_{nf}}PrD_f\Phi_r,$$

$$c_{1,r} = \frac{\eta}{2}(1-\xi)Sc + \xi f_{r+1}, \qquad c_{2,r} = -Sc\xi\gamma,$$

$$R_{3,r} = -ScSr\theta''_{r+1}.$$

Equations (4.7)-(4.9) are now linear and decoupled. The equations can be solved sequentially to obtain approximate solutions for $f(\eta,\xi)$, $\theta(\eta,\xi)$ and $\phi(\eta,\xi)$. In this study, the Chebyshev spectral collocation method was used to discretize in η and finite differences

used to discretize in ξ directions. Starting from initial guesses for f, θ and ϕ, equations (4.7)-(4.9) were solved iteratively until the approximate solutions converged within a certain prescribed tolerance level. The accuracy of the results was validated against results from the literature for some special cases of the governing equations.

5 Results and discussion

The system of partial differential equations (2.13) to (2.15) subject to boundary conditions (2.18) were solved numerically using the spectral relaxation method (SRM) for Cu-water and Ag-water nanofluids. The thermophysical properties of the nanofluids used in the numerical simulations are given in Table 1.

To determine the accuracy of our numerical results, the skin friction coefficient is compared with the published results of Jafar *et al.* [15], Wang [31] and Suali *et al.* [32] in Tables 2-4. Here we have varied the stretching parameter while keeping other physical parameters fixed. Table 2 gives a comparison of the SRM results with those obtained by Jafar *et al.* [15] and Wang [31] when $Ha = Gr_t = Gr_c = \delta = D_f = Sc = Sr = \gamma = \phi = 0$, $Pr = 1$ and $\xi = 1$ for different values of the stretching/shrinking parameter. It is observed that for increasing λ, the present results are in good agreement with results in the literature.

Table 4 gives the skin friction coefficient for selected stretching λ parameter values. Here we note that as the stretching rate decreases, the skin friction coefficient increases. These results are in good agreement with those obtained by Suali *et al.* [32].

The effects of the nanoparticle volume fraction on the fluid velocity, temperature, concentration profiles as well as skin friction, local Nusselt and Sherwood numbers are given

Table 1 Thermophysical properties of the base fluid and the nanoparticles [29] and [30]

Physical properties	Base fluid (Water)	Copper (Cu)	Silver (Ag)
C_p (J/kgK)	4,179	385	235
ρ (Kg/m^3)	997.1	8,933	10,500
k (W/mK)	0.613	401	429
$\alpha \times 10^7$ (m^2/s)	1.47	1,163.1	1,738.6
$\beta \times 10^5$ (K^{-1})	21	1.67	1.89

Table 2 Comparison of the SRM result with Wang [31] and Jafar *et al.* [15] for the skin friction coefficient $f''(0,1)$ for different stretching rates

λ	Wang [31]	Jafar *et al.* [15]	Present result (SRM)
	$f''(0,1)$	$f''(0,1)$	$f''(0,1)$
0	1.232588	1.2326	1.23258
0.1	1.14656	1.1466	1.14655
0.2	1.05113	1.0511	1.05112
0.5	0.71330	0.7133	0.71328
1	0.00000	0.00000	0.00000
2	−1.88731	−1.8873	−1.88690
5	−10.26475	−10.2648	−10.24531

Table 3 Comparison of the SRM results with Wang [31] and Jafar *et al.* [15] for the skin friction coefficient $f''(0,1)$ for different stretching rates

λ	−0.25	−0.5	−0.75	−1
Wang [31]	1.40224	1.49576	1.48930	1.32882
Jafar *et al.* [15]	1.4022	1.4957	1.4893	1.32880
SRM result	1.40224	1.49565	1.48913	1.32795

Table 4 Comparison of the SRM result with Suali *et al.* [32] for the skin friction coefficient for different stretching/shrinking sheet rates

λ	Suali *et al.* [32]	SRM result
	$f''(0,1)$	$f''(0,1)$
4	−7.086378	−7.086378
3	−4.276545	−4.276542
0.2	1.051130	1.051130
0.1	1.146561	1.146561
−0.2	1.373886	1.373886
−0.5	1.495672	1.495670

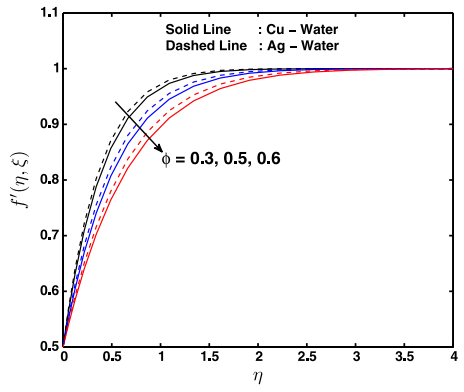

Figure 1 Effect of nanoparticle value fraction ϕ on velocity for $D_f = 0.01$, $\lambda = 0.5$, $Gr_t = 0.01$, $Gr_c = 0.01$, $Pr = 7$, $Ha = 2$, $\delta = 0.1$, $Sc = 1$, $Sr = 1$, $f_w = 1$, $\gamma = 0.1$ and $\xi = 0.5$.

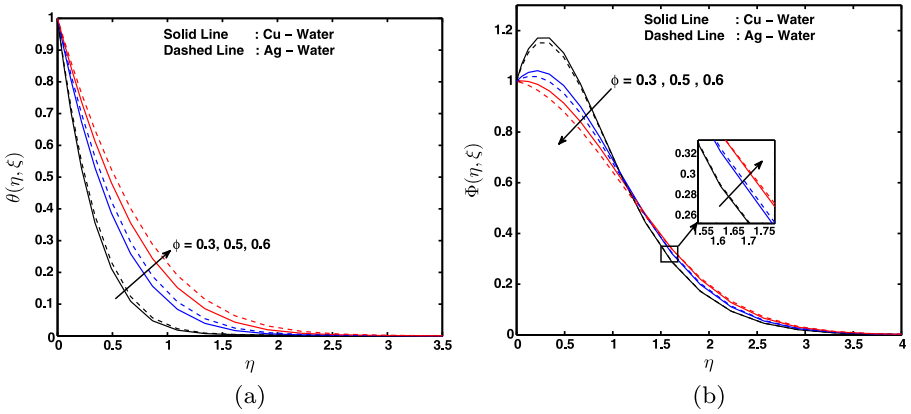

Figure 2 Effect of various nanoparticle value fractions ϕ on (a) temperature profiles and (b) concentration profiles when $D_f = 0.01$, $\lambda = 0.5$, $Gr_t = 0.01$, $Gr_c = 0.01$, $Pr = 7$, $Ha = 2$, $\delta = 0.1$, $Sc = 1$, $Sr = 1$, $f_w = 1$, $\gamma = 0.1$ and $\xi = 0.5$.

in Figures 1-4. It is evident that the solute concentration, skin friction and the local Nusselt number decrease with increasing nanoparticle volume fraction while the velocity, temperature, and the local Sherwood number increase. This is because with an increase in nanoparticles volume fraction, the thermal conductivity of the nanofluid increases, which reduces the thermal boundary layer thickness and the temperature gradient at the wall.

The axial velocity in the case of an Ag-water nanofluid is comparatively higher than that in the case of a Cu-water nanofluid. The temperature distribution in an Ag-water nanofluid is higher than that in a Cu-water nanofluid and this is explained by the observa-

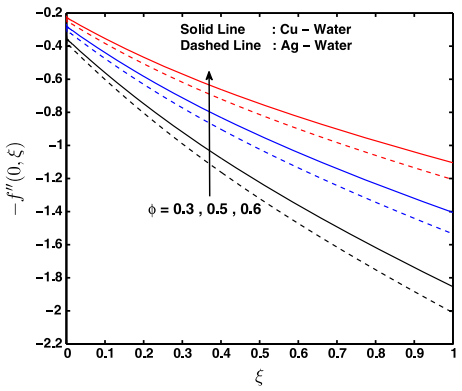

Figure 3 Effect of various nanoparticle value fractions ϕ on the skin friction coefficient for $D_f = 0.01$, $\lambda = 0.5$, $Gr_t = 0.01$, $Gr_c = 0.01$, $Pr = 7$, $Ha = 2$, $\delta = 0.1$, $Sc = 1$, $Sr = 1$, $f_w = 1$ and $\gamma = 0.1$.

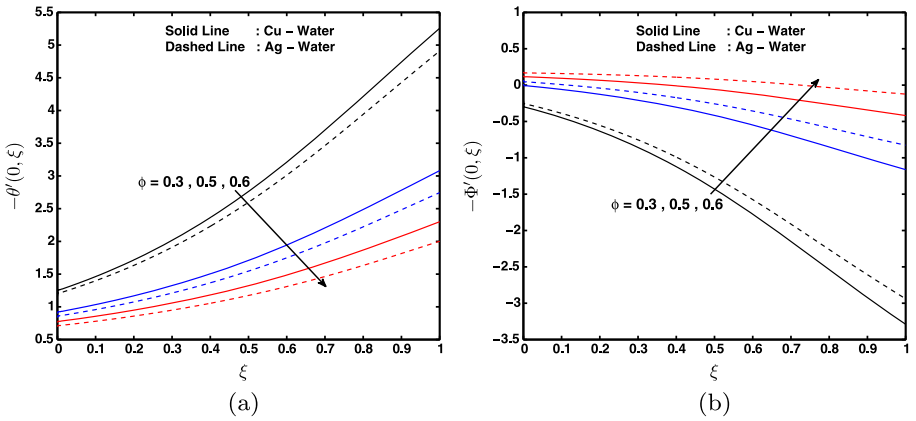

Figure 4 Effect of nanoparticle volume fraction ϕ on (a) the heat transfer coefficient and (b) the mass transfer coefficient when $D_f = 0.01$, $\lambda = 0.5$, $Gr_t = 0.01$, $Gr_c = 0.01$, $Pr = 7$, $Ha = 2$, $\delta = 0.1$, $Sc = 1$, $Sr = 1$, $f_w = 1$ and $\gamma = 0.1$.

tion that the thermal conductivity of silver is higher than that of copper. The concentration boundary layer thickness is higher for the case of a Cu-water than that for the case of an Ag-water nanofluid.

Figure 3 shows that the skin friction coefficient decreases monotonically with increasing ξ. The result is true for both types of fluids. The maximum value of the skin friction in the case of a Cu-water nanofluid is achieved at a smaller value of ξ in comparison with an Ag-water nanofluid. Furthermore, in this paper it is found that the Ag-water nanofluid shows less drag as compared to the Cu-water nanofluid. The dimensionless wall heat transfer rate and the dimensionless wall mass transfer rate are shown as functions of ξ in Figure 4(a) and (b), respectively. We observe that the wall heat transfer rate decreases while the opposite is true in case of the wall mass transfer rate. The Cu-water nanofluid exhibits higher wall heat transfer rate as compared to the Ag-water nanofluid, while the Cu-water nanofluid exhibits less than the Ag-water nanofluid. The presence of nanoparticle tends to increase the wall heat transfer rate and to reduce the wall mass transfer rates with increasing the values of ξ.

Figures 5-7 show the influence of the Hartmann number on the velocity, temperature, skin friction, the local Nusselt number and the local Sherwood number. The effect of the Hartmann number *Ha* is to increase the nanofluid velocity and the wall heat transfer rate,

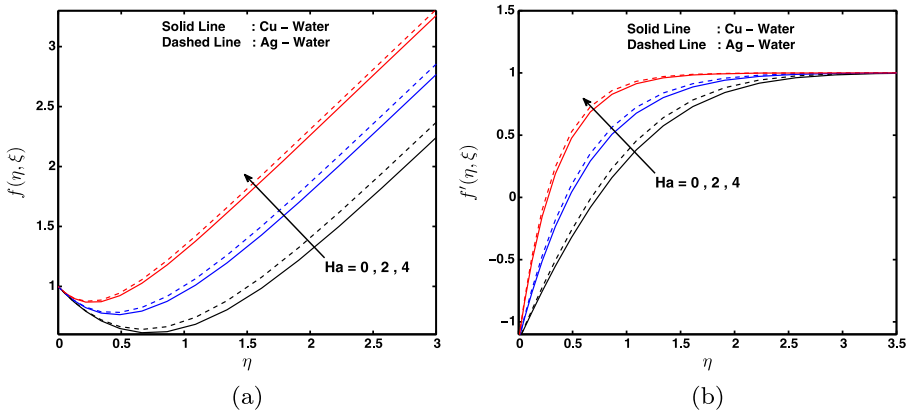

Figure 5 Effect of the Hartmann number *Ha* on velocity profiles for $D_f = 0.01$, $\phi = 0.2$, $Gr_t = 0.01$, $Gr_c = 0.01$, $Pr = 7$, $f_w = 1$, $\delta = 0.1$, $Sc = 1$, $Sr = 1$, $\lambda = -1.15$, $\gamma = 3$ and $\xi = 0.5$.

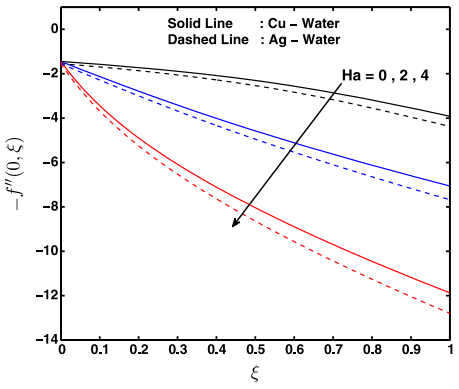

Figure 6 Effect of the Hartmann number *Ha* on the skin friction coefficient for $D_f = 0.01$, $\phi = 0.2$, $Gr_t = 0.01$, $Gr_c = 0.01$, $Pr = 7$, $f_w = 1$, $\delta = 0.1$, $Sc = 1$, $Sr = 1$, $\lambda = -1.15$ and $\gamma = 3$.

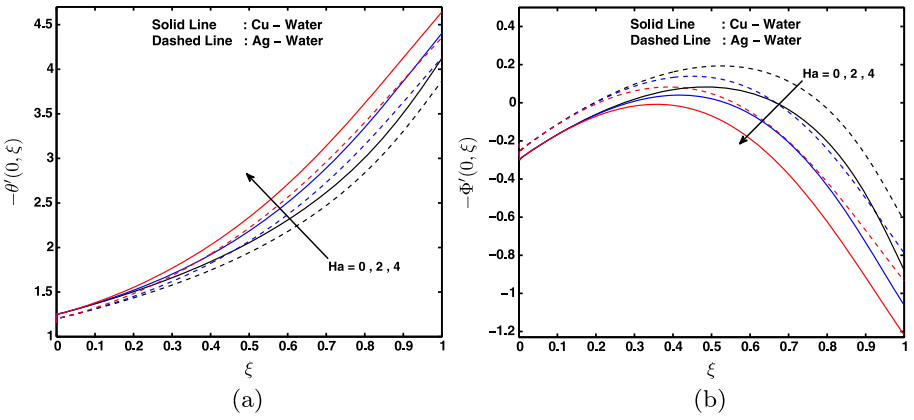

Figure 7 Effect of various values of the Hartmann number *Ha* on (a) the heat transfer coefficient and (b) the mass transfer coefficient when $D_f = 0.01$, $\phi = 0.2$, $Gr_t = 0.01$, $Gr_c = 0.01$, $Pr = 7$, $f_w = 1$, $\delta = 0.1$, $Sc = 1$, $Sr = 1$, $\lambda = -1.15$ and $\gamma = 3$.

whereas it reduced the skin friction coefficient and the wall mass transfer rate. A similar observation was made by Jafar *et al.* [15]. The momentum boundary layer thickness increases with increase in the Hartmann number.

Figure 6 shows the skin friction coefficient as a function of ξ. It is clear that for Ag-water and Cu-water nanofluids, the skin friction reduces when ξ increases. We note that the Cu-water nanofluid exhibits higher drag to the flow as compared to the Ag-water nanofluid. Figure 7 shows the wall heat and mass transfer rates for a different Hartmann number *Ha*, it is clear that the value of wall heat transfer rate increases as ξ increases, in the case of an Ag-water nanofluid it is less than in the case of a Cu-water nanofluid. Further, the wall mass transfer rate increases up to the value of ξ before reducing.

Figures 8-11 show the velocity, temperature, concentration of nanofluid with skin friction, the wall heat and mass transfer rates for various values of the suction/injection parameter. We observe that the velocity boundary layer thickness decreases with increasing values of the suction parameter. This is because due to suction, the fluid is removed from the system which reduces the momentum boundary layer thickness. Similarly, the bound-

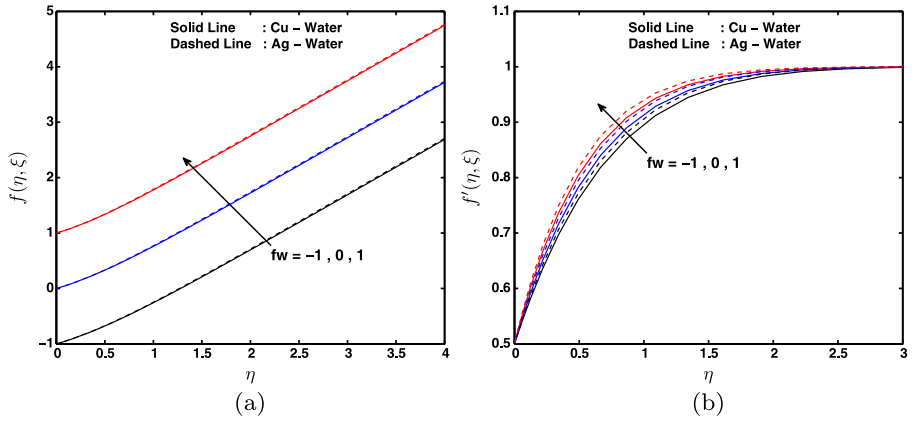

Figure 8 Effect of suction/injection on velocity profiles when $D_f = 0.01$, $\phi = 0.2$, $Gr_t = 0.01$, $Gr_c = 0.01$, $Pr = 7$, $Ha = 2$, $\delta = 0.2$, $Sc = 1$, $Sr = 1$, $\lambda = 0.5$, $\gamma = 3$ and $\xi = 0.5$.

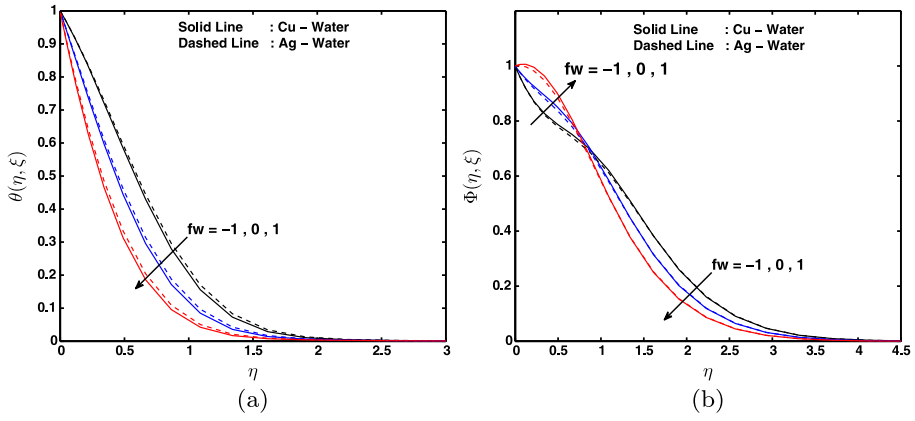

Figure 9 Effect of suction/injection on (a) temperature profiles and (b) concentration profiles for $D_f = 0.01$, $\phi = 0.2$, $Gr_t = 0.01$, $Gr_c = 0.01$, $Pr = 7$, $Ha = 2$, $\delta = 0.2$, $Sc = 1$, $Sr = 1$, $\lambda = 0.5$, $\gamma = 3$ and $\xi = 0.5$.

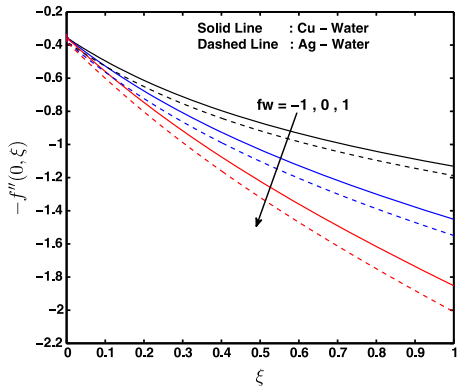

Figure 10 Effect of the suction/injection parameter on the skin friction coefficient for $D_f = 0.01$, $\phi = 0.2$, $Gr_t = 0.01$, $Gr_c = 0.01$, $Pr = 7$, $Ha = 2$, $\delta = 0.2$, $Sc = 1$, $Sr = 1$, $\lambda = 0.5$ and $\gamma = 3$.

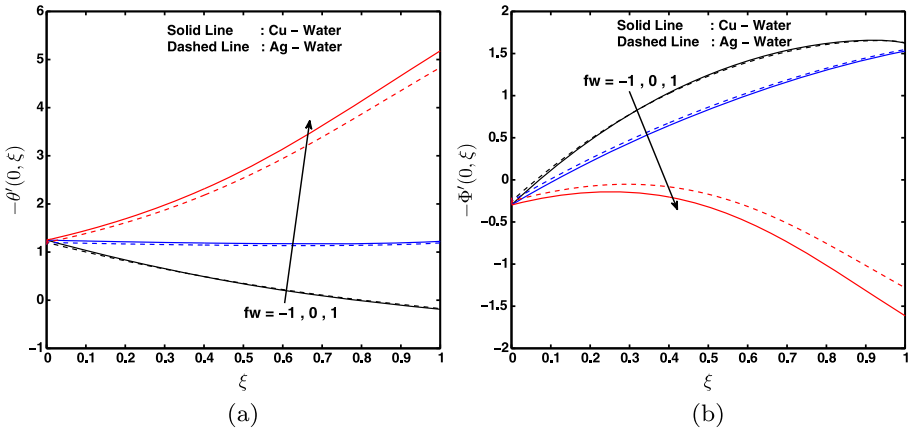

Figure 11 Effect of the suction/injection parameter on (a) the heat transfer coefficient and (b) the mass transfer coefficient when $D_f = 0.01$, $\phi = 0.2$, $Gr_t = 0.01$, $Gr_c = 0.01$, $Pr = 7$, $Ha = 2$, $\delta = 0.2$, $Sc = 1$, $Sr = 1$, $\lambda = 0.5$ and $\gamma = 3$.

ary layer thickness increases with increase of the injection parameter as injection allows the fluid to enter the system. The thermal boundary layer thickness decreases due to injection, while it increases with suction. The effect of the suction/injection parameter is to increase the concentration profile at the surface. Beyond this critical value, the concentration profile decreases with increasing suction/injection. The solute concentration boundary layer thickness is larger for the case of a Cu-water nanofluid than that for the case of an Ag-water nanofluid (see Figure 9). The skin friction coefficient decreases with increasing the values of ξ. It is obvious that the skin friction for the case of an Ag-water nanofluid is relatively less than that for the case of a Cu-water nanofluid (see Figure 10).

The axial distributions of the wall heat and mass transfer rates are shown in Figure 11(a) and (b), respectively. The wall heat transfer rate increased with ξ, and we observe that the heat transfer rate is higher for a Cu-water nanofluid than for an Ag-water nanofluid. It is interesting to note that with suction ($f_w = -1$), the heat transfer rate is less for an Ag-water nanofluid than for a Cu-water nanofluid up to a certain value of ξ. Beyond this point, the heat transfer rate is higher for an Ag-water nanofluid as compared to a Cu-water nanofluid, while the wall mass transfer rate increases monotonically with ξ to a maximum values before reducing. It is shown that the mass transfer rate is higher for a Cu-water nanofluid

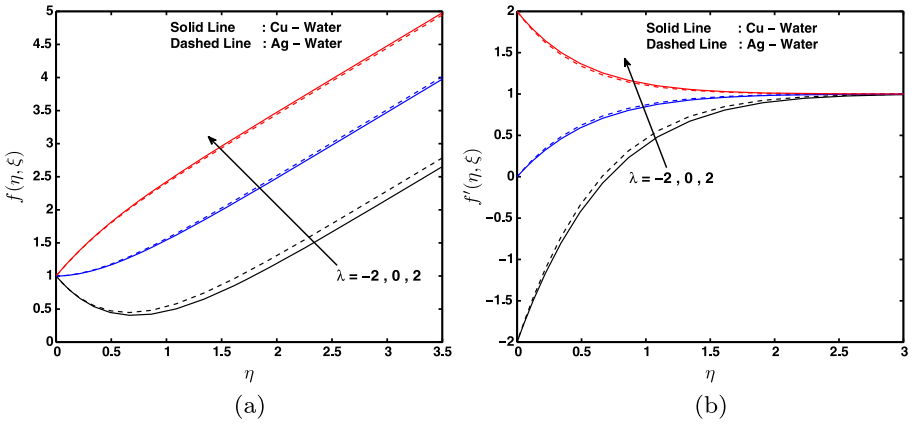

Figure 12 Effect of stretching/shrinking parameter values λ on velocity profiles for $D_f = 0.01$, $\phi = 0.2$, $Gr_t = 0.01$, $Gr_c = 0.01$, $Pr = 7$, $Ha = 2$, $\delta = 0.1$, $Sc = 1$, $Sr = 1$, $f_w = 1$, $\gamma = 0.1$ and $\xi = 0.5$.

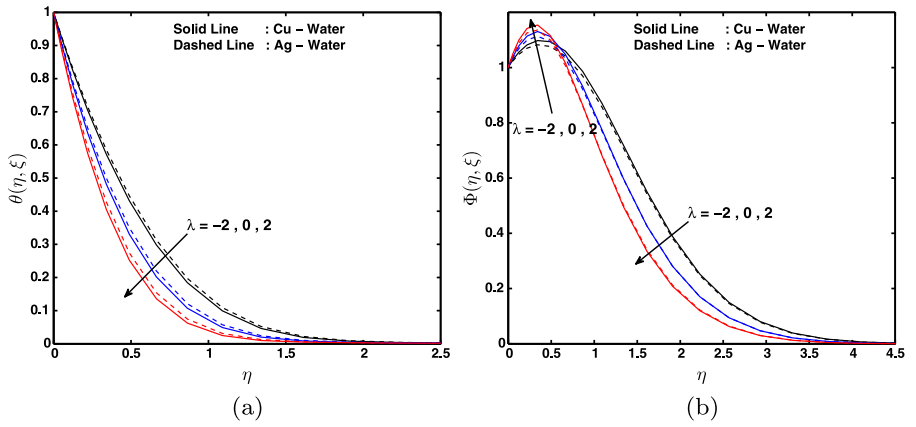

Figure 13 Effect of various stretching/shrinking parameter values λ on (a) temperature profiles and (b) concentration profiles for $D_f = 0.01$, $\phi = 0.2$, $Gr_t = 0.01$, $Gr_c = 0.01$, $Pr = 7$, $Ha = 2$, $\delta = 0.1$, $Sc = 1$, $Sr = 1$, $f_w = 1$, $\gamma = 0.1$ and $\xi = 0.5$.

than for an Ag-water nanofluid. The opposite behavior is observed in the case of suction when $f_w = -1$. The mass transfer rate for an Ag-water nanofluid is higher than that for a Cu-water nanofluid up to a certain value of ξ, and beyond this critical value, the mass transfer in an Ag-water nanofluid is less than that in a Cu-water nanofluid, Figure 11(b).

The influence of stretching/shrinking on velocity, temperature, solutal concentration profiles, the skin friction coefficient, wall heat and mass transfer rates are shown in Figures 12-15. Figure 12 shows that the momentum boundary layer thickness increases with the stretching/shrinking rate. This may be attributed to the fact than an increase in the stretching parameter enhances the velocity of the nanofluid which in turn enhances the momentum boundary layer thickness.

Figure 13 shows that the thermal and concentration boundary layer thicknesses decrease as the stretching rate increases. For the shrinking case, when $\lambda = -2$, the momentum boundary layer for an Ag-water nanofluid is greater than that for a Cu-water nanofluid, while the opposite is observed for the stretching case when $\lambda = 2$. The Ag-water nanofluid

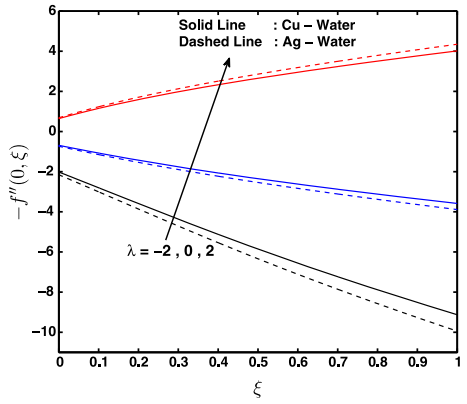

Figure 14 Effect of stretching/shrinking parameter values λ on the skin friction coefficient for $D_f = 0.01$, $\phi = 0.2$, $Gr_t = 0.01$, $Gr_c = 0.01$, $Pr = 7$, $Ha = 2$, $\delta = 0.1$, $Sc = 1$, $Sr = 1$, $f_w = 1$ and $\gamma = 0.1$.

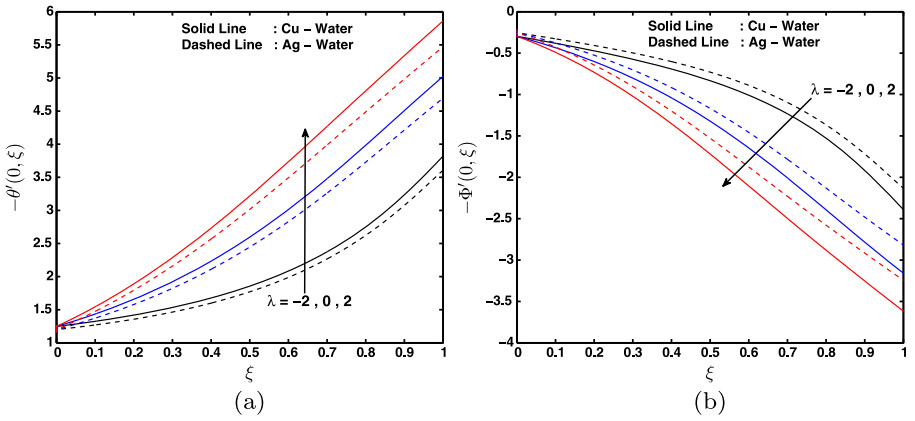

Figure 15 Effect of various stretching/shrinking parameter values λ on (a) the heat transfer coefficient and (b) the mass transfer coefficient for $D_f = 0.01$, $\phi = 0.2$, $Gr_t = 0.01$, $Gr_c = 0.01$, $Pr = 7$, $Ha = 2$, $\delta = 0.1$, $Sc = 1$, $Sr = 1$, $f_w = 1$ and $\gamma = 0.1$.

thermal boundary is higher than that of a Cu-water nanofluid (see Figure 13(a)). The solutal concentration increases up to a critical η, and beyond this critical value the concentration profile decreases (see Figure 13(b)). We observe that solute concentration profiles are larger for the case of a Cu-water than those for the case of an Ag-water nanofluid for the shrinking sheet with $\lambda = -2$, while the opposite is true for the stretching sheet with $\lambda = 2$.

Figure 14 shows the effect of stretching/shrinking on the shear stress, while Figure 15 shows the effect of the stretching rate on the wall heat and mass transfer rates. From Figure 14 we note that the shear stress increases with the stretching/shrinking parameter. The shear stress decreases with ξ. Figure 15(a) shows that the heat transfer rate increases with increasing λ. The mass transfer at the wall decreases with the increase in λ. The heat transfer rate is larger for the case of an Ag-water nanofluid compared to that of a Cu-water nanofluid, while the opposite is true for the mass transfer rate (see Figure 15).

6 Conclusions

We have investigated heat and mass transfer in unsteady MHD mixed convection in a nanofluid due to a stretching/shrinking sheet with heat generation and viscous dissipation. Other parameters of interest in this study included the Soret and Dufour effects. In this

paper we considered Cu-water and Ag-water nanofluids and assumed that the nanoparticle volume fraction can be actively controlled at the boundary surface. We have solved the model equations using the spectral relaxation method, and to benchmark our solutions, we compared our results with some limiting cases from the literature. These results were found to be in good agreement.

The numerical simulations show, *inter alia*, that the skin friction factor increases with both an increase in the nanoparticle volume fraction and the stretching rate and that an increase in the nanoparticle volume fraction leads to a reduction in the wall mass transfer rate.

Abbreviations

a: a positive constant; B_0: magnetic field; C_∞: ambient concentration; C_{fx}: skin friction coefficient; C: solutal concentration; C_w: surface concentration; C_s: concentration susceptibility; D_m: concentration mass diffusivity; D_f: Dufour number; f: dimensionless stream function; g: acceleration due to gravity; Gr_c: solutal Grashof number; Gr_t: thermal Grashof number; Ha: Hartmann number; k_f: fluid thermal conductivity; k_s: solid volume fraction; k_{nf}: nanofluid thermal conductivity; K_T: thermal diffusion ratio; Nu_x: local Nusselt number; p: fluid pressure; Pr: Prandtl number; q_w: wall heat flux; q_m: wall mass flux; Q: volumetric rate of heat generation; R: chemical reaction parameter; Re_x: local Reynolds number; Sc: Schmidt number; Sh_x: local Sherwood number; Sr: Soret number; t: time; T: fluid temperature; T_m: mean fluid temperature; T_w: wall temperature; T_∞: ambient temperature; u, v: fluid velocity components; v_w: suction velocity.
Greek symbols: α_{nf}: nanofluid thermal diffusivity; β_C: volumetric solutal expansion coefficient; β_T: volumetric thermal expansion coefficient; δ: heat generation parameter; μ_f: base fluid dynamic viscosity; μ_{nf}: nanofluid effective dynamic viscosity; ν_{nf}: nanofluid kinematic viscosity; ρ_f: density of the base fluid; ρ_{nf}: nanofluid density; ρ_s: density of the solid fractions; σ: electrical conductivity; τ_w: wall shear stress; ϕ: nanoparticle solid volume fraction; ψ: stream function.

Competing interests

The authors declare that they have no competing interests.

Authors' contributions

All the authors participated in the design of this study and helped to draft and proofread the manuscript. NAHH produced the initial draft.

Acknowledgements

The authors wish to thank the University of KwaZulu-Natal for financial support.

Received: 24 September 2014 Accepted: 15 January 2015 Published online: 31 January 2015

References

1. Kuznetsov, AV, Nield, DA: Natural convective boundary layer flow of a nanofluid past a vertical plate. Int. J. Therm. Sci. **49**, 243-247 (2010)
2. Ishak, A, Nazar, R, Pop, I: Hydromagnetic flow and heat transfer adjacent to a stretching vertical sheet. Heat Mass Transf. **44**, 921-927 (2008)
3. Mahapatra, TR, Mondal, S, Pal, D: Heat transfer due to magnetohydrodynamic stagnation-point flow of a power-law fluid towards a stretching surface in the presence of thermal radiation and suction/injection. ISRN Thermodyn. **9**, 1-9 (2012)
4. Das, SK, Choi, SUS, Yu, W, Pradeep, T: Nanofluids: Science and Technology. Wiley, New York (2007)
5. Crane, LJ: Flow past a stretching plate. Z. Angew. Math. Phys. **21**, 645-647 (1970)
6. Khan, WA, Pop, I: Boundary layer flow of a nanofluid past a stretching sheet. Int. J. Heat Mass Transf. **53**, 2477-2483 (2010)
7. Chen, C-H: Laminar mixed convection adjacent to vertical, continuously stretching sheets. Heat Mass Transf. **33**, 471-476 (1988)
8. Abo-Eldahab, EM, Abd El-Aziz, M: Blowing/suction effect on hydromagnetic heat transfer by mixed convection from an inclined continuously stretching surface with internal heat generation/absorption. Int. J. Therm. Sci. **43**, 709-719 (2004)
9. Abd El-Aziz, M: Thermal-diffusion and diffusion-thermo effects on combined heat and mass transfer by hydromagnetic three-dimensional free convection over a permeable stretching surface with radiation. Phys. Lett. **372**(3), 263-272 (2007)
10. Hady, FM, Ibrahim, FS, Abdel-Gaied, SM, Eid, MR: Radiation effect on viscous flow of a nanofluid and heat transfer over a nonlinearly stretching sheet. Nanoscale Res. Lett. **7**, 229 (2012)
11. Bachok, N, Ishak, A, Pop, I: Unsteady boundary-layer flow and heat transfer of a nanofluid over a permeable stretching/shrinking sheet. Int. J. Heat Mass Transf. **55**, 2102-2109 (2012)
12. Rohni, AM, Ahmad, S, Ismail, AIM, Pop, I: Flow and heat transfer over an unsteady shrinking sheet with suction in a nanofluid using Buongiorno's model. Int. Commun. Heat Mass Transf. **43**, 75-80 (2013)
13. Buongiorno, J: Convective transport in nanofluids. J. Heat Transf. **128**, 240-250 (2006)
14. Pavlov, KB: Magnetohydromagnetic flow of an incompressible viscous fluid caused by deformation of a surface. Magn. Gidrodin. **4**, 146-147 (1974)

15. Jafar, K, Nazar, R, Ishak, A, Pop, I: MHD flow and heat transfer over stretching/shrinking sheets with external magnetic field, viscous dissipation and Joule effects. Can. J. Chem. Eng. **99**, 1-11 (2011)
16. Chamka, AJ: MHD flow of a uniformly stretched vertical permeable surface in the presence of heat generation/absorption and a chemical reaction. Int. Commun. Heat Mass Transf. **30**, 413-422 (2003)
17. Kandasamy, R, Palanimani, PG: Effects of chemical reactions, heat, and mass transfer on nonlinear magnetohydrodynamic boundary layer flow over a wedge with a porous medium in the presence of ohmic heating and viscous dissipation. J. Porous Media **10**, 489-502 (2007)
18. Rashidi, MM, Erfani, E: Analytical method for solving steady MHD convective and slip flow due to a rotating disk with viscous dissipation and Ohmic heating. Eng. Comput. **29**, 562-579 (2012)
19. Rashidi, MM, Momoniat, E, Rostami, B: Analytic approximate solutions for MHD boundary-layer viscoelastic fluid flow over continuously moving stretching surface by homotopy analysis method with two auxiliary parameters. J. Appl. Math. **2012**, Article ID 780415 (2012)
20. Rashidi, MM, Keimanesh, M: Using differential transform method and Padé approximant for solving MHD flow in a laminar liquid film from a horizontal stretching surface. Math. Probl. Eng. **2010**, Article ID 491319 (2010)
21. Anjali-Devi, SP, Thiyagarajan, M: Steady nonlinear hydromagnetic flow and heat transfer over a stretching surface of variable temperature. Heat Mass Transf. **42**, 671-677 (2006)
22. Postelnicu, A: Influence of chemical reaction on heat and mass transfer by natural convection from vertical surfaces in porous media considering Soret and Dufour effects. Heat Mass Transf. **43**, 595-602 (2007)
23. Motsa, SS: A new spectral relaxation method for similarity variable nonlinear boundary layer flow systems. Chem. Eng. Commun. **201**, 241-256 (2014)
24. Motsa, SS, Dlamini, PG, Khumalo, M: Spectral relaxation method and spectral quasilinearization method for solving unsteady boundary layer flow problems. Adv. Math. Phys. **2014**, Article ID 341964 (2014). doi:10.1155/2014/341964
25. Motsa, SS, Makukula, ZG: On spectral relaxation method approach for steady von Karman flow of a Reiner-Rivlin fluid with Joule heating and viscous dissipation. Cent. Eur. J. Phys. **11**, 363-374 (2013)
26. Yang, KT: Unsteady laminar boundary layers in an incompressible stagnation flow. J. Appl. Mech. **25**, 421-427 (1958)
27. Brinkman, HC: The viscosity of concentrated suspensions and solution. J. Chem. Phys. **20**, 571-581 (1952)
28. Liao, SJ: An analytic solution of unsteady boundary layer flows caused by an impulsively stretching plate. Commun. Nonlinear Sci. Numer. Simul. **11**, 326-329 (2006)
29. Sheikholeslami, M, Bandpy, MG, Ganji, DD, Soleimani, S, Seyyedi, SM: Natural convection of nanofluids in an enclosure between a circular and a sinusoidal cylinder in the presence of magnetic field. Int. Commun. Heat Mass Transf. **39**, 1435-1443 (2012)
30. Oztop, HF, Abu-Nada, E: Numerical study of natural convection in partially heated rectangular enclosures filled with nanofluids. Int. J. Heat Fluid Flow **29**, 1326-1336 (2008)
31. Wang, CY: Stagnation flow towards a shrinking sheet. Int. J. Non-Linear Mech. **43**, 377-382 (2008)
32. Suali, M, Long, NMAN, Ishak, A: Unsteady stagnation point flow and heat transfer over a stretching/shrinking sheet with prescribed surface heat flux. Appl. Math. Comput. Intell. **1**, 1-11 (2012)

Chapter 3

Heat and mass transfer of nanofluid through an impulsively vertical stretching surface using the spectral relaxation method

In this chapter we investigate unsteady heat and mass transfer in nanofluid flow through an impulsively vertical stretching surface. The flow is subject to a heat source, a homogeneous chemical reaction, Brownian motion, and thermophoresis parameters which are assumed to be significant. The transformed non-similar partial differential equations are solved numerically using SRM and SQLM.

Haroun et al. *Boundary Value Problems* (2015) 2015:161
DOI 10.1186/s13661-015-0424-3

Boundary Value Problems
a SpringerOpen Journal

RESEARCH Open Access

Heat and mass transfer of nanofluid through an impulsively vertical stretching surface using the spectral relaxation method

Nageeb AH Haroun[1], Precious Sibanda[1], Sabyasachi Mondal[1*], Sandile S Motsa[1] and Mohammad M Rashidi[2]

*Correspondence:
sabya.mondal.2007@gmail.com
[1]School of Mathematics, Statistics and Computer Science, University of KwaZulu-Natal, Private Bag X01, Scottsville, Pietermaritzburg, 3209, South Africa
Full list of author information is available at the end of the article

Abstract

In this paper, we investigate heat and mass transfer in a magnetohydrodynamic nanofluid flow due to an impulsively started stretching surface. The flow is subject to a heat source, a chemical reaction, Brownian motion and thermophoretic parameters which are assumed to be significant. We have further assumed that the nanoparticle volume fraction at the wall may be actively controlled. The physical problem is modeled using systems of nonlinear differential equations which have been solved numerically using the spectral relaxation method. Comparing with previously published results by Khan and Pop (Int. J. Heat Mass Transf. 53:2477-2483, 2010) shows an excellent agreement. Some of the particular findings are that the skin friction coefficient decreases with an increase in the nanoparticle volume fraction, the heat transfer coefficient decreases with an increase in the nanoparticle volume fraction and that the mass transfer coefficient increases with an increase in the nanoparticle volume fraction.

Keywords: nanofluids; impulsively stretching surface; magnetohydrodynamic; chemical reaction parameter; spectral relaxation method

1 Introduction

The term nanofluid denotes a liquid in which nanoscale particles are suspended in a base fluid with low thermal conductivity such as water, oils and ethylene glycol. In recent years, the concept of nanofluid has been proposed as a route for increasing the performance of heat transfer liquids. Due to the increasing importance of nanofluids, there is now a large amount of literature on convective transport of nanofluids and problems linked to a stretching surface. Choi [1] initially pointed out that addition of these nanoparticles to the base fluid appreciably enhances the effective thermal conductivity of the fluid. An excellent collection of articles on this topic can be found in [2, 3] and Das *et al.* [4]. A non-homogenous equilibrium model proposed by Buongiorno [5] revealed that the massive increase in the thermal conductivity occurs due to the presence of two main effects; namely the Brownian diffusion and the thermophoretic diffusion of nanoparticles. The study of a steady boundary layer flow of a nanofluid towards a stretching sheet was reported by Khan and Pop [6]. Radiation effects on the viscous flow of a nanofluid and heat transfer over a nonlinearly stretching sheet were studied by Hady *et al.* [7]. Kuznetsov and Nield

[8] carried out a numerical investigation of mixed convection in the nanofluid flow over a vertical flat plate. In related work, Nield and Kuznetsov [9] studied the Cheng-Minkowycz problem for the natural convection in nanofluid flow over a flat plate. Yacob *et al.* [10] studied the stagnation point flow of a nanofluid flow due to a stretching/shrinking sheet using a shooting technique together with a fourth-fifth order Runge-Kutta method. Recently, results of MHD mixed convection in unsteady nanofluid flow due to a stretching/shrinking surface with suction/injection were reported by Haroun *et al.* [11]. In this study the model equations were solved using a spectral relaxation method. Stagnation point flow of a nanofluid with heat generation/absorption and suction/blowing was investigated by Hamad and Ferdows [12]. Rashidi and Erfani [13] used the modified differential transform method to investigate boundary layer flow due to stretching surfaces. Some excellent articles on the flow of nanofluids include those by Rashidi *et al.* [14], Anwar Bég *et al.* [15] and Garoosi *et al.* [16]. Some interesting results on discrete problems were presented by [17, 18].

Magnetohydrodynamic (MHD) flow and heat and mass transfer over a stretching surface have many important technological and industrial applications such as in micro MHD pumps, micro mixing of physiological samples, biological transportation and in drug delivery. An excellent collection of articles on this topic can be found in [19, 20]. The application of magnetic field produces a Lorentz force which assists in mixing processes as an active micromixing technology technique. Hence, transportation of conductive biological fluids in micro systems may greatly benefit from theoretical research in this area (see Yazdi *et al.* [21]). Studies on magneto-hydrodynamics (MHD) free convective boundary layer flow of nanofluids are very limited. More recently, Chamkha and Aly [22] studied magneto-hydrodynamics (MHD) free convective boundary layer flow of a nanofluid along a permeable isothermal vertical plate in the presence of heat generation or absorption effects. Matin *et al.* [23] studied magneto-hydrodynamics (MHD) mixed convective flow of nanofluid over a stretching sheet. Magneto-hydrodynamics (MHD) forced convective flow of nanofluid over a horizontal stretching flat plate with variable magnetic field including the viscous dissipation was investigated by Nourazar *et al.* [24]. The effect of a transverse magnetic field on the flow and heat transfer over a stretching surface was examined by Anjali Devi and Thiyagarajan [25].

Despite all the previous work, there is still a lot that is unknown about the flow and heat and mass transfer properties of different nanofluids. For instance, the composition and make of nanoparticles may have an impact on the performance of nanofluid as a heat transfer medium. The aim of the present study is to analyze the effects of Brownian motion parameter and thermophoresis parameter on unsteady boundary layer flow heat and mass transfer of a nanofluid flow past an impulsively stretching surface in the presence of a chemical reaction and an applied magnetic field. The model equations are solved using the spectral relaxation method (SRM) that was recently proposed by Motsa [26]. The spectral relaxation method promises fast convergence with good accuracy, has been successfully used in a limited number of boundary layer flow, heat and mass transfer studies (see [27, 28]). A comparative study for a special case is presented, which shows good agreement with Khan and Pop [6].

2 Governing equations

Consider the two-dimensional unsteady boundary layer flow heat and mass transfer in a nanofluid past an impulsively stretching vertical surface situated at $y = 0$ with stretching

velocity $u(x) = ax$, where a is a constant. The temperature and nanoparticle concentration at the stretching surface are T_w and C_w, respectively, and those of the ambient nanofluid are T_∞ and C_∞, respectively. The x and y directions are taken along and perpendicular to the sheet, respectively. Here we focus mainly in the region $x, y \geq 0$. The Boussinesq approximation is applied here. The continuity, momentum, energy and concentration equations of an unsteady, incompressible nanofluid boundary layer flow are as follows (see Kuznetsov and Nield [8]):

$$\frac{\partial u}{\partial x} + \frac{\partial v}{\partial y} = 0, \tag{1}$$

$$\frac{\partial u}{\partial t} + u\frac{\partial u}{\partial x} + v\frac{\partial u}{\partial y} = \frac{\mu_{nf}}{\rho_{nf}}\frac{\partial^2 u}{\partial y^2} + g\beta_T(T - T_\infty) + g\beta_C(C - C_\infty) - \frac{\sigma B_0^2}{\rho_{nf}}u, \tag{2}$$

$$\frac{\partial T}{\partial t} + u\frac{\partial T}{\partial x} + v\frac{\partial T}{\partial y} = \alpha_{nf}\frac{\partial^2 T}{\partial y^2} + \tau^*\left[D_B\frac{\partial C}{\partial y}\frac{\partial T}{\partial y} + \frac{D_T}{T_\infty}\left(\frac{\partial T}{\partial y}\right)^2\right], \tag{3}$$

$$\frac{\partial C}{\partial t} + u\frac{\partial C}{\partial x} + v\frac{\partial C}{\partial y} = D_B\frac{\partial^2 C}{\partial y^2} + \frac{D_T}{T_\infty}\frac{\partial^2 T}{\partial y^2} - K(C - C_\infty), \tag{4}$$

where u and v are the fluid velocity and normal velocity components along x- and y-directions, respectively; μ_{nf}, ρ_{nf}, σ, B_0, g are the effective dynamic viscosity of the nanofluid, nanofluid density, electrical conductivity, the uniform magnetic field in the y-direction and gravitational acceleration; β_T, β_C, T, C, α_{nf}, τ^* $(= (\rho c)_p/(\rho c)_f)$ are the volumetric thermal expansion coefficient, volumetric solutal expansion coefficient, temperature of fluid in the boundary layer, fluid solutal concentration, the thermal diffusivity of the nanofluid, the ratio of effective heat capacity of the nanoparticle material to heat capacity of the fluid; D_B, D_T, T_∞, K are the Brownian motion coefficient, the thermophoretic diffusion coefficient, mean fluid temperature and the chemical reaction parameter.

The boundary conditions are

$$\begin{aligned} t \geq 0:\quad & u = U_w(x) = ax, \qquad v = 0, \qquad T = T_w, \qquad C = C_w \quad \text{at } y = 0, \\ & T_w(x) = T_\infty + T_0 x, \qquad C_w(x) = C_\infty + C_0 x, \\ t \geq 0:\quad & u, v \to 0, \qquad T \to T_\infty, \qquad C \to C_\infty \quad \text{as } y \to \infty, \end{aligned} \tag{5}$$

and the initial conditions are

$$\begin{aligned} t < 0:\quad & u(x, y, t) = 0, \qquad v(x, y, t) = 0, \\ & T(x, y, t) = T_\infty, \qquad C(x, y, t) = C_\infty, \quad \forall x, y, \end{aligned} \tag{6}$$

where a is the stretching/shrinking rate and stagnation flow rate parameters, with $a < 0$ for shrinking, $a > 0$ for stretching.

The effective dynamic viscosity of the nanofluid was given by Brinkman [29] as

$$\mu_{nf} = \frac{\mu_f}{(1 - \phi)^{2.5}}, \tag{7}$$

where ϕ and μ_f are the solid volume fraction of nanoparticles and the dynamic viscosity of the base fluid.

In equations (1) to (4), the quantities $(\rho c_p)_{nf}$, ρ_{nf} and α_{nf} are given by

$$\begin{aligned}
&(\rho c_p)_{nf} = (1-\phi)(\rho c_p)_f + \phi(\rho c_p)_s,\\
&\rho_{nf} = (1-\phi)\rho_f + \phi\rho_s, \qquad \nu_{nf} = \frac{\mu_{nf}}{\rho_{nf}},\\
&\alpha_{nf} = \frac{k_{nf}}{(\rho c_p)_{nf}}, \qquad \frac{k_{nf}}{k_f} = \frac{(k_s+k_f)-2\phi(k_f-k_s)}{(k_s+k_f)+\phi(k_f-k_s)},
\end{aligned} \tag{8}$$

where ν_{nf}, ρ_{nf}, $(\rho cp)_{nf}$, k_{nf}, k_f, k_s, ρ_s, $(\rho c_p)_f$, $(\rho c_p)_s$ are the nanofluid kinematic viscosity, the electrical conductivity, the nanofluid heat capacitance, thermal conductivity of the nanofluid, thermal conductivity of the fluid, the thermal conductivity of the solid fractions, the density of the solid fractions, the heat capacity of the base fluid, the effective heat capacity of nanoparticles, respectively (see Abu-Nada [30]).

The continuity equation (1) is satisfied by introducing a stream function $\psi(x,y)$ such that

$$u = \frac{\partial\psi}{\partial y}, \qquad \nu = -\frac{\partial\psi}{\partial x}. \tag{9}$$

Introducing the following non-dimensional variables (see Liao [31]):

$$\begin{aligned}
&\psi = [a\nu_f\xi]^{\frac{1}{2}} x f(\xi,\eta), \quad \xi = 1-\exp(-\tau), \tau = at, \eta = \left[\frac{a}{\nu_f\xi}\right]^{\frac{1}{2}} y,\\
&\theta(\xi,\eta) = \frac{T-T_\infty}{T_w-T_\infty}, \qquad \Phi(\xi,\eta) = \frac{C-C_\infty}{C_w-C_\infty},
\end{aligned} \tag{10}$$

where η, ξ and τ are dimensionless variables and the dimensionless time, $f(\xi,\eta)$ is the dimensionless stream function, $\theta(\xi,\eta)$ is the dimensionless temperature and $\phi(\xi,\eta)$ is the dimensionless solute concentration. By using (10) the governing equations (2) to (4) along with the boundary conditions (5) are reduced to the following two-point boundary value problem:

$$\begin{aligned}
&f''' + \phi_1\left[(1-\xi)\frac{1}{2}\eta f'' + \xi\left(ff''' - f'^2 - Ha^2 f' + Gr_t\theta + Gr_c\phi\right)\right]\\
&\quad = \phi_1\xi(1-\xi)\frac{\partial f'}{\partial\xi},
\end{aligned} \tag{11}$$

$$\begin{aligned}
&\theta'' + \phi_2 Pr\left(\frac{k_f}{k_{nf}}\right)\left[(1-\xi)\frac{1}{2}\eta\theta' + \xi f\theta' + N_b\theta'\phi' + N_T\theta' 2\right]\\
&\quad = \phi_2 Pr\left(\frac{k_f}{k_{nf}}\right)(1-\xi)\frac{\partial\theta}{\partial\xi},
\end{aligned} \tag{12}$$

$$\phi'' + Sc\left[(1-\xi)\frac{1}{2}\eta\phi' + \xi f\phi'\right] + \frac{N_T}{N_b}\theta'' - \gamma\xi Sc\phi = Sc\xi(1-\xi)\frac{\partial\phi}{\partial\xi}, \tag{13}$$

subject to the boundary conditions

$$f(\xi,0) = 0, \qquad f'(\xi,0) = 1, \qquad \theta(\xi,0) = 1, \qquad \Phi(\xi,0) = 1, \quad \eta = 0, \xi \geq 0, \tag{14}$$

$$f'(\xi,\infty) = 0, \qquad \theta(\xi,\infty) = 0, \qquad \Phi(\xi,\infty) = 0, \quad \eta\to\infty, \xi \geq 0, \tag{15}$$

where the prime denotes differentiation with respect to η, $\alpha_f = k_f/(\rho c_p)_f$ and $\nu_f = \mu_f/\rho_f$ are the thermal diffusivity and kinetic viscosity of the base fluid, respectively. Other non-dimensional parameters appearing in equations (11) to (13) Ha, Gr_t, Gr_c, Pr, N_b, N_T, Sc, and γ denote the Hartman number, the local temperature Grashof number and the local concentration Grashof number (see Mahdy [32] and Hsiao [33]), the Prandtl number, Brownian motion parameter and thermophoresis parameter (see Khan and Pop [6], Nadeem and Saleem [34]), the Schmidt number and scaled chemical reaction parameter. These parameters are defined mathematically as

$$\begin{aligned} &Ha^2 = \frac{\sigma B_0^2}{a\rho_{nf}}, \qquad Gr_t = \frac{g\beta_T(T_w - T_\infty)}{a^2 x}, \\ &Gr_c = \frac{g\beta_C(C_w - C_\infty)}{a^2 x}, \qquad Pr = \frac{\nu_f}{\alpha_f}, \\ &N_b = \frac{(\rho_c)_p D_B(C_w - C_\infty)}{\nu_f(\rho_p)_f}, \qquad Sc = \frac{\nu_f}{D_B}, \\ &\gamma = \frac{K}{a}, \qquad N_T = \frac{(\rho_c)_p D_T(T_w - T_\infty)}{T_\infty \nu_f(\rho_p)_f}. \end{aligned} \tag{16}$$

The nanoparticle volume fraction parameters ϕ_1 and ϕ_2 are defined as

$$\phi_1 = (1-\phi)^{2.5}\left[1 - \phi + \phi\left(\frac{\rho_s}{\rho_f}\right)\right], \qquad \phi_2 = \left[1 - \phi + \phi\frac{(\rho c)_s}{(\rho c)_f}\right]. \tag{17}$$

2.1 Skin friction, heat and mass transfer coefficients

The skin friction coefficient C_f, the local Nusselt number Nu_x and the local Sherwood number Sh_x characterize the surface drag, wall heat and mass transfer rates, respectively.

The shearing stress at the surface of the wall τ_w is defined as

$$\tau_w = -\mu_{nf}\left(\frac{\partial u}{\partial y}\right)_{y=0} = -\frac{U_w\mu_f}{(1-\phi)^{2.5}x}\sqrt{\frac{U_w x}{\nu_f \xi}}f''(0,\xi), \tag{18}$$

where μ_{nf} is the coefficient of viscosity.

The skin friction coefficient is obtained as

$$C_{fx} = \frac{2\tau_w}{\rho_f U_w^2}, \tag{19}$$

and using equation (18) in (19) we obtain

$$\frac{1}{2}(1-\phi)^{2.5}C_{fx} = -\xi^{-\frac{1}{2}}Re_x^{-\frac{1}{2}}f''(0,\xi). \tag{20}$$

The heat transfer rate at the surface flux at the wall is defined as

$$q_w = -k_{nf}\left(\frac{\partial T}{\partial y}\right)_{y=0} = -k_{nf}\frac{(T_w - T_\infty)}{x}\sqrt{\frac{U_w x}{\nu_f \xi}}\theta'(0,\xi), \tag{21}$$

where k_{nf} is the thermal conductivity of the nanofluid.

The local Nusselt number (heat transfer coefficient) is defined as

$$Nu_x = \frac{xq_w}{k_f(T_w - T_\infty)}. \tag{22}$$

Using equation (21) in equation (22), the dimensionless wall heat transfer rate is obtained as

$$\left(\frac{k_f}{k_{nf}}\right)Nu_x = -\xi^{-\frac{1}{2}} Re_x^{\frac{1}{2}} \theta'(0,\xi). \tag{23}$$

The mass flux at the wall surface is defined as

$$q_m = -D\left(\frac{\partial C}{\partial y}\right)_{y=0} = -D\frac{(C_w - C_\infty)}{x}\sqrt{\frac{U_w x}{\nu_f \xi}}\Phi'(0,\xi), \tag{24}$$

and the local Sherwood number (mass transfer coefficient) is obtained as

$$Sh_x = \frac{xq_m}{D(C_w - C_\infty)}. \tag{25}$$

The dimensionless wall mass transfer rate is obtained as

$$Sh_x = -\xi^{-\frac{1}{2}} Re_x^{\frac{1}{2}} \Phi'(0,\xi), \tag{26}$$

where Re_x represents the local Reynolds number and is defined as

$$Re_x = \frac{xu_\infty}{\nu_f}. \tag{27}$$

3 Cases of special interest

In this section some particular cases of equations (11) to (13) where the equations are reduced to ordinary differential equations are considered.

Case (1): *initial steady-state flow*. For steady flow when $\phi = 0$ (regular fluid), we have $\xi = 0$ corresponding to $t = 0$, thus $f(\eta,0) = f(\eta)$, $\theta(\eta,0) = \theta(\eta)$ and $\Phi(\eta,0) = \Phi(\eta)$. In this case equations (11) to (13) reduce to

$$f''' + \frac{1}{2}\phi_1 \eta f'' = 0, \tag{28}$$

$$\theta'' + \frac{1}{2}\frac{k_f}{k_{nf}} Pr\phi_2 \eta\theta' + \phi_2 \frac{k_f}{k_{nf}} PrN_b\theta'\phi' + \phi_2 \frac{k_f}{k_{nf}} PrN_T\theta' 2 = 0, \tag{29}$$

$$\phi'' + \frac{1}{2} Sc\eta\phi' + \frac{N_T}{N_b}\theta'' = 0, \tag{30}$$

subject to the boundary conditions

$$\begin{aligned} &f(0) = 0, \qquad f'(0) = 1, \qquad \theta(0) = 1, \qquad \Phi(0) = 1, \\ &f'(\infty) = 0, \qquad \theta(\infty) = 0, \qquad \Phi(\infty) = 0, \end{aligned} \tag{31}$$

where prime denotes differentiation with respect to η. Equation (28) subject to the boundary conditions (31) admits the exact solution (see Liao [31])

$$f(\eta) = \eta\left(1 - \operatorname{erf}\left(\frac{\eta}{2}\right)\right) + \frac{2}{\sqrt{\pi}}\left(1 - \exp^{(-\eta^2/4)}\right), \tag{32}$$

where $\operatorname{erf}(\nu)$ is the error function defined as

$$\operatorname{erf}(\nu) = \frac{2}{\sqrt{\pi}} \int_0^{\nu} e^{-z^2}\, dz. \tag{33}$$

Case (2): *final steady-state flow*. In this case, we have $\xi = 1$ ($t \to \infty$), corresponding to $f(\eta,1) = f(\eta)$, $\theta(\eta,1) = \theta(\eta)$ and $\phi(\eta,1) = \phi(\eta)$.

Equations (11) to (13) reduce to the following forms:

$$f''' + ff'' - f'^2 + 1 - Ha^2 f' + Gr_t\theta + Gr_c\phi = 0, \tag{34}$$

$$\theta'' + \frac{k_f}{k_{nf}} Pr\phi_2\left(f\theta' + N_b\theta'\phi'\right) + \frac{k_f}{k_{nf}} PrN_T\theta'^2 = 0, \tag{35}$$

$$\phi'' + Sc\left(f\phi' - \gamma\phi + \frac{N_T}{N_b}\theta''\right) = 0, \tag{36}$$

subject to the boundary conditions (31). Equations (11) to (13) were solved using the SRM, Motsa [26]. The SRM is an iterative procedure that employs the Gauss-Seidel type of relaxation approach to linearize and decouple the system of differential equations. Further details of the rules of the SRM can be found in [27, 28]. The linear terms in each equation are evaluated at the current iteration level (denoted by $r+1$) and nonlinear terms are assumed to be known from the previous iteration level (denoted by r). The linearized form of (11) to (13) is

$$f'''_{r+1} + a_{1,r} f''_{r+1} + a_{2,r} f'_{r+1} - \phi_1 \xi(1-\xi)\frac{\partial f'}{\partial \xi} = R_{1,r}, \tag{37}$$

$$\theta''_{r+1} + b_{1,r}\theta'_{r+1} - \frac{k_f}{k_{nf}} Pr\phi_2\xi(1-\xi)\frac{\partial \theta}{\partial \xi} = R_{2,r}, \tag{38}$$

$$\phi''_{r+1} + c_{r,1}\phi'_{r+1} + c_{2,r}\phi_{r+1} - Sc\xi(1-\xi)\frac{\partial \phi}{\partial \xi} = R_{3,r}, \tag{39}$$

where

$$a_{1,r} = \phi_1\left[\frac{\eta}{2}(1-\xi) + \xi f_r\right], \qquad a_{2,r} = -\phi_1\xi Ha^2,$$

$$R_{1,r} = -\phi_1\xi\left[Gr_t\theta_r + Gr_c\phi_r - f'^2_r\right],$$

$$b_{1,r} = \frac{k_f}{k_{nf}} Pr\phi_2\left[\frac{\eta}{2}(1-\xi) + \xi f_{r+1} + N_b\phi'_{r+1}\right], \qquad R_{2,r} = -\frac{k_f}{k_{nf}} Pr\phi_2\xi N_T\theta'^2_r,$$

$$c_{1,r} = \frac{\eta}{2}(1-\xi)Sc + Sc\xi f_{r+1}, \qquad c_{2,r} = -Sc\xi\gamma,$$

$$R_{3,r} = -\frac{N_T}{N_b}\theta''_{r+1}.$$

It must be noted that equations (37)-(39) are now linear and, being decoupled, can be solved sequentially to obtain approximate solutions for $f(\eta,\xi)$, $\theta(\eta,\xi)$ and $\phi(\eta,\xi)$. In this study, the Chebyshev spectral collocation method was used to discretize in η and finite differences with central differencing for derivatives was used to discretize in ξ. Starting from initial guesses for f, θ and ϕ, equations (37)-(39) were solved iteratively until the approximate solutions converged within a certain prescribed tolerance level. The accuracy of the results was validated against results from literature for some special cases of the governing equations.

4 Results and discussion

The nonlinear boundary value problem (11) to (13) subject to the boundary conditions (14) and (15) cannot be solved in closed form, so these equations are solved numerically using the spectral relaxation method (SRM) for Cu-water and Ag-water nanofluids for $0 \leq \xi \leq 1$. The thermophysical properties of the nanofluids used in the numerical simulations are given in Table 1. Extensive calculations have been performed to obtain the velocity, temperature, concentration profiles as well as skin friction, the local Nusselt number and the local Sherwood number for various values of physical parameters such as ϕ, Ha, Gr_t, Gr_c, Pr, N_b, N_T, Sc and γ.

To determine the accuracy of our numerical results, the heat and the mass transfer coefficients are compared with the published results of Khan and Pop [6] in Tables 2 and 3. Here, we have varied the N_T with N_b while keeping other physical parameters fixed. Ta-

Table 1 Thermophysical properties of the base fluid and the nanoparticles [35] and [36]

Physical properties	Base fluid (water)	Copper (Cu)	Silver (Ag)
C_p (J/kgK)	4,179	385	235
ρ (Kg/m^3)	997.1	8,933	10,500
k (W/mK)	0.613	401	429
$\alpha \times 10^7$ (m^2/s)	1.47	1,163.1	1,738.6
$\beta \times 10^5$ (K^{-1})	21	1.67	1.89

Table 2 Comparison of values of $-\theta'(0,\xi)$ for various values of N_T and N_b with $\phi = 0$ (regular fluid), $Ha = Gr_t = Gr_c = \gamma = 0$, $\xi = 1$, $Pr = 10$, $Sc = 10$

N_T	$N_b = 0.1$		$N_b = 0.2$		$N_b = 0.3$	
	[6]	Present results	[6]	Present results	[6]	Present results
0.1	0.9524	0.9519	0.5056	0.5052	0.2522	0.2522
0.2	0.6932	0.6930	0.3654	0.3662	0.1816	0.1841
0.3	0.5201	0.5219	0.2731	0.2760	0.1355	0.1394
0.4	0.4026	0.4040	0.2110	0.2117	0.1046	0.1044
0.5	0.3211	0.3185	0.1681	0.1639	0.0833	0.0779

Table 3 Comparison of values of $-\phi'(0,\xi)$ for various values of N_T and N_b with $\phi = 0$ (regular fluid), $Ha = Gr_t = Gr_c = \gamma = 0$, $\xi = 1$, $Pr = 10$, $Sc = 10$

N_T	$N_b = 0.1$		$N_b = 0.2$		$N_b = 0.3$	
	[6]	Present results	[6]	Present results	[6]	Present results
0.1	2.1294	2.1294	2.3819	2.3817	2.4100	2.4097
0.2	2.2740	2.2745	2.5152	2.5145	2.5150	2.5134
0.3	2.5286	2.5242	2.6555	2.6513	2.6088	2.6047
0.4	2.7952	2.7883	2.7818	2.7787	2.6876	2.6862
0.5	3.0351	3.0413	2.8883	2.8944	2.7519	2.7574

Table 4 Comparison of the SRM solutions for $f''(\xi,0)$, $-\theta'(\xi,0)$, and $-\phi'(\xi,0)$ against those of the SQLM at different values of ξ, $N_T = 0.1$, $N_b = 0.1$, $Pr = 7$, $Gr_t = 0.1$, $Gr_c = 0.1$, $Sc = 1$, $\phi = 0.2$, $\gamma = 2$, $Ha = 3$

ξ	$f''(\xi,0)$		$-\theta'(\xi,0)$		$-\phi'(\xi,0)$	
	SRM	SQLM	SRM	SQLM	SRM	SQLM
0.1	−1.024404	−1.024404	0.861024	0.861024	0.372386	0.372386
0.2	−1.062742	−1.062742	0.864900	0.864900	0.389380	0.389380
0.3	−1.088333	−1.088333	0.872739	0.872739	0.386305	0.386305
0.4	−1.108200	−1.108200	0.882753	0.882753	0.372517	0.372517
0.5	−1.124261	−1.124261	0.894651	0.894651	0.350129	0.350129
0.6	−1.136890	−1.136890	0.908632	0.908632	0.318838	0.318838
0.7	−1.145390	−1.145390	0.925350	0.925350	0.276272	0.276272
0.8	−1.146964	−1.146964	0.946411	0.946411	0.216141	0.216141
0.9	−1.127531	−1.127531	0.977047	0.977047	0.118365	0.118365
1.0	−4.252384	−4.252384	1.495226	1.495226	0.463421	0.463421

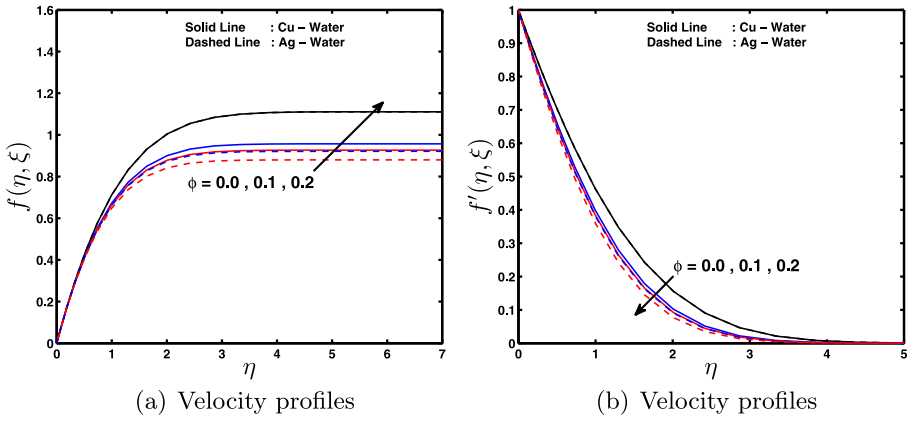

Figure 1 Effect of various nanoparticle values fraction ϕ on (a) and (b) for $Gr_t = 0.2$, $Ha = 0.2$, $Gr_c = 0.2$, $N_T = 0.01$, $Pr = 7$, $N_b = 0.01$, $\gamma = 1$, $Sc = 1$ and $\xi = 0.5$.

bles 2 and 3 give a comparison of the SRM results with those obtained by Khan and Pop [6] when $Ha = Gr_t = Gr_c = \gamma = \phi = 0$, $Pr = 10$, $Sc = 10$ and $\xi = 1$ for different values of the Brownian motion and thermophoresis parameters. It is observed that the present results are in good agreement with results in the literature. In Table 4, approximate solutions of the skin friction coefficient, surface heat transfer and surface mass transfer rates at different values of flow parameters are presented and compared with the SQLM solutions. Values of the skin friction coefficient, reduced Nusselt and Sherwood numbers at different values of ξ are presented in Table 4. The table also shows a comparison of the SHAM and SQLM results. As can be seen from the table, the results match perfectly well for the set accuracy level.

The effects of physical parameters on various fluid dynamic quantities are show in Figures 1-11.

Figures 1-4 illustrate the effect of the nanoparticle volume fraction ϕ on the velocity, temperature and concentration profiles, respectively, in the case of a Cu-water nanofluid. It is clear that as the nanoparticle volume fraction increases, the nanofluid velocity and the temperature profile increase while the opposite trend is observed for the concentration profile. Increasing the volume fraction of nanoparticles increases the thermal conductivity of the nanofluid, and we observe that thickening of the thermal boundary layer and the

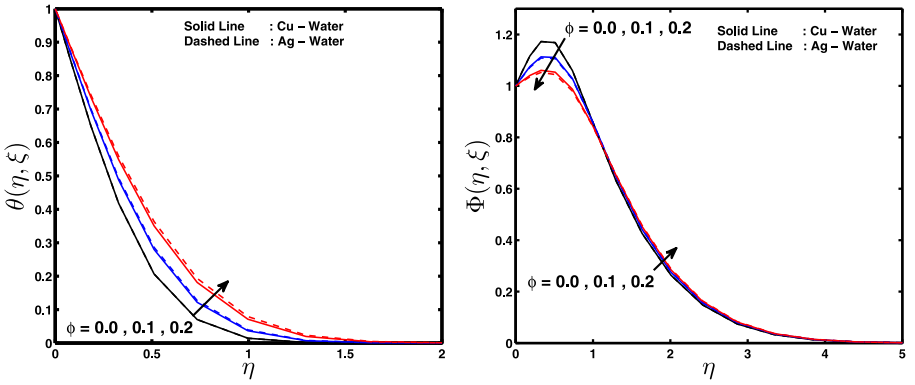

(a) Temperature profiles (b) Concentration profiles

Figure 2 Effect of various nanoparticle values fraction ϕ on (a) and (b) for $Gr_t = 0.2$, $Ha = 0.2$, $Gr_c = 0.2$, $N_T = 0.01$, $Pr = 7$, $N_b = 0.01$, $\gamma = 1$, $Sc = 1$ and $\xi = 0.5$.

Figure 3 Effect of various nanoparticle values fraction ϕ on skin friction coefficient for $Gr_t = 0.2$, $Ha = 0.2$, $Gr_c = 0.2$, $N_T = 0.01$, $Pr = 7$, $N_b = 0.01$, $\gamma = 1$ and $Sc = 1$.

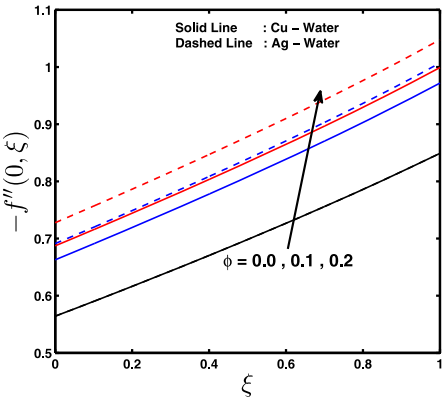

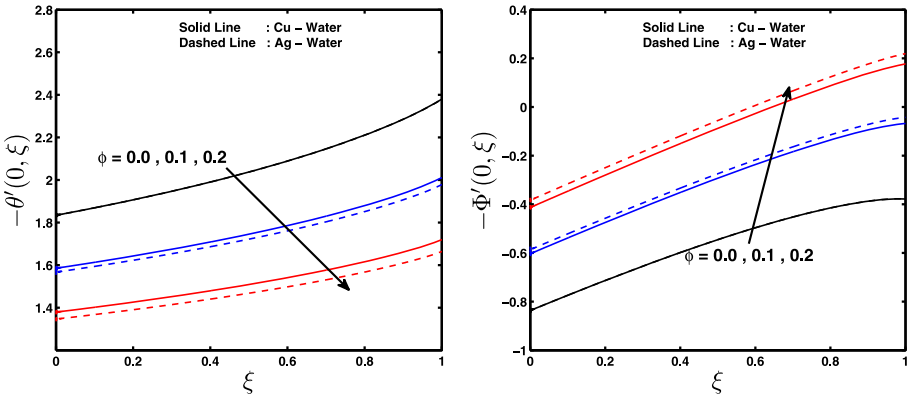

(a) Heat transfer coefficient (b) Mass transfer coefficient

Figure 4 Effect of various nanoparticle values fraction ϕ on (a) and (b) for $Gr_t = 0.2$, $Ha = 0.2$, $Gr_c = 0.2$, $N_T = 0.01$, $Pr = 7$, $N_b = 0.01$, $\gamma = 1$ and $Sc = 1$.

velocity in the case of an Ag-water nanofluid are relatively less than in the case of a Cu-water. We also note that since the conductivity of silver is higher than that of copper, the temperature distribution in the Ag-water nanofluid is higher than that in the Cu-water nanofluid. With increase in the nanoparticle volume fraction, the concentration boundary layer thickness increases for both types of nanofluids considered, and the opposite trend is observed when the concentration profile decreases.

Figure 3 shows that the skin friction coefficient $-f''(0,\xi)$ increases monotonically with increasing ξ. The result is true for both types of nanofluids. The minimum value of the skin friction in the case of the Cu-water nanofluid is achieved at a smaller value of ξ in comparison with the Ag-water nanofluid. Furthermore, in this paper it is found that the Ag-water nanofluid shows higher drag as compared to the Cu-water nanofluid. The dimensionless wall heat transfer rate and the dimensionless wall mass transfer rate are shown as functions of ξ in Figure 4(a) and (b), respectively. We observe that the wall heat transfer rate $-\theta'(0,\xi)$ decreases, while the opposite trend is observed in the case of the wall mass transfer rate $-\Phi'(0,\xi)$. The Cu-water nanofluid exhibits higher wall heat transfer rate as compared to the Ag-water nanofluid, while the opposite trend is observed for the wall mass transfer rate. The presence of nanoparticle tends to increase the wall heat transfer rate and to decrease the wall mass transfer rate with increasing the values of dimensionless variable ξ.

Figures 5-7 show the influence of the Hartman number on the velocity, temperature, skin friction coefficient $-f''(0,\xi)$, the local Nusselt number $-\theta'(0,\xi)$ and the local Sherwood number $-\Phi'(0,\xi)$. The effect of Hartman number *Ha* is to decrease the nanofluid velocity and the wall heat transfer coefficient, whereas it increases the skin friction coefficient and the wall mass transfer coefficient. A similar observation was made by Haroun *et al.* [11]. The momentum boundary layer thickness decreases with increase in the Hartman number. In the case of the Cu-water nanofluid it is relatively higher than that of the Ag-water nanofluid for nanofluid velocity. Figure 6 shows the skin friction coefficient as a function of ξ. It is clear that for the Cu-water nanofluid and the Ag-water nanofluid, the skin friction coefficient increases when ξ increases. We note that the Ag-water nanofluid exhibits higher drag to the flow as compared to the Cu-water nanofluid. Figure 7 shows the wall heat and mass transfer rates for different values of the Hartman number *Ha*, it is clear that the value of wall heat transfer rate decreases when ξ increases, in the case of

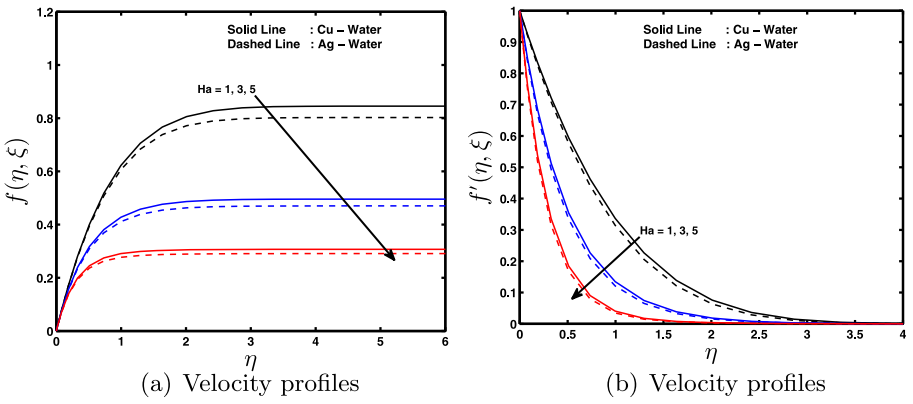

(a) Velocity profiles (b) Velocity profiles

Figure 5 Effect of various values of the Hartman number *Ha* on (a) and (b) for $Gr_t = 0.2$, $\phi = 0.2$, $Gr_c = 0.2$, $N_T = 0.01$, $Pr = 7$, $N_b = 0.01$, $\gamma = 1$, $Sc = 1$ and $\xi = 0.5$.

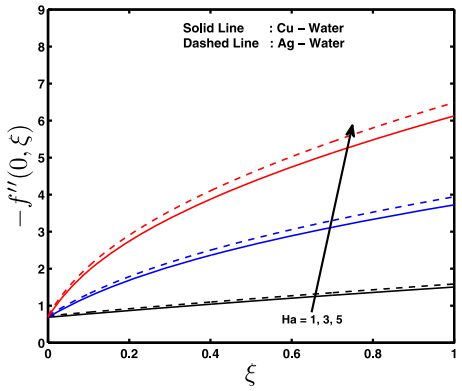

Figure 6 Effect of various values of the Hartman number *Ha* on skin friction coefficient for $Gr_t = 0.2$, $\phi = 0.2$, $Gr_c = 0.2$, $N_T = 0.01$, $Pr = 7$, $N_b = 0.01$, $\gamma = 1$ and $Sc = 1$.

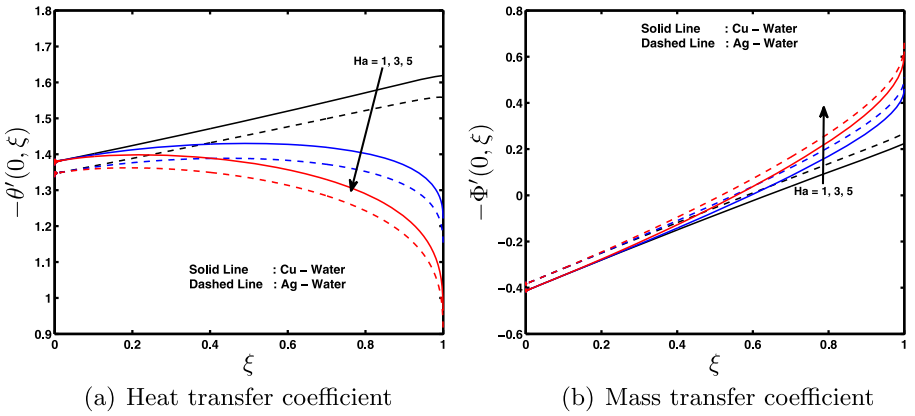

(a) Heat transfer coefficient (b) Mass transfer coefficient

Figure 7 Effect of various values of the Hartman number *Ha* on (a) and (b) for $Gr_t = 0.2$, $\phi = 0.2$, $Gr_c = 0.2$, $N_T = 0.01$, $Pr = 7$, $N_b = 0.01$, $\gamma = 1$ and $Sc = 1$.

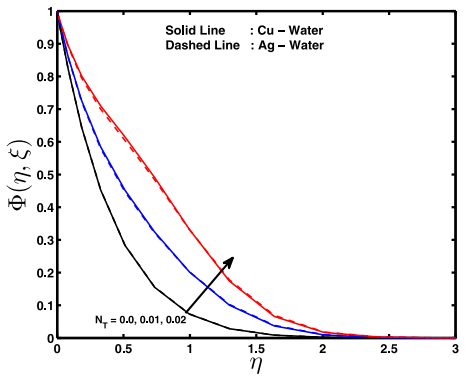

Figure 8 Effect of thermophoretic parameter N_T on concentration profiles for $Gr_t = 0.2$, $\phi = 0.2$, $Gr_c = 0.2$, $Ha = 2$, $Pr = 7$, $N_b = 0.01$, $\gamma = 4$, $Sc = 1$ and $\xi = 0.5$.

the Ag-water nanofluid it is less than that in the case of the Cu-water nanofluid. Further, the wall mass transfer rate increases when ξ increases, we observe that in the case of a Cu-water nanofluid it is less than that of an Ag-water nanofluid.

Figures 8 to 9 show the effect of the thermophoretic parameter N_T on the concentration profile, wall heat and mass transfer rates, respectively. In the case of a Cu-water nanofluid and an Ag-water nanofluid the concentration profile increases and the wall heat and mass

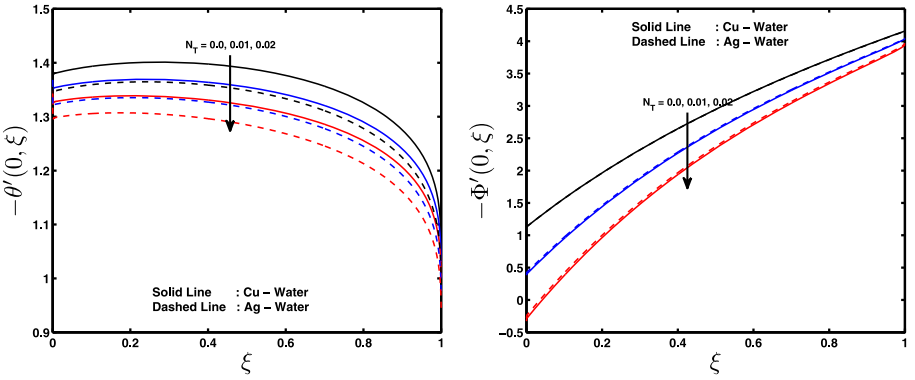

Figure 9 Effect of thermophoretic parameter N_T on (a) and (b) for $Gr_t = 0.2$, $\phi = 0.2$, $Gr_c = 0.2$, $Ha = 4$, $Pr = 7$, $N_b = 0.01$, $\gamma = 4$ and $Sc = 4$.

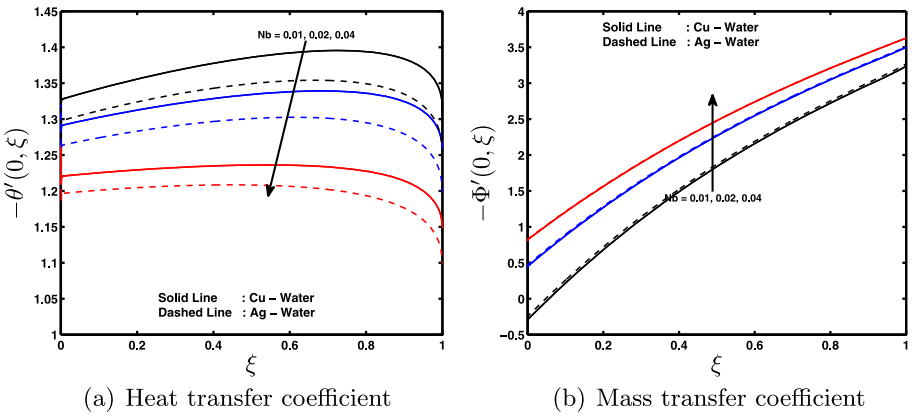

Figure 10 Effect of Brownian motion parameter N_b on (a) and (b) for $Gr_t = 0.2$, $\phi = 0.2$, $Gr_c = 0.2$, $Ha = 2$, $Pr = 7$, $N_T = 0.02$, $\gamma = 3$ and $Sc = 4$.

transfer rates decrease with an increase in the thermophoretic parameter. It is observed that the concentration profile and the wall heat transfer rate in the case of the Ag-water nanofluid are less than those of the Cu-water nanofluid, while the opposite trend is observed in the case of the wall mass transfer rate. We found that the wall heat transfer rate got higher value when $\xi = 0$, and then the opposite trend is observed when $\xi = 1$. The mass transfer rate got less value when $\xi = 0$, while in the case $\xi = 1$ it got the higher value. The fast flow from the stretching sheet carries with it nanoparticles leading to an increase in the mass volume fraction boundary layer thickness.

Figure 10(a) and (b) shows the effect of the Brownian motion parameter N_b on the wall heat and mass transfer rates. Figure 10(a) shows that the heat transfer rate decreases with increasing N_b. The mass transfer at the wall increases with the increase in N_b. The heat transfer rate for the Cu-water nanofluid is higher than that for the Ag-water nanofluid, while the opposite is true for the mass transfer rate (see Figure 10).

Figure 11(a) and (b) shows the impact of the Soret number on the concentration profiles and the mass transfer coefficient, where the concentration profiles grow less while the mass transfer coefficient increases with an increase in the Soret number. Again, Fig-

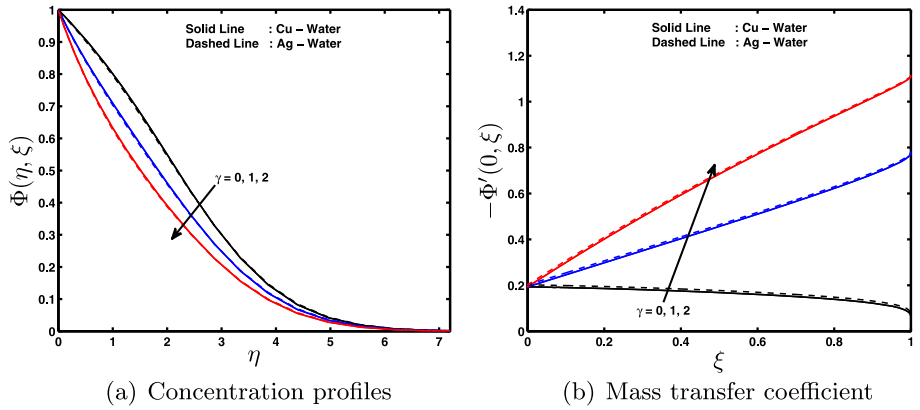

Figure 11 Effect of chemical reaction parameter γ on concentration profiles and the local Sherwood number for $Gr_t = 0.2$, $\phi = 0.2$, $Gr_c = 0.2$, $Ha = 2$, $Pr = 7$, $N_T = 0.01$, $N_b = 0.01$, $Sc = 0.6$ and $\xi = 0.5$.

ure 11(a) and (b) shows that as the Soret number increases, the boundary layer thickness for the solute concentration reduces. The mass transfer coefficient is increasing when the Soret number is positive.

5 Conclusions

We have investigated the heat and mass transfer in unsteady MHD boundary layer flow in nanofluid due to an impulsively stretching surface with chemical reaction and an applied magnetic field. Other parameters of interest in this study included the Brownian motion parameter and thermophoresis parameter. In this paper we considered Cu-water and Ag-water nanofluids and assumed that the nanoparticle volume fraction can be actively controlled at the boundary surface. We have solved the model equations using the spectral relaxation method, and to benchmark our solutions we compared our results with some limiting cases from the literature. These results were found to be in a good agreement. From the numerical simulations, some results can be drawn as follows:

(i) The velocity profiles increase with increase in the nanoparticle volume fraction, while the opposite trend is observed with increase in the value of the Hartman number.

(ii) The temperature profiles increase with increasing nanoparticle volume fraction values.

(iii) The skin friction decreases with an increase in the values of the nanoparticle volume fraction, while the opposite trend is observed for increasing values of the Hartman number.

(iv) The heat transfer coefficient decreases with increase in the values of the nanoparticle volume fraction, the Hartman number, thermophoretic and Brownian motion parameters.

(v) The mass transfer coefficient increases with an increase in the nanoparticle volume fraction, chemical reaction parameter, Hartman number and Brownian motion parameter, while the opposite trend is observed for increasing values of the thermophoretic parameter.

Abbreviations

t: time; p: pressure; a: positive constant; q_w: wall heat flux; q_m: wall mass flux; Pr: Prandtl number; Sc: Schmidt number; Ha: Hartman number; N_T: thermophoresis parameter; N_b: Brownian motion parameter; Sh_x: local Sherwood number; Re_x: local Reynolds number; Nu_x: local Nusselt number; Gr_t: local temperature Grashof number; Gr_c: local concentration Grashof number; k_{nf}: thermal conductivity of nanofluid; C_{fx}: skin friction coefficient; $f(\xi, \eta)$: dimensionless stream function; T_∞: ambient temperature; C_∞: ambient concentration; g: acceleration due to gravity; B_0: uniform magnetic field; u, v: velocity components along x, y directions; x: coordinate along the sheet; y: coordinate normal to the sheet; T: local fluid temperature; T_w: temperature at the stretching surface; D_B: Brownian motion coefficient; D_T: thermophoretic diffusion coefficient; C: solutal concentration; C_s: concentration susceptibility; C_w: concentration at the stretching surface; v_w: prescribed suction velocity; K: chemical reaction parameter; k_s: solid volume fraction; k_f: thermal conductivity of fluid. *Greek symbols*: ρ_{nf}: nanofluid density; ν_{nf}: nanofluid kinematic viscosity; μ_{nf}: coefficient of viscosity; $(\rho cp)_{nf}$: nanofluid heat capacitance; α_{nf}: thermal diffusivity of nanofluid; μ_{nf}: effective dynamic viscosity nanofluid; $(cp)_{nf}$: specific heat of fluid at constant pressure; τ_w: shearing stress at the surface of the wall; γ: scaled chemical reaction parameter; σ: electrical conductivity; ϕ: fraction of nanoparticles; ϕ_1, ϕ_2: nanoparticle volume fraction; $\psi(x, y)$: dimensionless stream function; $(\rho c_p)_f$: heat capacity of base fluid; ρ_f: density of base fluid; μ_f: dynamic viscosity of fluid; ϕ: fraction of nanoparticles; ρ_s: density of solid fractions; β_C: volumetric solutal expansion coefficient; β_T: volumetric thermal expansion coefficient; $(\rho c_p)_s$: effective heat capacity of nanoparticle. *Subscripts*: f: fluid; nf: nanofluid; s: solid.

Competing interests

The authors have declared that they have no competing interests.

Authors' contributions

All authors contributed equally to the writing of this paper. All authors read and approved the final manuscript.

Author details

[1]School of Mathematics, Statistics and Computer Science, University of KwaZulu-Natal, Private Bag X01, Scottsville, Pietermaritzburg, 3209, South Africa. [2]Shanghai Key Lab of Vehicle Aerodynamics and Vehicle Thermal Management Systems, Tongji University, 4800 Cao An Rd., Jiading, Shanghai, 201804, China.

Received: 29 May 2015 Accepted: 25 August 2015 Published online: 15 September 2015

References

1. Choi, SUS: Enhancing thermal conductivity of fluids with nanoparticles. In: The Proceedings of the ASME International Mechanical Engineering Congress and Exposition (San Francisco, USA, ASME, FED, 231/MD), vol. 66, pp. 99-105 (1995)
2. Isha, A, Nazar, R, Pop, I: Hydromagnetic flow and heat transfer adjacent to a stretching vertical sheet. Heat Mass Transf. **44**, 921-927 (2008)
3. Mahapatra, TR, Mondal, S, Pal, D: Heat transfer due to magnetohydrodynamic stagnation-point flow of a power-law fluid towards a stretching surface in the presence of thermal radiation and suction/injection. ISRN Thermodyn. **2012**, Article ID 465864 (2012)
4. Das, SK, Cho, SUS, Yu, W, Pradeep, T: Nanofluids: Science and Technolog. Wiley, New York (2007)
5. Buongiorno, J: Convective transport in nanofluids. J. Heat Transf. **128**, 240-250 (2006)
6. Khan, WA, Pop, I: Boundary layer flow of a nanofluid past a stretching sheet. Int. J. Heat Mass Transf. **53**, 2477-2483 (2010)
7. Hady, FM, Ibrahim, FS, Abdel-Gaied, SM, Mohamed, R: Radiation effect on viscous flow of a nanofluid and heat transfer over a nonlinearly stretching sheet. Nanoscale Res. Lett. **7**, 229 (2012)
8. Kuznetsov, AV, Nield, DA: Natural convective boundary layer flow of a nanofluid past a vertical plate. Int. J. Therm. Sci. **49**, 243-247 (2010)
9. Nield, DA, Kuznetsov, AV: The Cheng-Minkowycz problem for natural convective boundary layer flow in a porous medium saturated with a nanofluid. Int. J. Heat Mass Transf. **52**, 5792-5795 (2009)
10. Yacob, NA, Ishak, A, Pop, I, Vajravelu, K: Boundary layer flow past a stretching/shrinking surface beneath an external uniform shear flow with a convective surface boundary condition in a nanofluid. Nanoscale Res. Lett. **6**, 314 (2011). doi:10.1186/1556-276X-6-314
11. Haroun, NAH, Sibanda, P, Mondal, S, Motsa, SS: On unsteady MHD mixed convection in a nanofluid due to a stretching/shrinking surface with suction/injection using the spectral relaxation method. Bound. Value Probl. **2015**, 24 (2015). doi:10.1186/s13661-015-0289-5
12. Hamad, MAA, Ferdows, M: Similarity solution of boundary layer stagnation point flow towards a heated porous stretching sheet saturated with a nanofluid with heat absorption/generation and suction/blowing. Commun. Nonlinear Sci. Numer. Simul. **17**, 132-140 (2012)
13. Rashidi, MM, Erfani, E: The modified differential transform method for investigating nano boundary-layers over stretching surfaces. Int. J. Numer. Methods Heat Fluid Flow **21**, 864-883 (2011)
14. Rashidi, MM, Freidoonimehr, N, Hosseini, A, Anwar Bég, O, Hung, TK: Homotopy simulation of nanofluid dynamics from a non-linearly stretching isothermal permeable sheet with transpiration. Meccanica **49**, 469-482 (2014)
15. Anwar Bég, O, Rashidi, MM, Akbari, M, Hosseini, A: Comparative numerical study of single-phase and two-phase models for bio-nanofluid transport phenomena. J. Mech. Med. Biol. **14**, 1450011 (2014)
16. Garoosi, F, Jahanshaloo, L, Rashidi, MM, Badakhsh, A, Ali, MA: Numerical simulation of natural convection of the nanofluid in heat exchangers using a Buongiorno model. Appl. Math. Comput. **254**, 183-203 (2015)
17. Mălin, M: Multiple solutions for a class of oscillatory discrete problems. Adv. Nonlinear Anal. (2015). doi:10.1515/anona-2015-0027
18. Mălin, M: Emden-Fowler problem for discrete operators with variable exponent. Electron. J. Differ. Equ. **2014**, 55 (2014)
19. Kleinstreuer, C, Li, J, Koo, J: Microfluidics of nano-drug delivery. Int. J. Heat Mass Transf. **51**, 5590-5597 (2008)

20. Capretto, L, Cheng, W, Hill, M, Zhang, X: Micromixing within microfluidic devices. Top. Curr. Chem. **304**, 27-68 (2011)
21. Yazdi, MH, Abdullah, S, Hashim, I, Sopian, K: Slip MHD liquid flow and heat transfer over non-linear permeable stretching surface with chemical reaction. Int. J. Heat Mass Transf. **54**, 3214-3225 (2011)
22. Chamkha, AJ, Aly, AM: MHD free convection flow of a nanofluid past a vertical plate in the presence of heat generation or absorption effects. Chem. Eng. Commun. **198**, 425-441 (2011)
23. Matin, MH, Nobari, MRH, Jahangiri, P: Entropy analysis in mixed convection MHD flow of nanofluid over a non-linear stretching sheet. J. Therm. Sci. Techonol. **7**(1), 104-119 (2012)
24. Nourazar, SS, Matin, MH, Simiari, M: The HPM applied to MHD nanofluid flow over a horizontal stretching plate. J. Appl. Math. **2011**, Article ID 876437 (2011). doi:10.1155/2011/876437
25. Anjali Devi, SP, Thiyagarajan, M: Steady nonlinear hydromagnetic flow and heat transfer over a stretching surface of variable temperature. Heat Mass Transf. **42**, 671-677 (2006)
26. Motsa, SS: A new spectral relaxation method for similarity variable nonlinear boundary layer flow systems. Chem. Eng. Commun. **201**, 241-256 (2014)
27. Motsa, SS, Dlamini, PG, Khumalo, M: Spectral relaxation method and spectral quasilinearization method for solving unsteady boundary layer flow problems. Adv. Math. Phys. **2014**, Article ID 341964 (2014). doi:10.1155/2014/341964
28. Motsa, SS, Makukula, ZG: On spectral relaxation method approach for steady von Karman flow of a Reiner-Rivlin fluid with Joule heating and viscous dissipation. Cent. Eur. J. Phys. **11**, 363-374 (2013)
29. Brinkman, HC: The viscosity of concentrated suspensions and solution. J. Chem. Phys. **20**, 571-581 (1952)
30. Abu-Nada, E: Application of nanofluids for heat transfer enhancement of separated flows encountered in a backward facing step. Int. J. Heat Fluid Flow **29**, 242-249 (2008)
31. Liao, SJ: An analytic solution of unsteady boundary layer flows caused by an impulsively stretching plate. Commun. Nonlinear Sci. Numer. Simul. **11**, 326-329 (2006)
32. Mahdy, A: Unsteady mixed convection boundary layer flow and heat transfer of nanofluids due to stretching sheet. Nucl. Eng. Des. **249**, 248-255 (2012)
33. Hsiao, KL: Nanofluid flow with multimedia physical features for conjugate mixed convection and radiation. Comput. Fluids **104**, 1-8 (2014)
34. Nadeem, S, Saleem, S: Analytical study of third grade fluid over a rotating vertical cone in the presence of nanoparticles. Int. J. Heat Mass Transf. **85**, 1041-1048 (2015)
35. Sheikholeslami, M, Bandpy, MG, Ganji, DD, Soleimani, S, Seyyedi, SM: Natural convection of nanofluids in an enclosure between a circular and a sinusoidal cylinder in the presence of magnetic field. Int. Commun. Heat Mass Transf. **39**, 1435-1443 (2012)
36. Oztop, HF, Abu-Nada, E: Numerical study of natural convection in partially heated rectangular enclosures filled with nanofluids. Int. J. Heat Fluid Flow **29**, 1326-1336 (2008)

Chapter 4

On couple stress effects on unsteady nanofluid flow over stretching surfaces with vanishing nanoparticle flux at the wall

In this chapter we study flow of an unsteady nanofluid subject to couple stress effects. The couple stress slows down fluid motion due to an increasing drag force which is equivalent to an apparent decrease in the fluid viscosity. The highly non-linear equations are solved numerically using a novel SRM and SQLM. Comparison of the results with previously published work was undertaken and the validation of our new techniques is discussed.

Journal of Applied Fluid Mechanics, Vol. 9, No. 4, pp. 1937-1944, 2016.
Available online at www.jafmonline.net, ISSN 1735-3572, EISSN 1735-3645.

On Couple Stress Effects on Unsteady Nanofluid Flow over Stretching Surfaces with Vanishing Nanoparticle Flux at the Wall

F. Awad[1, 2†], N. A. H. Haroun[2, 3], P. Sibanda[3] and M. Khumalo[1]

[1] *Department of pure & applied mathematics, university of Johannesburg, P.O. Box 524, Auckland Park 2006, Johannesburg, South Africa*
[2]*Department of Mathematics, Omdurman. I. University, Omdurman, Khartoum, Sudan*
[3]*School of Mathematics, Statistics and Computer Science, University of KwaZulu-Natal, Bag X01, Scottsville, Pietermaritzburg,3209, South Africa*

†*Corresponding Author Email: awad.fga@gmail.com*

(Received April 21, 2015; accepted August 8, 2015)

ABSTRACT

In this paper the problem of unsteady nanofluid flow over a stretching sheet subject to couple stress effects is presented. Most previous studies have assumed that the nanoparticle volume fraction at the boundary surface may be actively controlled. However, a realistic boundary condition for the nanoparticle volume fraction model is that the nanoparticle flux at the boundary be set to zero. This paper differs from previous studies in that we assume there is no active control of the nanoparticle volume fraction at boundary. The spectral relaxation method has been used to solve the governing equations, moreover the results were further confirmed by using the quasi-linearization method. The qualitative and quantitative effects of the dimensionless parameters in the problem such as the couple stress parameter, the Prandtl number, the Brownian motion parameter, the thermophoresis parameter, the Lewis number on the fluid behavior are determined.

Keywords: Nanofluid; Couple stress; Stretching surface; Vanishing nanoparticle flux; Spectral relaxation method.

NOMENCLATURE

b& $c$are	positive constants with dimensions time^{-1}
D_B	Brownian diffusion coefficient
D_T	thermophoresis diffusion coefficient
f	dimensionless velocity
g	acceleration due to gravity
i	time index during navigation
L	scale
Le	Lewis number
N	number of grid points
N_B	Brownian motion parameter
N_T	thermophoresis parameter
p	fluid pressure
Pr	Prandtl number
S	unsteadiness parameter
t	time
T	fluid temperature
T_w	temperature at the stretching surface
T_∞	ambient fluid temperature
T_{ref}	reference temperature
u & v	velocity components (along xand y)
Q_x	couple stress parameter
α_m	effective thermal diffusivity
η	similarity variable
θ	Dimensionless temperature
$v = \frac{\mu}{\rho}$	kinematic viscosity of the fluid
$v' = \frac{\varsigma}{\rho}$	couple stress viscosity
ς	couple stress viscosity coefficient
ρ	fluid density v
μ	fluid viscosity
$(\rho c)_f$	effective heat capacity of the fluid
$(\rho c)_p$	effective heat capacity of the nanoparticle material
τ	parameter defined by $(\rho c)_f/(\rho c)_p$
ϕ	Dimensionless nanoparticles volume
$\hat{\phi}$	nanoparticle volume concentration
$\hat{\phi}_\infty$	ambient nanoparticle volume fraction
ω	Gauss-Lobatto points
U	stretching velocity
$V = V(u, v)$	fluid velocity
x & y	Cartesian coordinates

1. INTRODUCTION

In the past few years, convective heat and mass transfer in nanofluids has become a topic of major interest. The thermal conductivity of a fluid plays an important role in the heat transfer between the fluid medium and a solid surface. Conventional heat transfer fluids including oil, water and ethylene glycol, etc., are poor heat transfer fluids due to low thermal conductivities. Nanofluids are engineered by suspending metallic nanoparticles with sizes below $100nm$ in traditional heat transfer fluids. Heat transfer enhancement using nanofluids in convective boundary-layer flow over a vertical plate, stretching sheet and moving surfaces has been studied by numerous authors, and are discussed in the review papers Buongiorno (2006), Oztop and Abu-Nada (2008), Daungthongsuk and Wongwises (2007, Nield and Kuznetsov (2009), Kuznetsov and Nield (2010a), Kuznetsov and Nield (2010b), Ahmad and Pop (2010), Khan and Pop (2010), Bachok, Ishak, and Pop (2010)andRashidi *et al*. (2014).

The couple stress fluid model is one of numerous viscoelastic models that have been proposed to describe the characteristics and Behavior of non-Newtonian fluids. The constitutive equations of these fluids are often very complex involving a large number of parameters. The couple stress fluid model is the simplest generalization of the classical theory of fluids which allows for polar effects such as couple stresses and body couples in the fluid medium. The theory of couple stress fluids was introduced in Stokes (1966) to explain the rheological behaviour of various complex non-Newtonian fluids with body stresses and body couples which cannot be treated by the classical theory of continuum mechanics. Due to the rotational interaction of particles, the force-stress tensor is not symmetric and the flow behaviour of such fluids is not similar to Newtonian fluids. Couple stress fluids have applications in engineering and chemical industries. The peristaltic transport of a couple stress fluid in an asymmetric channel with an induced magnetic field has been considered by Nadeem and Akram (2011). An analysis of the effects of couple stresses on the blood flow through a thin artery with a mild stenosis was carried out by Sinha and Singh (1984). Malashetty, Pop, Kollur, and Sidram (2012) investigated double diffusive convection in a couple stress fluid saturated porous layer with Soret effects. Hayat *et al*. (2013) observed that the velocity and the boundary layer thickness decrease with the couple stress fluid parameter in his study of melting heat transfer in the boundary layer flow of a couple stress fluid. Khan, Mahmood, and Ara (2013) found the approximate solution of the couple stress fluid between expanding and contracting walls. An analysis has been provided for three-dimensional magnetohydrodynamic flow of couple stress fluid with Newtonian heating by Ramzan, Farooq, Alsaedi, and Hayat (2013). Murthy and Nagaraju (2009) considered the flow of a couple stress fluid generated by a circular cylinder subjected to longitudinal and torsional oscillations, and the time dependence of the run up flow of a couple stress fluid between rigid parallel plates is examined by Devakar and Iyengar (2010) in which the flow was induced by a constant pressure gradient which is suddenly withdrawn and the parallel plates set to move instantaneously with different velocities in the direction of the applied pressure gradient. In this work we study the unsteady nanofluid flow over a stretching sheet in the presence of couple stress effects. To the best of our knowledge, most published work in the field of nanofluid, employed boundary conditions on the nanoparticle volume fraction analogous to those on the temperature thereby assuming that the nanoparticle volume fraction could be actively controlled at the boundary. A recent series of papers by Kuznetsov and Nield (2014), Nield and Kuznetsov (2014a), Nield and Kuznetsov (2014b), Nield and Kuznetsov (2014c) have suggested that a more realistic boundary condition is that the nanoparticle volume fraction flux at the boundary be set to zero. These boundary conditions have not been used on previous studies on couple stress fluids.

2. MATHEMATICAL FORMULATION

Consider the problem of two-dimensional flow of unsteady incompressible nanofluid over a stretching sheet subject to couple stress effect see Fig. (1).

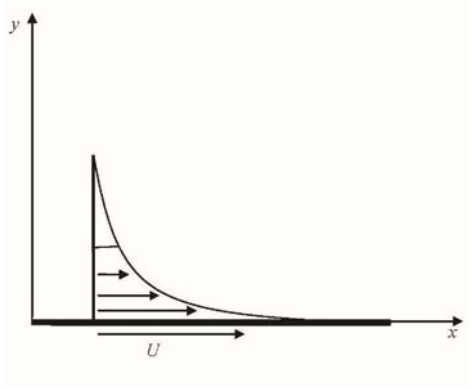

Fig. 1. Schematic diagram for the problem.

The continuous sheet isplaced at $y = 0$ and moves parallel to the $x - axis$ with velocity,

$$U = \frac{bx}{1 - ct} \tag{1}$$

where b and c are constants and t represents time. The boundary layer temperature and nanoparticle volume concentration are$T$ and $\hat{\phi}$ respectively. The ambient fluid temperature and nanoparticle volume fraction are $T_\infty$and $\hat{\phi}_\infty$respectively. At the surface, both the nanofluid and the sheet arekept at a constant temperature T_w where $T_w > T_\infty$is for aheated stretching surface and $T_w < T_\infty$corresponds to acooled surface.The boundary layer equations

governing the flow of an incompressible couple stress fluid are (see Hayat *et al*. (2013))

$$div\, V = 0, \tag{2}$$

$$\rho \frac{DV}{Dt} = -\nabla p - \mu(\nabla \times \nabla \times \mathrm{V}) - \varsigma\left(\nabla \times \nabla \times \nabla \times \nabla \times V\right) \tag{3}$$

The continuity, momentum, energy and nanoparticles fraction equations for the nanofluid can be expressed as,

$$\frac{\partial \mathrm{u}}{\partial \mathrm{x}} + \frac{\partial \mathrm{v}}{\partial \mathrm{y}} = 0 \tag{4}$$

$$\frac{\partial \mathrm{u}}{\partial \mathrm{t}} + \mathrm{u}\frac{\partial \mathrm{u}}{\partial \mathrm{x}} + \mathrm{v}\frac{\partial \mathrm{u}}{\partial \mathrm{x}} = \nu \frac{\partial^2 \mathrm{u}}{\partial \mathrm{y}^2} - \nu' \frac{\partial^4 \mathrm{u}}{\partial \mathrm{y}^4}, \tag{5}$$

$$\frac{\partial \mathrm{T}}{\partial \mathrm{t}} + \mathrm{u}\frac{\partial \mathrm{T}}{\partial \mathrm{x}} + \mathrm{v}\frac{\partial \mathrm{T}}{\partial \mathrm{y}} = \alpha_{\mathrm{m}} \frac{\partial^2 \mathrm{T}}{\partial \mathrm{y}^2} + \tau\left[\mathrm{D_B}\frac{\partial \hat{\phi}}{\mathrm{y}}\frac{\partial \mathrm{T}}{\partial \mathrm{y}} + \frac{\mathrm{D_T}}{\mathrm{T}_\infty}\left(\frac{\partial \mathrm{T}}{\partial \mathrm{y}}\right)^2\right], \tag{6}$$

$$\frac{\partial \hat{\phi}}{\partial \mathrm{t}} + \mathrm{u}\frac{\partial \hat{\phi}}{\partial \mathrm{x}} + \mathrm{v}\frac{\partial \hat{\phi}}{\partial \mathrm{y}} = \mathrm{D_B}\frac{\partial^2 \hat{\phi}}{\partial \mathrm{y}^2} + \frac{\mathrm{D_T}}{\mathrm{T}_\infty}\frac{\partial^2 \mathrm{T}}{\partial \mathrm{y}^2},$$

equations (4)-(7) are subject to the boundary conditions

(7)

$$\mathrm{v} = 0,\ \mathrm{u} = \mathrm{U},\ \mathrm{T} = \mathrm{T_s},\ \mathrm{D_B}\frac{\partial \hat{\phi}}{\partial \mathrm{y}} + \frac{\mathrm{D_T}}{\mathrm{T}_\infty}\frac{\partial \mathrm{T}}{\partial \mathrm{y}} = 0 \quad \text{on } \mathrm{y} = 0 \tag{8}$$

$$\mathrm{u} \to 0,\ \mathrm{T} \to \mathrm{T}_\infty, \hat{\phi} \to \hat{\phi}_\infty,\ \text{as } \mathrm{y} \to \infty \tag{9}$$

For two-dimensional flow, it is convenient to introduce the stream function$\psi(\mathrm{x},\ \mathrm{y},\ \mathrm{t})$and the following similarity transformations$\psi(\mathrm{x}, \mathrm{y}, \mathrm{t}) = \sqrt{\frac{\mathrm{bv}}{1-\mathrm{ct}}}\mathrm{xf}(\eta)$,

$$\eta = \sqrt{\frac{b}{\nu(1-ct)}}\, y,$$

$$T(x,y,t) = T_\infty + T_{ref}\left[\frac{bx^2}{2\nu}\right](1-ct)^{-\frac{3}{2}}\theta(\eta),$$

$$\hat{\phi}(x,y,t) = \hat{\phi}_\infty + C_{ref}\left[\frac{bx^2}{2\nu}\right](1-ct)^{-\frac{3}{2}}\phi(\eta),$$

Equations (5)-(7) can now be presented in the form

$$f''' - Qf^{(5)} + ff'' - f'^2 - S\left(f' + \frac{1}{2}\eta f''\right) = 0, \tag{10}$$

$$\theta'' + Pr\left[f\theta' - 2f'\theta - \frac{S}{2}(3\theta + \eta\theta')\right] + N_b\phi'\theta' + N_t\theta'^2 = 0, \tag{11}$$

$$\phi'' + Le\left[f\phi' - 2f' - \frac{S}{2}(3\phi + \eta\phi)\right] + \frac{N_t}{N_b}\theta'' = 0, \tag{12}$$

with boundary conditions

$$f = 0,\ f' = \theta = 1,\ N_b\phi' + N_t\,\theta' = 0, \tag{13}$$

$$f' \to 0,\ \theta \to 0,\ \phi \to 0\ as\ \eta \to \infty, \tag{14}$$

where the couple stress parameter$Q$, the dimensionless measure of unsteadiness S, the Prandtl number Pr, the Brownian motion parameter N_b, the thermophoresis parameter N_t and the Lewis number Le are defined as

$$Q_x = \frac{v'U}{v^2 x},\ S = \frac{c}{b},\ N_t = \frac{\tau D_T(T_w - T_\infty)}{T_\infty \alpha_m},$$

$$N_b = \frac{\tau D_B \hat{\phi}_{ref}\left[\frac{bx^2}{2v}\right]}{\alpha_m}(1-ct)^{-\frac{3}{2}},$$

$$Pr = \frac{\nu}{\alpha_m},\ Le = \frac{\nu}{D_B},$$

3- NUMERICAL SOLUTION

In this section, we apply the spectral relaxation method (SRM) to solve the nonlinear ODEs (10) - (12) along with boundary conditions (13)-(14). For the implementation of the spectral collocation method, it is convenient to reduce the order of equation (10) from five to four. To this end, we set$f' = g$, so that equation (10) becomes

$$-Qg'''' + g'' + \left(\mathrm{f} + \frac{1}{2}\eta\right)g' - Sg = g^2,$$

$$g(0) = 1,\ \mathrm{g}(\infty) = 0, \tag{15}$$

$$f' = g,\ \mathrm{f}(0) = 0, \tag{16}$$

The spectral relaxation method algorithm (see Motsa, Dlamini, and Khumalo (2012), Motsa and Makukula (2013), Motsa, Dlamini, and Khumalo (2013)) first decouples the system of equations (10) - (12). From the decoupled equations an iteration scheme is developed by evaluating linear terms in the current iteration level which is denoted by the subscript $r+1$ and nonlinear terms in the previous iteration level denoted by the subscript$r$. Applying the SRM to (11) - (12) and (15) - (16) gives the following linearordinary differential equations;

$$-Qg''''_{r+1} + g''_{r+1} + \left(f_r + \frac{1}{2}\eta\right)g'_{r+1} - Sg_{r+1} = {g_r}^2, \tag{17}$$

$$f'_{r+1} = g_{r+1},\ f_{r+1}(0) = 0, \tag{18}$$

$$\theta''_{r+1} + Pr\left(f_{r+1} - \frac{1}{2}S\eta + N_b\phi'_r\right)\theta'_{r+1} - Pr\left(2g_{r+1} + \frac{3}{2}S\right)\theta_{r+1} = -N_t\theta'^2_r, \tag{19}$$

$$\phi''_{r+1} + Le\left(f_{r+1} - \frac{1}{2}S\eta\right)\phi'_{r+1} - Le\left(2g_{r+1} + \frac{3}{2}S\right)\phi_{r+1} = -\frac{N_t}{N_b}\theta''_r, \tag{20}$$

$$g_{r+1}(0) = 1,\ \theta_{r+1}(0) = 1,\ N_b\phi'_{r+1}(0) + N_t\theta'_{r+1}(0) = 0, \tag{21}$$

$$g_{r+1}(\infty) = 0,\ \theta_{r+1}(\infty) = 0,\ \phi_{r+1}(\infty) = 0. \tag{22}$$

Starting from given initial approximationsf_0, g_0, θ_0 and ϕ_0, the iteration schemes (17) - 20) can be solved iteratively using a spectral collocation method. In applying the spectral collocation method, we find the unknown function at the collocation points by requiring that equations (17) - (20) be satisfied exactly at these points. A convenient set of collocation points are the Gauss-Lobatto points defined by

$$\omega_j = \cos\frac{\pi_j}{N}, \quad \mathrm{j} = 0, 1, \ldots, \mathrm{N} \tag{23}$$

For convenience, in numerical computations, the semi-infinite domain is approximated by the truncated domain $[0, L]$ and using thelinear transformation $\eta = L(\omega + 1)/2$, we convert $[0, L]$ intothe interval $[-1,1]$ in which the spectral method can be used,where $L = \eta_\infty$is a finite number selected to be largeenough to represent the behavior of the flow properties when $\eta$is very large. The derivative are defined as

$$\frac{df}{d\eta} = \sum_{k=0}^{N} D_{jk} f(\omega_k) = Df,\ j = 0, 1, \dots, N \qquad (24)$$

where $N + 1$is the number of collocation points,

$D = 2D/L\ and\ F = [f(\omega_0),$
$f(\omega_1), \dots, f(\omega_N)]^T$is the vector of unknown functions at the collocation points. Applying the Chebyshevspectral collocation method to the system (17) - (20) we obtain the following matrix equations

$$A_{1,r} g_{r+1} = R_{1,r},\ g_{r+1}(\omega_N) = 1, g_{r+1}(\omega_0) = 0$$
$$Df_{r+1} = g_{r+1},\ f_{r+1}(\omega_N) = 0,$$
$$A_{2,r}\theta_{r+1} = R_{2,r},\ \theta_{r+1}(\omega_N) = 1,$$
$$\theta_{r+1}(\omega_0) = 0,$$
$$A_{3,r}\phi_{r+1} = R_{3,r}, N_b\phi_{r+1}(\omega_N) + N_t\phi_{r+1}(\omega_N)$$
$$\phi_{r+1}(\omega_0) = 0,$$

where

$$A_{1,r} = -QD^4 + D^2 + diag\left[f_r - \frac{1}{2}S\eta\right]D - SI, R_{1,r} = g_r^2 \qquad (25)$$

$$A_{2,r} = D^2 + Pr\ diag\left[f_{r+1} - \frac{1}{2}S\eta + N_b\phi_r'\right]D - \left[2f_{r+1} + \frac{3}{2}S\right]I,\ R_{2,r} = -N_t\theta_r'^2 \qquad (26)$$

$$A_{3,r} = D^2 + Le\ diag\left[f_{r+1} - \frac{1}{2}S\eta\right]D - \left[2f_{r+1} + \frac{3}{2}S\right]I,\ R_{3,r} = -\frac{N_t}{N_b}\theta_r'' \qquad (27)$$

Here $I$is an $(N + 1) \times (N + 1)$diagonal matrix and $diag$ []denotes a diagonal matrix. Starting from stable initial approximations f_0, g_0, $\theta_0\ and\ \phi_0$ whichsatisfy the boundary conditions of governing equations:

$$f_0 = \left(\frac{\eta^2}{6} - 1\right)e^{-\eta} \qquad (28)$$

$$g_0 = \left(1 + \frac{\eta}{3} - \frac{\eta^2}{6}\right)e^{-\eta} \qquad (29)$$

$$\theta_0 = e^{-\eta},\ \phi_0 = -\frac{N_t}{N_b}e^{-\eta} \qquad (30)$$

4- RESULTS AND DISCUSSION

To obtain clear insights into the physics of the problem of unsteady nanofluid flow over a stretching sheet with couple stresses, the set of ordinary differential equations (10) – (12) were solved using the spectral relaxation method. We determined through numerical experimentation that $\eta_\infty = 20$with grid points$N = 100$, gave sufficient accuracy for the spectral relaxationmethod. The effects of the fluid parameters such as the thermophoresis parameterN_t, the Brownian motion N_b on thevelocity, temperature and nanoparticle profiles have beendetermined.

Table 1 Effects of S, Q on $f''(0)$ when $Nt = 0{:}5, Nb = 0{:}5, Pr = 10$ and $Le = 10$.

S		SRM Q	QLM Ord 7	QLM Ord 8
0.2	0.1	0.8310757	0.8310757	0.8310757
0.4	0.1	0.8640531	0.8640531	0.8640532
0.6	0.1	0.8959227	0.8959227	0.8959227
0.8	0.1	0.9263125	0.9263125	0.9263125
1.0	0.1	0.9551785	0.9551785	0.9551785
1.2	0.1	0.9825941	0.9825941	0.9825941
1.4	0.1	1.0086687	1.0086687	1.0086687
1.6	0.1	1.0335168	1.0335168	1.0335168
1.8	0.1	1.0572473	1.0572473	1.0572473
2.0	0.1	1.0799590	1.0799590	1.0799590
0.2	0.1	0.8310757	0.8310757	0.8310757
0.2	0.2	0.7746540	0.7746540	0.7746540
0.2	0.3	0.7393373	0.7393373	0.7393375
0.2	0.4	0.7135600	0.7135600	0.7135601
0.2	0.5	0.6932968	0.6932968	0.6932969
0.2	0.6	0.6766463	0.6766463	0.6766463
0.2	0.7	0.6625540	0.6625539	0.6625540
0.2	0.8	0.6503734	0.6503734	0.6503734
0.2	0.9	0.6396800	0.6396800	0.6396800
0.2	1.0	0.6301808	0.6301809	0.6301809

Table 2.Effects of $S, Q, Nb$and Nton $-\theta'(0)$ when$Pr = 10$ and $Le = 10$.

S		SRM Q	QLM Ord 7	QLM Ord 8
0.2	0.1	0.8310757	0.8310757	0.8310757
0.4	0.1	0.8640531	0.8640531	0.8640532
0.6	0.1	0.8959227	0.8959227	0.8959227
0.8	0.1	0.9263125	0.9263125	0.9263125
1.0	0.1	0.9551785	0.9551785	0.9551785
1.2	0.1	0.9825941	0.9825941	0.9825941
1.4	0.1	1.0086687	1.0086687	1.0086687
1.6	0.1	1.0335168	1.0335168	1.0335168
1.8	0.1	1.0572473	1.0572473	1.0572473
2.0	0.1	1.0799590	1.0799590	1.0799590
0.2	0.1	0.8310757	0.8310757	0.8310757
0.2	0.2	0.7746540	0.7746540	0.7746540
0.2	0.3	0.7393373	0.7393373	0.7393375
0.2	0.4	0.7135600	0.7135600	0.7135601
0.2	0.5	0.6932968	0.6932968	0.6932969
0.2	0.6	0.6766463	0.6766463	0.6766463
0.2	0.7	0.6625540	0.6625539	0.6625540
0.2	0.8	0.6503734	0.6503734	0.6503734
0.2	0.9	0.6396800	0.6396800	0.6396800
0.2	1.0	0.6301808	0.6301809	0.6301809

In order to have a sense of the accuracy and reliability of the spectral relaxation method, benchmark results were obtained. Tables (1) and (2) give a comparison between the results obtained using the spectral relaxation method and the quasi-linearization technique. The two sets of results are comparable up to six decimal places for all orders of the SRM from order five onwards.

Table (1) shows the effects of the unsteadiness and couple stress parameters on the skin-friction

coefficient. It is evident that increasing Sleads to an increase in the skin frictioncoefficient. On the other hand, increasing Qleads to increases in skin friction coefficient. Table (2) shows the effects of S, Q, N_t *and* $N_b$on the Nusselt number. Here the Nusselt number increases as both the unsteadiness parameter and the couple stress parameter increase. We observe that increasing the thermophoresis parameter N_t increases the heat transfer coefficients increasewhile no effect occurs as the Brownian motion parameter increases.

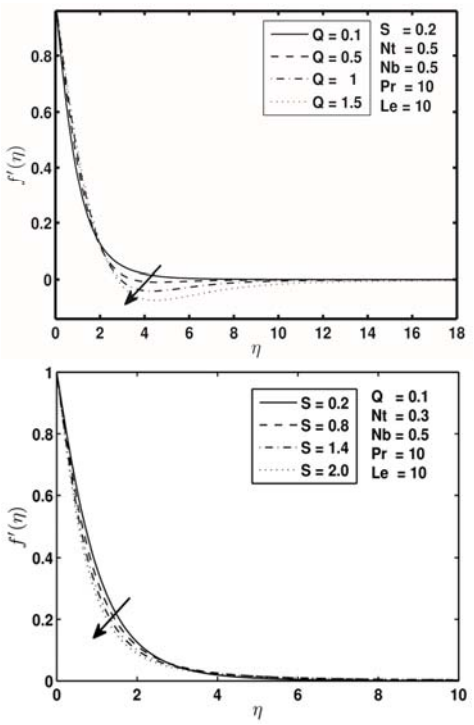

Fig. 2. Effect of the couple stress parameter $Q$and the unsteadiness parameter S on $f(\eta)$ for $Nt = 0.5$, $Nb = 0.5, Pr = 10$ and $Le = 10$.

Figure 2 shows the effect of the couple stress parameter$Q$ and the unsteadiness parameter S on velocity profilesrespectively within the boundary layer. We observe that, asexpected, strengthening the couple stress slows down the fluid motion due to an increasing drag force which is equivalent to an apparent decrease in the fluid viscosity. The velocity decreases with increasing Q until we obtain back flow in the range $2 \leq \eta \leq 8$. We also observe that the unsteadiness parameters lows the motion of the fluid within the boundary layer. It is clear that the boundary layer thickness reduces with increasing$S$.

Figure 3 shows the effect of the couple stress parameter Q on the temperature and mass volume fraction profiles respectively. Increasing Qleads to an increase in the thicknessof both the thermal and mass volume fraction boundary layers, henceincreasing Qreduces both the temperature and the mass volumefraction within the boundary layer.

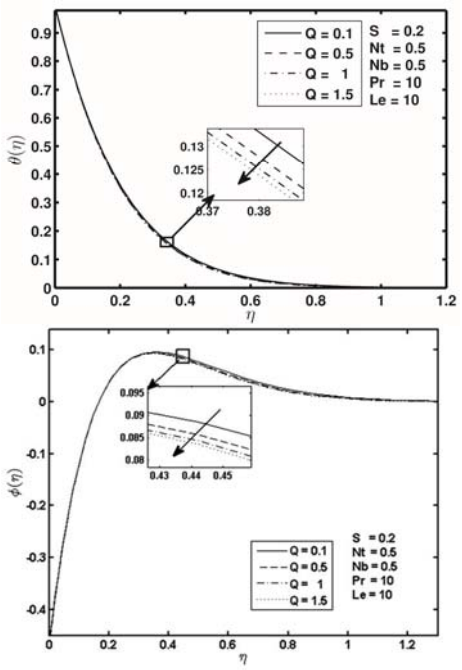

Fig. 3. Effect of the couple stress parameter Qon $\theta(\eta)$ and $\phi(\eta)$ for $S = 0.2$, $Nt = 0.5$, $Nb = 0,5$, $Pr = 10$ and $Le = 10$.

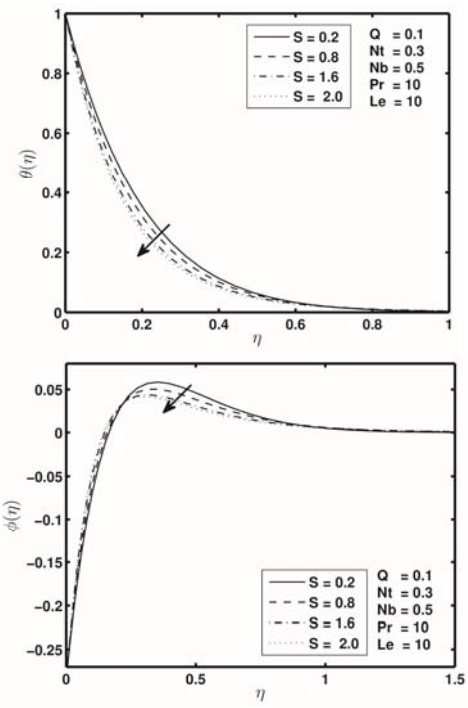

Fig. 4. Effect of the unsteadiness parameter Son $\theta(\eta)$ and $\phi(\eta) Q = 0.1, Nt = 0.3, Nb = 0.5, Pr = 10andLe = 10$.

The effect of the unsteadiness parameter S on the temperature andmass volume fraction are shown in Figure 4. We observe thatas Sincreases, the boundary layer velocity decreases causing adecrease in the heat and nanoparticle transfer

rates, hence the temperature and the nanoparticle inside boundary layer reduce. The influence of the thermophoresis parameter N_t on the temperature and nanoparticle profiles is given in Figure 5. Fast flowaway from the stretching surface exists due to the thermophoresis force generated by the temperature gradient. Therefore as $N_t$increases more a heated fluid travel away from the surface, hencethe temperature within the boundary layer increases. The fast flowfrom the stretching sheet carries with it nanoparticles leading to an increase in the mass volume fraction boundary layer thickness.

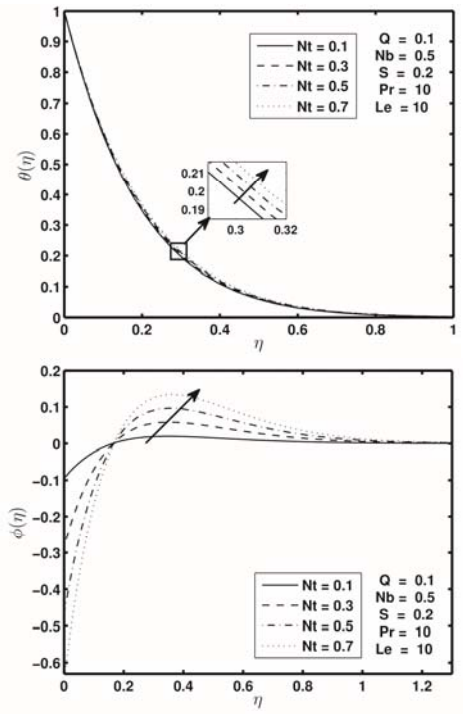

Fig. 5. Effect of the thermophoresis parameter Nton $\theta(\eta)$ and $\phi(\eta)$for $Q = 0,1,\ S = 0,2,\ Nb = 0.5, Pr = 10$ and $Le = 10$.

5. CONCLUSION

In this paper we have studied the flow of an unsteady nanofluid subject to couple stress effects. Numerical solutions of the equations governing the flow were found using the spectral relaxation method (SRM). The validation of the numerical results was done via a careful comparison between the solutions obtained using

The effect of the random motion of nanoparticles suspended in the fluid on the nanoparticle volume fraction is shown in Figure 6. It is evident that increasing N_b leads to a decrease in the mass volume fraction. Moreover, Figure 6illustrates the effect of the Lewis number Leon the mass volumefraction within boundary layer. Increasing Leleads to a decreasein the nanoparticle volume fraction within the thermal boundarylayer, this, in turn, leads to a decrease in the mass volume fraction gradient at the sheet surface.

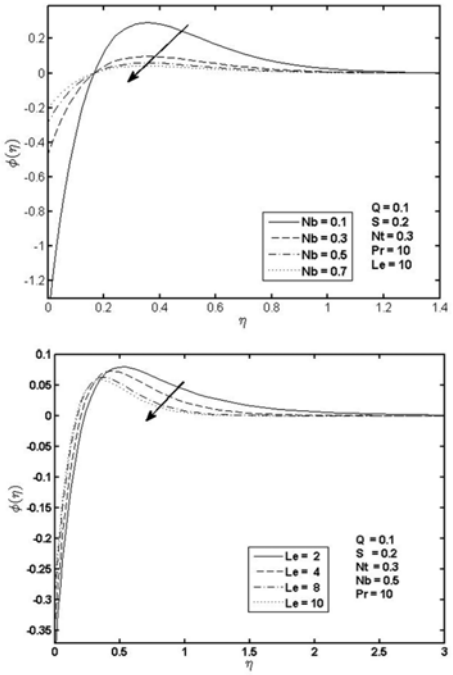

Fig. 6. Effect of the Brownian motion parameter Nb and the Lewis $number\ Le$ on$\phi(\eta)$for$Q = 0.1,\ S = 0.2,\ Nt = 0.5$ and $Pr = 10$.

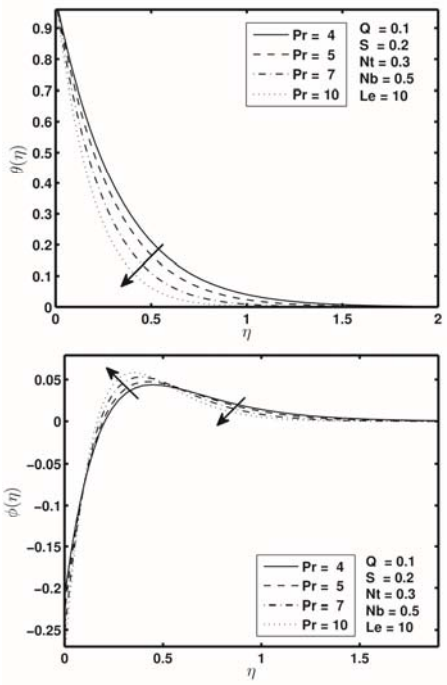

Fig. 7. Effect of the Prandtl number Pr on$\theta(\eta)$ and$\phi(\eta)$for$Q = 0,1,\ S = 0,2,\ Nt = 0.5,\ Nb = 0.5$and $= 10$.

Figure 7 illustrates the variation of the temperature profile $\theta(\eta)$ and mass volume fraction profile $\phi(\eta)$for some values of Prandtl number Pr. The results shows that increasing Prreduces the

temperature profile, while the oppositeresults occurs when we vary the mass volume fraction with Pr.

The results in Figures 3 - 7 show that the nanoparticle volume fraction profiles starts from negative values and later become positive. This, as explained in Kuznetsov and Nield (2010b),is due to the fact the effect of thermophoresis is such that an elevation (above the ambient value of the surface temperature)results in a depression in the relative value of the nanoparticle fraction at the sheet.

the spectral relaxation and the quasi-linearization methods. We have presented the results graphically in order to illustrate the effects of various fluid parameters on the velocity, thermal and nanoparticle volume fraction profiles. The nanoparticle profiles are initially negative and become positive due to the effect of thermophoresis. The velocity is reduced by increasing the unsteadiness parameter. The temperature as well as the mass volume fraction decrease with an increase in the unsteadiness parameter. The stronger couple stress reduces the nanofluid velocity, as well as increasing the thickness of both the thermal and mass volume fraction boundary layers. The effect of the Brownian motion on the mass volume fraction within the boundary is much more significant rather than on the temperature.

REFERENCES

Ahmad, S. and I. Pop (2010). Mixed convection boundary layer flow from a vertical flat plate embedded in a porous medium filled with nanofluids. *International Communications in Heat and Mass Transfer* 37, 987-991.

Bachok, N., A. Ishak and I. Pop (2010). Boundary-layer flow of nanofluids over a moving surface in a flowing fluid. *International Scientific Journal Thermal Science* 49, 1663-1668.

Buongiorno, J. (2006). Convective transport in nanofluids. *ASME Jouraenal Heat Transfer* 128, 240-250.

Daungthongsuk, W. and S. Wongwises (2007). A critical review of convective heat transfer nanofluids. *Renewable and Sustainable Energy Reviews* 11, 797-817.

Daungthongsuk, W. and S. Wongwises (2007). nanofluidover a stretching sheet inthe presence stretching sheet inthe presence thermathermalradiation**,** *Journal of Molecular Liquids* 198, 234–238.

Devakar, M. and T. Iyengar (2010). Run up flow of a couple stress fluid between parallel plates. *Nonlinear Analy-sis: Modelling and Control* 15, 29-37.

Devakar, M. and T. K. V. Iyengar (2010). Run up flow of a couple stress fluid between parallel plates. *Nonlinear Analysis: Modelling and Control* 15, 29-37.

Hayat, T., M. Mustafa, Z. Iqbal and A. Alsaedi (2013). Stagnation point flow of couple stress fluid with melting heat transfer. *Applied Mathematics and Mechanics* 34, 167-176.

Khan, N. A., A. Mahmood and A. Ara (2013). Approximate solution of couple stress fluid with expanding or contracting porous channel. *Engineering Computations* 30, 399-408.

Khan,W. A. and I. Pop (2010). Boundary layer flow of a nanofluid past a stretching sheet. *International Journal Heat Mass Transfer* 53, 2477-2483.

Kuznetsov, A. V. and D. A. Nield (2010a). Effect of local thermal non-equilibrium on the onset of convection in a porous medium layer saturated by a nanofluid. *Transportation in Porous Media* 83, 425-436.

Kuznetsov, A. V. and D. A. Nield (2010b). Natural convective boundary layer flow of a nanofluid past a vertical plate. *International Scientific Journal Thermal Science* 49, 243-247.

Kuznetsov, A. V. and D. A. Nield (2014). Natural convective boundary layer flow of a nanofluid past a vertical plate: A revised model. *International Journal of Thermal Sciences* 77, 126-129.

Malashetty, M. S., I. Pop, P. Kollur and W. Sidram (2012). Soret effect on double diffusive convection in a Darcy porous medium saturatedwith a couple stress fluid. *International Journal of Thermal Sciences* 53, 130-140.

Motsa, S. S., P. G. Dlamini and M. Khumalo (2012). Solving hyperchaotic systems using the spectral relaxation method. *Abstract and Applied Analysis*, V 203461,18.

Motsa, S. S., P. G. Dlamini and M. Khumalo (2013). On spectral relaxation method approach for steady von Kármán flow of a Reiner-Rivlin fluid with Joule heating, viscous dissipation and suction or injection. *Central European Journal of Physics 11*, 363-374.

Nadeem, S. and S. Akram (2011). Peristaltic flowof a couple stress fluid under the effect of induced magnetic field in an asymmetric channel. *Archive of Applied Mechanics* 81, 97-109.

Nield, D. A. and A. V. Kuznetsov (2009). The Cheng Minkowycz problem for natural convective boundary layer flow in a porous medium saturated by nanofluids. *International Journal Heat Mass Transfer* 52, 5792-5795.

Nield, D. A. and A. V. Kuznetsov (2014a). Thermal instability in a porous medium layer saturated by a nanofluid: A revised model. *International Journal of Heat and Mass Transfer* 68, 211-214.

Nield, D. A. and A. V. Kuznetsov (2014b). Forced convection in a parallel-plate channel occupied by a nanofluid or a porous medium saturated

by a nanofluid. *International Journal of Heat and Mass Transfer* 70, 430-433.

Nield, D. A. and A. V. Kuznetsov (2014c). The onset of convection in a horizontal nanofluid layer of finite depth: A revised model. *International Journal of Heat and Mass Transfer* 77, 915-918.

Oztop, H. F. and E. Abu-Nada (2008). Numerical study of natural convection in partially heated rectangular enclosures filled with nanofluids. *International Journal Heat Fluid Flow* 29, 1326-1336.

Oztop, H. F. and E. Abu-Nada (2008). Numerical study of natural convection in partially heated rectangular enclosures filled with nanofluids. *International Journal Heat Fluid Flow* 29, 1326-1336.

Ramana Murthy, J. V. and G. Nagaraju (2009). Flow of a couple stress fluid generated by a circular cylinder subjected to longitudinal and torsional oscillations. *Contemporary Engineering Sciences* 2, 451-461.

Ramzan, M., M. Farooq, A. Alsaedi and T. Hayat (2013). MHD threedimensional flow of couple stress fluid with Newtonian heating. *The European Physical Journal Plus* 128, 49.

Rashidi, M., N. Vishnu Ganesh, A. Abdul Hakeem and B**.** Ganga (2014). Buoyancy effect on MHD flow of

Sinha, P. and C. Singh (1984). Effects of couple stresses on the blood flow through an artery with mild stenosis. *Biorheology* 21, 303-315.

Stokes, V. K. (1966). Couple stresses in fluids. *Physics of Fluids* 9, 1709-1715.

Chapter 5

Unsteady natural convective boundary-layer flow of MHD nanofluid over a stretching surfaces with chemical reaction using the spectral relaxation method: A revised model

In this chapter we consider two types of nanofluids, namely copper-water and silver-water embedded with dust particles. The cross-diffusion effects arise in abroad range of fluid flow situations in many areas of science and engineering. Here we chose the revised nanofluid boundary condition which is more realistic than the previously discussed nanofluid models. Again, here, the cross-diffusion, the combined significance of Brownion motion and the thermophoresis parameters in nanofluids have a significant impact on heat and mass transfer processes. The temperature distribution on a silver-water nanofluid is higher than on a copper-water nanofluid, and for this reason it is important to know that the thermal conductivity of silver-water is less than that of copper-water. The concentration boundary layer thickness is higher in copper-water than in a silver-water nanofluid. The model equations for the conservation of momentum, heat and solute concentration transfer rates are solved using the spectral relaxation method.

Available online at www.sciencedirect.com

ScienceDirect

Procedia Engineering 127 (2015) 18 – 24

Procedia Engineering

www.elsevier.com/locate/procedia

International Conference on Computational Heat and Mass Transfer-2015

Unsteady natural convective boundary-layer flow of MHD nanofluid over a stretching surfaces with chemical reaction using the spectral relaxation method: A revised model

Nageeb A.H. Haroun, Sabyasachi Mondal*, Precious Sibanda

School of Mathematics, Statistics and Computer Science, University of KwaZulu-Natal, Private Bag X01 Scottsville 3209, Pietermaritzburg, South Africa

Abstract

We investigate heat and mass transfer in an unsteady MHD nanofluid boundary layer flow due to a stretching surface. The traditional model which here includes the effects of Brownian motion and thermophoresis is revised, so that the nanofluid particle volume fraction on the boundary is passively rather than actively controlled. In this respect the problem is more realistic. This problem is modeled using systems of nonlinear partial differential equations which have been solved numerically using the spectral relaxation method. The results are benchmarked with previously published results.

Peer-review under responsibility of the organizing committee of ICCHMT – 2015

Keywords: MHD Nanofluids; chemical reaction parameter; spectral relaxation method.

1. Introduction

The mathematical study over stretching sheet is increasing recent years due it's importance in science and engineering ([1]). The nanofluid represents a liquid in which nanoscale particles are suspended in a base fluid with low thermal conductivity such as water, oils, rthylene glycol etc. In recent years, the concept of nanofluid has been proposed as a route for increasing the performance of heat transfer in liquids. The model for a nanofluid including the effects of Brownian motion and thermophoresis, introduced by Buongiorno [2] which was carried out by Kuznetsov and Nield [3] to the classical problem. In their pioneering problem they employed boundary conditions on the nanoparticle volume fraction. MHD flow, heat and mass transfer has many important technological and industrial applications such as micro MHD pumps, micromixing of physiological samples and drug delivery. Recently, on unsteady MHD mixed convection in a nanofluid due to a stretching/shrinking surface with suction/injection using a spectral relaxation method were reported by Haroun et al. [4]. The aim of the present study is to analyze the effects of Brownian motion and thermophoresis parameters on a boundary condition that is more realistic physically. In a recent paper, Kuznetsov

* Corresponding author. Tel.: +27-620908146.
E-mail address: sabya.mondal.2007@gmail.com

Peer-review under responsibility of the organizing committee of ICCHMT – 2015
doi:10.1016/j.proeng.2015.11.317

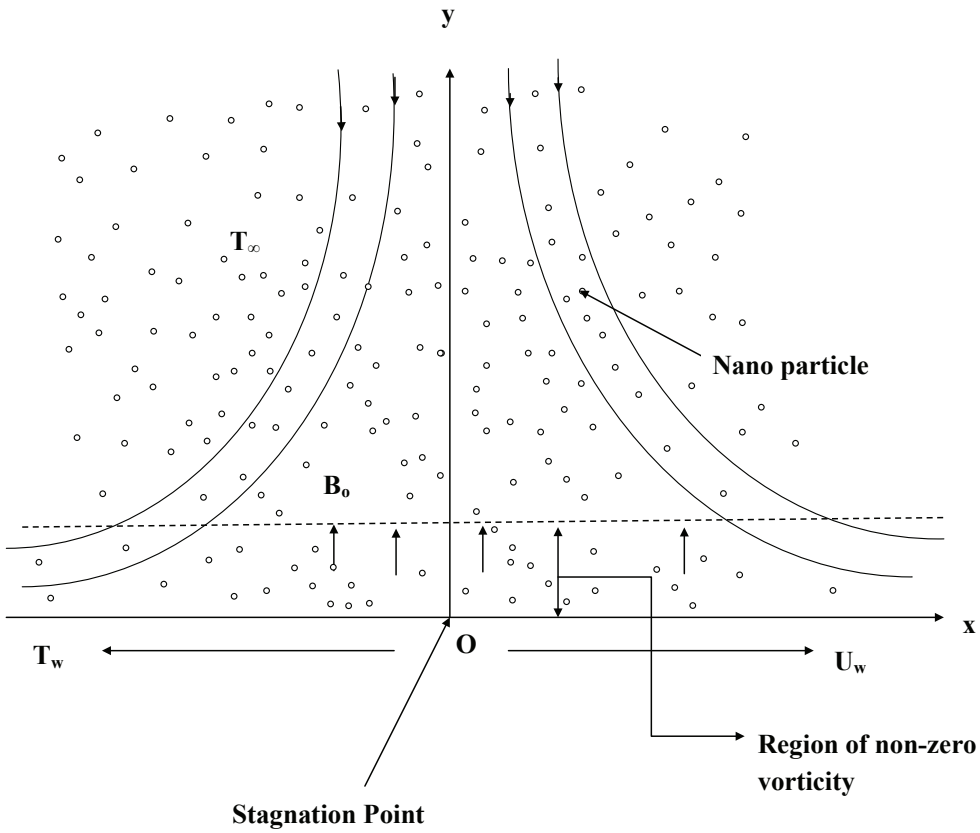

Fig. 1. Geometry of the physical model.

and Nield [5] suggested that the nanoparticle volume fraction flux at the boundary cannot be actively controlled. Very recently, Haroun et al. [12] investigated heat and mass transfer in a magnetohydrodynamic nanofluid flow due to an impulsively started stretching surface. The mathematical problem with this type of boundary conditions has not been studied extensively on previous studies on an unsteady nanofluid in presence of chemical reaction and magnetic field. In this study we solve this type of problem numerically by using spectral relaxation method (Motsa [6]).

2. Governing Equations

Consider the two-dimensional Unsteady natural convective boundary-layer flow of heat and mass transfer nanofluid past a vertical platesituated at $y = 0$ with stretching velocity $u(x) = ax$ where a is a positive constant as shown in Figures 1. At the surface both the nanofluid and the sheet are kept at a constant temperature T_w where $T_w > T_\infty$ is for a heated stretching surface and $T_w < T_\infty$ corresponds to a cooled surface. The boundary layer temperature and nanoparticle volume concentration are T and $\hat{\phi}$ respectively. The ambient fluid temperature and nanoparticle volume fraction are T_∞ and $\hat{\phi}_\infty$ respectively. Using the Boussinesq and the boundary layer approximations, the governing equations are,

$$\frac{\partial u}{\partial x} + \frac{\partial v}{\partial y} = 0, \tag{1}$$

$$\frac{\partial u}{\partial t} + u\frac{\partial u}{\partial x} + v\frac{\partial u}{\partial y} = \frac{\mu_{nf}}{\rho_{nf}}\frac{\partial^2 u}{\partial y^2} + g\beta_T(T - T_\infty) - \frac{\sigma B_0^2}{\rho_{nf}}u, \tag{2}$$

$$\frac{\partial T}{\partial t} + u\frac{\partial T}{\partial x} + v\frac{\partial T}{\partial y} = \alpha_{nf}\frac{\partial^2 T}{\partial y^2} + \tau^*\left[D_B\frac{\partial \hat{\phi}}{\partial y}\frac{\partial T}{\partial y} + \frac{D_T}{T_\infty}\left(\frac{\partial T}{\partial y}\right)^2\right], \tag{3}$$

$$\frac{\partial \hat{\phi}}{\partial t} + u\frac{\partial \hat{\phi}}{\partial x} + v\frac{\partial \hat{\phi}}{\partial y} = D_B\frac{\partial^2 \hat{\phi}}{\partial y^2} + \frac{D_T}{T_\infty}\frac{\partial^2 T}{\partial y^2} - K(\hat{\phi} - \hat{\phi}_\infty), \tag{4}$$

where u and v are the fluid velocity and normal velocity components along $x-$ and $y-$directions respectively, μ_{nf}, ρ_{nf}, σ, B_0, g are the the effective dynamic viscosity of the nanofluid, nanofluid density, electrical conductivity, the uniform magnetic field in the y-direction and gravitational acceleration, β_T, T, $\hat{\phi}$, α_{nf}, $\tau^*(= (\rho c)_p/(\rho c)_f)$ are the volumetric thermal expansion coefficient, volumetric solutal expansion coefficient, temperature of fluid in the boundary layer, nanoparticle volume fraction, the thermal diffusivity of the nanofluid, the ratio of effective heat capacity of the nanoparticle material to heat capacity of the fluid, D_B, D_T, T_∞, K are the Brownian motion coefficient, the thermophoretic diffusion coefficient, mean fluid temperature and the chemical reaction parameter.
The boundary conditions

$$\begin{aligned} &t \geq 0 \ : u = U_w(x) = ax,\ v = 0,\ T = T_{\mathrm{w}},\ D_B\frac{\partial \hat{\phi}}{\partial y} + \frac{D_T}{T_\infty}\frac{\partial T}{\partial y} = 0 \quad \text{at} \quad y = 0, \\ &t \geq 0 \ : u, v \to 0,\ T \ \to T_\infty,\ \hat{\phi} = \hat{\phi}_\infty, \quad \text{as} \quad y \to \infty, \end{aligned} \tag{5}$$

where a is the stretching/shrinking rate and stagnation flow rate parameters, with $a < 0$ for shrinking, $a > 0$ for a stretching. The effective dynamic viscosity of the nanofluid was given by Brinkman [7] as

$$\mu_{nf} = \frac{\mu_f}{(1-\phi)^{2.5}}, \tag{6}$$

$$(\rho c_p)_{nf} = (1-\phi)(\rho c_p)_f + \phi(\rho c_p)_s, \rho_{nf} = (1-\phi)\rho_f + \phi\rho_s, \quad \nu_{nf} = \frac{\mu_{nf}}{\rho_{nf}},$$

$$\alpha_{nf} = \frac{k_{nf}}{(\rho c_p)_{nf}}, \ \frac{k_{nf}}{k_f} = \frac{(k_s + k_f) - 2\phi(k_f - k_s)}{(k_s + k_f) + \phi(k_f - k_s)}, \tag{7}$$

where ϕ and μ_f are the solid volume fraction of nanoparticles and the dynamic viscosity of the base fluid. In equations (1) to (4) and ν_{nf}, ρ_{nf}, $(\rho cp)_{nf}$, k_{nf}, k_f, k_s, ρ_s, $(\rho c_p)_f$, $(\rho c_p)_s$ are the nanofluid kinematic viscosity, the density of nanofluid, the nanofluid heat capacitance, thermal conductivity of the nanofluid, thermal conductivity of the fluid, the thermal conductivity of the solid fractions, the density of the solid fractions, the heat capacity of base fluid, the effective heat capacity of nanoparticles, respectively.
The continuity equation is satisfied by introducing a stream function $\psi(x, y)$ and the following non-dimensional variables, (see Liao [8]) such that

$$u = \frac{\partial \psi}{\partial y}, \ \ v = -\frac{\partial \psi}{\partial x}. \tag{8}$$

$$\psi = \left[a\nu_f\xi\right]^{\frac{1}{2}}\ xf(\xi,\eta),\ \xi = 1 - \exp(-\tau),\ \ \tau = a\,t,\ \eta = \left[\frac{a}{\nu_f\xi}\right]^{\frac{1}{2}}\ y, \tag{9}$$

$$\theta(\xi,\eta) = \frac{T - T_\infty}{T_{\mathrm{w}} - T_\infty},\ \Phi(\xi,\eta) = \frac{\hat{\phi}}{\hat{\phi}_\infty}, \tag{10}$$

where η, ξ and τ are dimensionless variables and the dimensionless time, $f(\xi, \eta)$ is the dimensionless stream function, $\theta(\xi, \eta)$ is the dimensionless temperature and $\phi(\xi, \eta)$ is the dimensionless solute concentration.
We get the dimensionless governing equationa by using the dimensionless variables

$$f''' + \phi_1\left[(1-\xi)\frac{1}{2}\,\eta f'' + \xi\left(ff'' - f'^2 - Mf' + Gr_t\theta\right)\right] = \phi_1\xi(1-\xi)\frac{\partial f'}{\partial \xi}, \tag{11}$$

$$\theta'' + \phi_2 Pr\left(\frac{k_f}{k_{nf}}\right)\left[(1-\xi)\frac{1}{2}\,\eta\theta' + \xi f\theta' + N_b\theta'\Phi' + N_t\theta'^2\right] = \phi_2 Pr\left(\frac{k_f}{k_{nf}}\right)\xi(1-\xi)\frac{\partial \theta}{\partial \xi}, \tag{12}$$

$$\Phi'' + Sc\left[(1-\xi)\frac{1}{2}\,\eta\Phi' + \xi f\Phi'\right] + \frac{N_t}{N_b}\theta'' - \gamma\xi Sc\Phi = Sc\xi(1-\xi)\frac{\partial \Phi}{\partial \xi}, \tag{13}$$

subject to the boundary conditions

$$f(\xi,0)=0,\ \ f'(\xi,0)=1,\ \theta(\xi,0)=1,\ N_b\Phi'+N_t\theta'=0,\ \ \eta=0\,,\quad \xi\geq 0,$$
$$f'(\xi,\infty)=0,\ \theta(\xi,\infty)=0,\ \Phi(\xi,\infty)=0,\quad \eta\longrightarrow\infty,\quad \xi\geq 0. \tag{14}$$

Where primes denote differentiation with respect to η, $\alpha_f = k_f/(\rho c_p)_f$ and $\nu_f = \mu_f/\rho_f$ are the thermal diffusivity and kinetic viscosity of the base fluid, respectively. Other non-dimensional parameters appearing in equations (11) to (13) are Ha, Gr_t, Pr, N_b, N_t, Sc, and γ denote the Magnetic parameter, local temperature Grashof number, Prandtl number, Brownian motion parameter and thermal phoresis parameter, the Schmidt number and scaled chemical reaction parameter. These parameters are defined mathematically as

$$M=\frac{\sigma B_0^2}{a\rho_{nf}}\,, Gr_t=\frac{g\beta_T(T_w-T_\infty)x^3}{\nu_f^2},\ Pr=\frac{\nu_f}{\alpha_f},$$
$$N_b=\frac{(\rho_c)_p D_B\Phi_\infty}{\nu_f(\rho_p)_f},\ Sc=\frac{\nu_f}{D_B},\ \gamma=\frac{K}{a},\ N_t=\frac{(\rho_c)_p\, D_T(T_w-T_\infty)}{T_\infty\nu_f(\rho_p)_f}. \tag{15}$$

The nanoparticle volume fraction ϕ_1 and ϕ_2 are defined as

$$\phi_1=(1-\phi)^{2.5}\left[1-\phi+\phi\left(\frac{\rho_s}{\rho_f}\right)\right],\quad \phi_2=\left[1-\phi+\phi\frac{(\rho c)_s}{(\rho c)_f}\right]. \tag{16}$$

The skin friction coefficient, local Nusselt number are obtained as

$$C_{fx}=\frac{2\tau_w}{\rho_f U_w^2}, Nu_x=\frac{xq_w}{k_f\,(T_w-T_\infty)}. \tag{17}$$

The reader will note that the dimensionless mass flux represented by a Sherwood number Sh_x is now identically zero due to the revised nanofluid model.

3. Results and Discussion

Table 1. Comparison of the SRM solutions for $f''(\xi,0)$ for different values of ξ when the other parameters are same as those published papers

	Kechil and Hashim [10]	Srinivasa and Eswara [11]	Present Results
ξ			
0.0	-0.5643740	-0.5643740	-0.5641896
0.1	-0.6150550	-0.6106120	-0.6104676
0.3	-0.7115696	-0.7115610	-0.7115697
0.9	-0.9633761	-0.9623398	-0.9623380
1.0	-1.0000000	-1.0000000	-1.0000019

The equations (11) to (13) are solved using the SRM (Motsa [6]). The thermophysical properties of the nanofluids used in the numerical simulations are given in [9]. Extensive calculations have been performed to obtain the velocity, temperature, concentration profiles as well as skin friction etc for various values of physical parameters such as ϕ, M, Gr_t, Pr, N_b, N_t, Sc and γ. To determine the accuracy of our numerical results, the skin friction coefficient is compared with the published results of Kechil and Hashim [10], Srinivasa and Eswara [11] in Tables 1. Here we have varied the ξ while keeping other physical parameters fixed. Table 1 gives a comparison of the SRM results with those obtained by Kechil and Hashim [10], Srinivasa and Eswara [11] when $Gr_t = \gamma = \phi = 0$, $Pr = 7$, $Sc = 0.4$ and $M = 0.0$ for different values of the ξ. It is observed that the present results are in good agreement with the previously published results.

The effects of the nanoparticle volume fraction and M on the fluid velocity, temperature, concentration profiles as well as on skin friction are shown in Figures 2 - 4. From Figures 2 - 3, it is evident that the solute concentration decreases with increasing nanoparticle volume fraction while the velocity and temperature skin friction increase. This is because

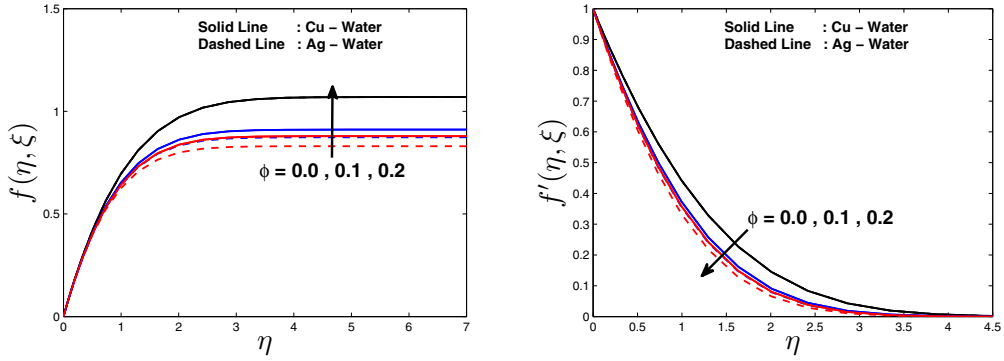

(a) Velocity profiles (b) Velocity profiles

Fig. 2. Effect of various nanoparticle values fraction ϕ on (a) and (b) for $Gr_t = 0.2$, $M = 0.2$, $N_t = 0.01$, $Pr = 7$, $N_b = 0.01$, $\gamma = 1$, $Sc = 1$ and $\xi = 0.5$.

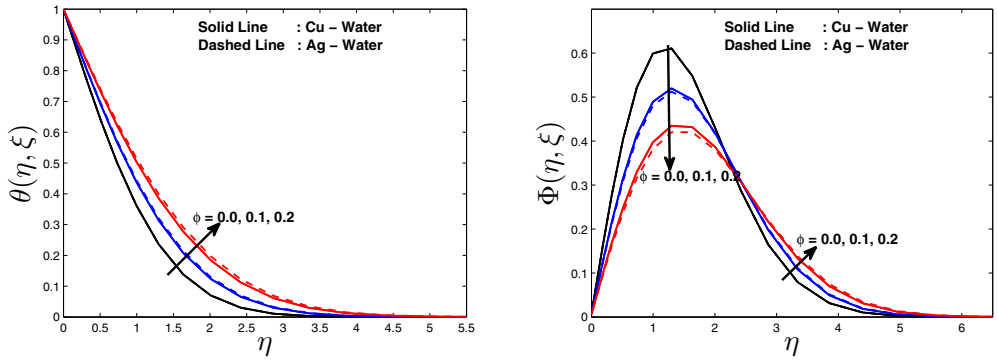

(a) Temperature profiles (b) Concentration profiles

Fig. 3. Effect of various nanoparticle values fraction ϕ on (a) and (b) for $Gr_t = 0.2$, $M = 0.2$, $N_t = 0.01$, $Pr = 7$, $N_b = 0.01$, $\gamma = 1$, $Sc = 1$ and $\xi = 0.5$.

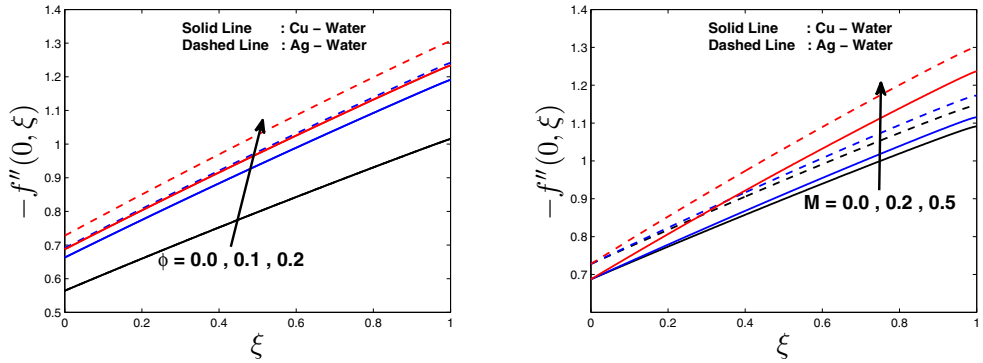

(a) Skin friction coefficient (b) Skin friction coefficient

Fig. 4. Effect of various nanoparticle values fraction ϕ and Magnetic parameter M respectively, on Skin friction coefficient for $Gr_t = 0.2$, $N_t = 0.01$, $Pr = 7$, $N_b = 0.01$, $\gamma = 1$ and $Sc = 1$.

with an increase in nanoparticles volume fraction, the thermal conductivity of the nanofluid increases, which reduces the thermal boundary layer thickness and the temperature gradient at the wall. The axial velocity in the case of an Ag-water nanofluid is comparatively less than that in the case of a Cu-water nanofluid. The temperature distribution in an Ag-water nanofluid is higher than that in a Cu-water nanofluid and this is explained by the observation that the thermal conductivity of silver is less than that of copper. The concentration boundary layer thickness is higher for the case of a Cu-water than that for the case of an Ag-water nanofluid. Figure 4 (a) and (b) show that the skin friction coefficients $-f''(0,\xi)$ increases monotonically with increasing ξ. The result is true for both types of nanofluids. The minimum value of the skin friction in the case of a Cu-water nanofluid is achieved at a smaller value of ξ in comparison with a Ag-water nanofluid. Furthermore, in this paper it is found that the Ag-water nanofluid shows higher drag as compared to the a Cu-water nanofluid. The maximum value of the skin friction in the case of a Ag-water nanofluid is achieved at the value of $\xi = 1$ in comparison with an Cu-water nanofluid in two figures (a) and (b)respectively.

4. Conclusions

We have investigated the heat and mass transfer in an unsteady MHD boundary layer flow in nanofluid due to a stretching surfaces with chemical reaction and an applied magnetic field. From the numerical simulations, some results can be drawn as follow:
[i] The velocity profile increase with increase in the nanoparticle volume fraction while the opposite trend is observed with increase in the value of the nanoparticle volume fraction.
[ii] The temperature and concentration profiles increase with increasing in the values of the nanoparticle volume fraction and thermophoresis parameter while the opposite trend is observed for the concentration profile with increasing in the values of Brownian motion parameter.
[iii] The values of skin friction increase with increase in the values of the nanoparticle volume fraction and magnetic parameter M.

Acknowledgement

This work is supported by the University of KwaZulu-Natal, South Africa.

Conflict of Interest

The authors declare that there is no conflict of interests regarding the publication of this article.

References

[1] T.R. Mahapatra, S. Mondal, D. Pal, Heat transfer due to magnetohydrodynamic stagnation-point flow of a power-law fluid towards a stretching surface in the presence of thermal radiation and suction/injection, ISRN Thermodynamics, 2012, Article ID 465864, doi:10.5402/2012/465864 128 (2006) 240–250.
[2] J. Buongiorno, Convective transport in nanofluids, Journal of Heat Transf. 128 (2006) 240–250.
[3] A.V. Kuznetsov, D.A. Nield, Natural convective boundary layer flow of a nanofluid past a vertical plate, International Journal Thermal Sciences, 49 (2010) 243–247.
[4] A.H. Nageeb, P. Sibanda, S. Mondal, S.S. Motsa, On unsteady MHD mixed convection in a nanofluid due to a stretching/shrinking surface with suction/injection using the spectral relaxation method, Boundary Value Problems, 24 (2015) DOI 10.1186/s13661–015–0289–5.
[5] A.V. Kuznetsov, D.A. Nield, Natural convective boundary layer flow of a nanofluid past a vertical plate: A revised model, International Journal Thermal Sciences, 77 (2014) 126–129.
[6] S.S. Motsa, A New spectral relaxation method for similarity variable nonlinear boundary layer flow systems, Chemical Engineering Communications, 201 (2014) 241–256.
[7] H.C. Brinkman, The viscosity of concentrated suspensions and solution, The Journal of Chemical Physics, 20 (1952) 571.
[8] S.J. Liao, An analytic solution of unsteady boundary layer flows caused by an impulsively stretching plate, Communications in Nonlinear Science and Numerical Simulation, 11 (2006) 326–329.
[9] M. Sheikholeslami, M.G. Bandpy, D.D. Ganji, S. Soleimani, S.M. Seyyedi, Natural convection of nanofluids in an enclosure between a circular and a sinusoidal cylinder in the presence of magnetic field, International Communications in Heat and Mass Transf. 39 (2012) 1435–1443.

[10] S.A. Kechil, I. Hashim, Series solution for unsteady boundary-layer flows due to impulsively stretching plate, Chinese Physics Letters, 24 (2007) 139–142.
[11] A.H. Srinivasa, A.T. Eswara, Unsteady MHD Laminar boundary layer flow due to an impulsively stretching surface, Proceedings of the World Congress on Engineering, WCE, July 6-8, London, U.K. 2011.
[12] A.H. Nageeb, P. Sibanda, S. Mondal, S.S. Motsa, M.M. Rashidi, Heat and mass transfer of nanofluid through an impulsively vertical stretching surface using the spectral relaxation method, Boundary Value Problems, 2015 (2015) 161, DOI 10.1186/s13661-015-0424-3.

Chapter 6

The effects of thermal radiation on an unsteady MHD axisymmetric stagnation-point flow over a shrinking sheet in presence of temperature dependent thermal conductivity with navier slip

In this chapter we investigate unsteady MHD axisymmetric stagnation-point flow with Navier slip conduction. The surface is assumed to be a two-dimensional plane and flow is permeated by a uniform magnetic field normal to the surface. We discuss two different types of heat transfer processes namely a prescribed surface temperature (PST) and a prescribed surface heat flux (PHF) and evaluate how the various parameters affect the fluid flow, heat transfer and temperature field. The temperature profiles in the two cases of PST and PHF are shown to increase with the thermal radiation parameter, which in turn increases the thermal boundary layer thickness. The SRM is used to solve the problem.

PLOS | ONE

RESEARCH ARTICLE

The Effects of Thermal Radiation on an Unsteady MHD Axisymmetric Stagnation-Point Flow over a Shrinking Sheet in Presence of Temperature Dependent Thermal Conductivity with Navier Slip

Sabyasachi Mondal*, Nageeb A. H. Haroun, Precious Sibanda

University of KwaZulu-Natal, School of Mathematics, Statistics and Computer Science, Private Bag X01, Scottsville, Pietermaritzburg 3209, South Africa

* sabya.mondal.2007@gmail.com

Citation: Mondal S, Haroun NAH, Sibanda P (2015) The Effects of Thermal Radiation on an Unsteady MHD Axisymmetric Stagnation-Point Flow over a Shrinking Sheet in Presence of Temperature Dependent Thermal Conductivity with Navier Slip. PLoS ONE 10(9): e0138355. doi:10.1371/journal.pone.0138355

Editor: Saeed Islam, Abdul Wali Khan University Mardan Pakistan, PAKISTAN

Received: April 24, 2015

Accepted: August 29, 2015

Published: September 28, 2015

Data Availability Statement: All the data underlying the findings are fully available without restriction.

Funding: This work is funded by the University of KwaZulu-Natal through SM's postdoctoral fellowship.

Competing Interests: The authors have declared that no competing interests exist.

Abstract

In this paper, the magnetohydrodynamic (MHD) axisymmetric stagnation-point flow of an unsteady and electrically conducting incompressible viscous fluid in with temperature dependent thermal conductivity, thermal radiation and Navier slip is investigated. The flow is due to a shrinking surface that is shrunk axisymmetrically in its own plane with a linear velocity. The magnetic field is imposed normally to the sheet. The model equations that describe this fluid flow are solved by using the spectral relaxation method. Here, heat transfer processes are discussed for two different types of wall heating; (a) a prescribed surface temperature and (b) a prescribed surface heat flux. We discuss and evaluate how the various parameters affect the fluid flow, heat transfer and the temperature field with the aid of different graphical presentations and tabulated results.

1 Introduction

The study of an unsteady fluid flow toward a stretching/shrinking sheet has great importance due to its various applications in science and engineering. Some often given examples in this regard include metal rolling, drawing and pultrusion. Heat transfer in such flows with both constant and variable wall temperature was investigated by Gupta and Gupta [1] and also investigated by Carragher and Crane [2]. Work on unsteady MHD flow with ramped wall temperature has been done by Khan et al.[3], Samiulhaq [4] and Khalid [5]. Wang [6] investigated the steady flow through a flat surface of a viscous fluid which is stretched in its own plane in two perpendicular directions. MHD free convection of unsteady flow in a porous medium with Newtonian heating and constant mass diffusion was studied by Hussanan [7]. Pavlov [8] studied exact similarity solution of the steady two-dimensional boundary layer flow equations in presence of magnetic field of an electrically conducting fluid due to the stretching of an elastic

surface in the presence of a uniform transverse magnetic field. Mabood et al. [9] solved the differential equations of the model flow and heat transfer in an axisymmetric channel using the optimal homotopy asymptotic method. Homann [10] studied three dimensional axisymmetric stagnation-point flow using a similarity transform for reducing the Navier-Stokes equations to third order ordinary differential equations.

Chiam [11] investigated steady axisymmetric stagnation-point flow of a viscous fluid over an axisymetrically stretched surface. Mahapatra and Gupta [12] examined axisymmetric stagnation-point flow of an incompressible viscous fluid towards a stretching surface. Axisymmetric stagnation-point flow in presence of a uniform magnetic field towards a stretching surface with heat generation was investigated by Attia [13].

Considerable interest has been shown on the boundary layer flow over a shrinking sheet in recent years. Some of the applications of the shrinking sheet problem in industry relate to the shrinking film that is can be unwrapped easily with adequate heat and used in the packaging of bulk products. The shrinking fluid flow study, which is essentially a backward flow, can also be applied to the study of hydraulic properties of agricultural clay soils, capillary effects in the shrinking-swell behaviour and small pores. The related changes in mechanical and hydraulic studies of such soils have a significant impact on the behaviour and the transport properties of the fluid. The fluid loses the memory of the perturbation produced by the slot for this backward flow configuration. Due this reason, the fluid flow due to a shrinking sheet has some quite distinct physical characteristics compared to the forward stretching case.

Miklavcic and Wang [14] studied axisymmetric flow with uniform suction induced by a shrinking surface. Wang [15] examined heat transfer from a shrinking sheet due to a steady two-dimensional axisymmetric stagnation-point flow. Qasim et al. [16] examined heat transfer in the case of a micropolar fluid through a stretching sheet with Newtonian heating. Recently, Mahapatra and Nanday [17] studied heat transfer in an axisymmetric stagnation-point flow in the presence of a magnetic field. Qayyum et al. [18] presented an analysis of unsteady axisymmetric squeezing fluid flow with slip boundary conditions through a porous channel. Some recent studies of boundary layer flow in presence of a magnetic field include those of Mabood and his group [19–21]. For the case of a nonlinearly stretching sheet, we note the work of Khan et al. [22].

In this paper, we generalize the study of MHD fluid flow with an unsteady conditions through a shrinking sheet including a temperature dependent thermal conductivity, radiation and a Navier slip condition. The surface with prescribed surface temperature (PST) and surface with prescribed wall heat flux (PHF) are considered as two examples of non-isothermal boundary conditions.

Ethical Statement: This study involved only numerical simulations and the analysis of fluid flow.

2 Formulation

Here, we consider the unsteady axisymmetric stagnation-point flow of an electrically conducting incompressible fluid from the surface which is shrunk axisymmetrically. We have used Cartesian axes instead of cylindrical axes due to possible non-alignment, Wang [15]. The flow configuration is shown in Fig 1. In this frame of reference, let the velocity components are u, v and w in the x- direction, y- direction and z-direction, respectively.

At the surface the fluid velocity components are

$$u = \frac{(l+x)c}{1-\lambda t}, \quad v = \frac{cy}{1-\lambda t} \quad \text{and} \quad w = 0,$$

where $-l$ is the location of the origin and c (< 0) denotes the shrinking rate (and if $c > 0$ the it

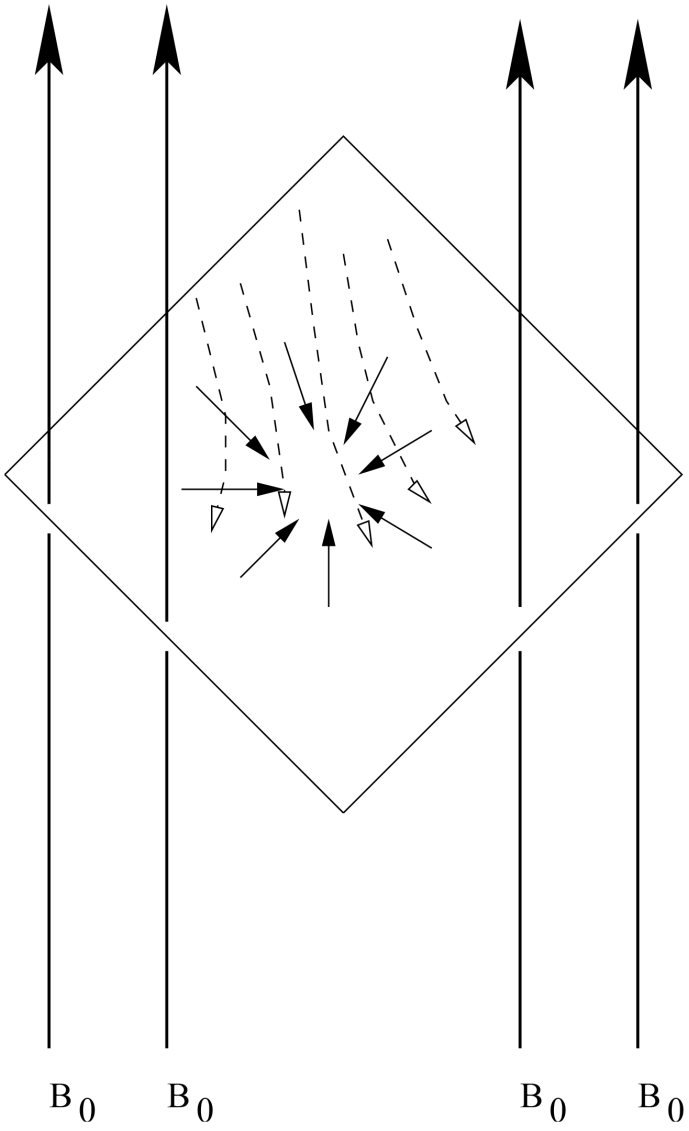

Fig 1. A sketch of the physical problem.

doi:10.1371/journal.pone.0138355.g001

denotes stretching rate). Here the sheet shrinkage is along the negative x-axis. Note that the stretching axis and the point flow are not always aligned (that is, $l \neq 0$).

The velocity components in the ambient region are given by

$$U = \frac{ax}{1-\lambda t}, \; V = \frac{ay}{1-\lambda t} \quad \text{and} \quad W = -\frac{2az}{1-\lambda t},$$

where a (> 0) is a constant that is a measure of the strength of the stagnation-point flow and λ quantifies the unsteadiness of the problem. For a decelerating shrinking sheet $\lambda < 0$ whereas for an accelerating sheet $\lambda > 0$. The magnetic field B_0 is imposed in the normal direction to the surface i.e., parallel to z-axis.

The continuity and momentum equations are (Bansal [23])

$$\frac{\partial u}{\partial x}+\frac{\partial v}{\partial y}+\frac{\partial w}{\partial z}=0, \tag{1}$$

$$\frac{\partial u}{\partial t}+u\frac{\partial u}{\partial x}+w\frac{\partial u}{\partial z}=-\frac{1}{\rho}\frac{\partial p}{\partial x}+\nu\frac{\partial^2 u}{\partial z^2}-\frac{\sigma B_0^2 u}{\rho}. \tag{2}$$

The pressure gradient in the free stream can be obtained from Eq (2) as

$$\frac{1}{\rho}\frac{\partial p}{\partial x}=-\frac{\partial U}{\partial t}-U\frac{\partial U}{\partial x}-\frac{\sigma B_0^2 U}{\rho}, \tag{3}$$

so that Eq (2) becomes

$$\frac{\partial u}{\partial t}+u\frac{\partial u}{\partial x}+w\frac{\partial u}{\partial z}=\frac{\partial U}{\partial t}+U\frac{\partial U}{\partial x}+\nu\frac{\partial^2 u}{\partial z^2}+\frac{\sigma B_0^2}{\rho}(U-u). \tag{4}$$

The appropriate boundary conditions with velocity partial slip are given by (see Jat and Rajotia [24]);

$$u = u_w(x,t)+L_1\nu\frac{\partial u}{\partial z}, \quad v=cy/(1-\lambda t), \quad w=0 \quad \text{at} \quad z=0, \tag{5}$$

$$u \rightarrow U(x,t)=ax/(1-\lambda t), \qquad \text{as} \qquad z\rightarrow\infty. \tag{6}$$

where $a(>0)$ is a constant. For the u-component boundary condition, we have assumed a velocity slip. This is proportional to local shear stress with slip factor $L_1 = L(1-\lambda t)^{1/2}$ where L is the initial velocity. Note that the essential slip factor L_1 changes with time and has dimensions (velocity)$^{-1}$. The velocity

$$u_w(x,t)\ (=c(x+l)/(1-\lambda t)), \tag{7}$$

is valid for time $t<\lambda^{-1}$.

We introduce the following similarity transformations to transform the govering equations

$$u=\frac{[a\,x\,f'(\eta)+c\;l\;h(\eta)]}{1-\lambda t}, \quad v=\frac{ayf'(\eta)}{1-\lambda t}, \; w=-2\sqrt{\frac{a\nu}{1-\lambda t}}\,f(\eta), \tag{8}$$

where

$$\eta=z\left(\frac{a}{\nu(1-\lambda t)}\right)^{1/2}, \tag{9}$$

and differentiation is with respect to η. Eqs (8) and (1) is identically satisfied. Substituting Eqs (8) and (9) in Eq (4) and equating the coefficients of x^0 and x^1, we obtain the coupled non-linear differential equations

$$f'''+2ff''-f'^2+1+M^2(1-f')-\beta\left[\frac{\eta}{2}f''+f'-1\right]=0, \tag{10}$$

$$h''+2fh'-hf'-M^2h-\beta\left[\frac{\eta}{2}h'+h\right]=0, \tag{11}$$

where $B=B_0\sqrt{(1-\lambda t)}$. In Eqs (10) and (11), $\beta=(\lambda/a)$ and $M=(\sigma B^2/a\rho)^{1/2}$ are respectively

the unsteadiness parameter and the magnetic parameter characterizing the strength of the imposed magnetic field.

The appropriate boundary conditions are obtained from Eqs (5) and (6) as

$$f(0) = 0, \qquad f'(0) = \alpha + \delta f''(0), \qquad f'(\infty) = 1, \tag{12}$$

$$h(0) = 1, \qquad h(\infty) = 0, \tag{13}$$

here $\delta = L(av)^{1/2}$ is the dimensionless velocity slip parameter and $\alpha = (c/a)$ is the velocity ratio parameter. It is worth mentioning that the non-dimensional velocity slip parameter (δ) is always positive.

The non-dimensional velocity components is be introduced from the Eq (8) as

$$u^* = u\sqrt{\frac{(1-\lambda t)}{av}} = \xi f'(\eta) + \alpha\ L\ h(\eta), \tag{14}$$

$$w^* = w\sqrt{\frac{(1-\lambda t)}{av}} = -2f(\eta), \tag{15}$$

where

$$\xi = x\left(\frac{a}{v(1-\lambda t)}\right)^{1/2} \quad \text{and} \quad L = l\left(\frac{a}{v(1-\lambda t)}\right)^{1/2}. \tag{16}$$

The dimensionless wall shear stress τ is then given by

$$\tau = \xi f''(0) + \alpha\ L\ h'(0). \tag{17}$$

3 Heat transfer

The unsteady heat equation for a fluid with viscous and ohmic heating and variable thermal conductivity is given by (see Chiam [25])

$$\frac{\partial T}{\partial t} + \rho c_p\left(u\frac{\partial T}{\partial x} + w\frac{\partial T}{\partial z}\right) = \frac{\partial}{\partial z}\left(\kappa(T)\frac{\partial T}{\partial z}\right) + \mu\left(\frac{\partial u}{\partial z}\right)^2 + \sigma B_0^2(u-U)^2 - \frac{\partial q_r}{\partial z}, \tag{18}$$

where$\kappa(T)$, c_p and q_r are the temperature dependent thermal conductivity, the specific heat at constant pressure and the radiative heat flux of the fluid, respectively. The second term on the right hand side of Eq (18) represents the viscous dissipation in the flow; the third term stands for the dissipation of the magnetic energy in the form of Joule heating (Shercliff [26]) while the last term is due to the thermal radiation. Here, the temperature dependent thermal conductivity is written in the form (see Chiam [25])

$$\kappa(T) = \kappa_\infty\left[1 + \frac{\epsilon}{\Delta T}\right], \tag{19}$$

where κ_∞ denotes the conductivity of the fluid away from the surface, $\Delta T = T_w - T_\infty$, T_∞ and T_w are free stream temperature and the sheet temperature. ϵ is a small parameter. Substituting Eq (19) into Eq (18), gives

$$\frac{\partial T}{\partial t} + \rho c_p u\frac{\partial T}{\partial x} + \left(\rho c_p w - \frac{\kappa_\infty \epsilon}{\Delta T}\frac{\partial T}{\partial z}\right)\frac{\partial T}{\partial z} = \kappa(T)\frac{\partial^2 T}{\partial z^2} + \mu\left(\frac{\partial u}{\partial z}\right)^2 + \sigma B_0^2(u-U)^2 - \frac{\partial q_r}{\partial z}, \tag{20}$$

where the radiation heat flux q_r is defined as

$$q_r = -\frac{4\sigma^*}{3k^*}\frac{\partial T^4}{\partial z}, \tag{21}$$

where k^* is the Rosseland mean absorption coefficient and σ^* is denoted as the Stefan-Boltzmann constant. Here, Taylor series expansion is used to expand the temperature variation T^4 about T_∞, and on neglecting higher order terms we obtain, $T^4 \cong 4T_\infty^3 T - 3T_\infty^4$. Eq (20) becomes

$$\frac{\partial T}{\partial t} + \rho c_p u\frac{\partial T}{\partial x} + \left(\rho c_p w - \frac{\kappa_\infty \epsilon}{\Delta T}\frac{\partial T}{\partial z}\right)\frac{\partial T}{\partial z} = \left(\kappa(T) + \frac{16\sigma^*}{3k^*}\right)\frac{\partial^2 T}{\partial z^2} + \mu\left(\frac{\partial u}{\partial z}\right)^2 + \sigma B_0^2(u-U)^2. \tag{22}$$

The thermal boundary conditions may vary depending on the different types of heating processes under consideration. In this study, prescribed surface temperature and prescribed wall heat flux conditions are considered as two different examples of heating processes.

3.1 Case 1: Prescribed Surface Temperature (PST)

We assume that the prescribed wall temperature is a quadratic function in x (see Mahapatra and Nanday [17]) given by,

$$T_w = T_\infty + A(x/l_1)^2(1-\lambda t)^{-3/2} \quad \text{at} \quad z = 0, \tag{23}$$

$$T \to T_\infty \quad \text{as} \quad z \to \infty, \tag{24}$$

where A is a constant, T_w is the variable wall temperature and l_1 is a reference length. The dimensionless temperature θ is defined as

$$\theta = \frac{T - T_\infty}{T_w - T_\infty}. \tag{25}$$

Substituting Eqs (23) and (25) into Eq (22), we get

$$\begin{aligned}(1+\epsilon\theta+N_r)\theta'' + \epsilon\theta'^2 + Pr[2f\theta' - 2(f' + \alpha RLh)\theta + E_c(f'' + \alpha RLh')^2 \\ + E_c M^2(f' - 1 + \alpha RLh)^2 - \frac{\beta}{2}(\eta\theta' + 3\theta)] = 0,\end{aligned} \tag{26}$$

where $N_r E_c$ and P_r denote the radiation parameter, Eckert and Prandtl numbers, respectively. We defined these physical parameters as follows:

$$N_r = \frac{16\sigma^* T_\infty^3}{3\kappa_\infty k^*}, \quad P_r = \frac{\rho c_p}{\kappa_\infty}, \quad E_c = \frac{a^2 l_1^2}{A_0 c_p}, \quad R = \frac{1}{\xi} \quad A = A_0/\sqrt{1-\lambda t}, \tag{27}$$

with boundary conditions

$$\theta(0) = 1, \qquad \theta(\infty) = 0. \tag{28}$$

3.2 Case 2: Prescribed Wall Heat Flux (PHF)

The heat flux q_w at the surface is assumed to vary as the square of the distance as follows (see Mahapatra and Nanday [17]):

$$-\kappa_\infty \frac{\partial T}{\partial z} = q_w = D(x/l_1)^2(1-\lambda t)^{-3/2} \quad \text{at} \quad z = 0, \tag{29}$$

$$T \to T_\infty \quad \text{as} \quad z \to \infty, \tag{30}$$

where D is a constant. Here we set

$$T - T_\infty = \frac{D}{\kappa_\infty}\sqrt{\frac{\nu}{a}}(x/l_1)^2(1-\lambda t)^{-3/2}g(\eta), \tag{31}$$

so that Eq (22), is transformed into the equation

$$\begin{aligned}(1+\epsilon g+N_r)g''+\epsilon g'^2+Pr[2fg'-2(f'+\alpha RLh)g+E_c(f''+\alpha RLh')^2\\ +E_cM^2(f'-1+\alpha RLh)^2-\frac{\beta}{2}(\eta g'+3g)]=0,\end{aligned} \tag{32}$$

with boundary conditions

$$g'(0)=-1, \qquad g(\infty)=0, \tag{33}$$

where the Eckert number $E_c = \frac{\kappa_\infty a^2 l_1^2\sqrt{a/\nu}}{D_0 c_p}$ and $D = D_0/(1-\lambda t)^{1/2}$. Eq (32) has exactly the same form as Eq (26) but with a different first boundary condition.

4 Method of Solution

Eqs (10), (11) and (26) were solved using the successive relaxation method (SRM), Motsa [27]. The SRM is an iterative procedure that works in a similar fashion to the Gauss-Seidel method for algebraic equations. In this case the technique is used to linearize and decouple a system of differential equations. Further details of the rules of the SRM can be found in [28, 29].

The linear terms in each equation are evaluated at the current iteration level $r+1$ and the non-linear terms are known from the previous iteration level r. The linearized form of Eqs (10), (11) and (26) are

$$f'''_{r+1}+a_{1,r}f''_{r+1}+a_{2,r}f'_{r+1}=R_{1,r}, \tag{34}$$

$$h''_{r+1}+b_{1,r}h'_{r+1}+b_{2,r}h_{r+1}=R_{2,r}, \tag{35}$$

$$(1+\epsilon\theta_r+Nr)\theta''_{r+1}+c_{r,1}\theta'_{r+1}+c_{2,r}\theta_{r+1}=R_{3,r}, \tag{36}$$

where

$$\begin{aligned}&a_{1,r}=2f_r-\frac{\beta\,\eta}{2}, a_{2,r}=\beta+M^2-f'_r,\\ &R_{1,r}=-[f'^2_r+M^2+1+\beta],\\ &b_{1,r}=2f_r-\frac{\beta\,\eta}{2}, \quad b_{2,r}=-[f'_r+M^2+\beta], \quad R_{2,r}=0,\\ &c_{1,r}=2\epsilon\,\theta'_r+2Pr\,f_r-\frac{Pr\beta\,\eta}{2}, \quad c_{2,r}=\epsilon\,\theta''_r-2Pr(f'_{r+1}+\alpha\;R\;L\;h)^2-\frac{3Pr\;\beta}{2},\\ &R_{3,r}=Pr\;E_c[(f''_r+\alpha\;R\;L\;h'_r)^2+M^2(f'_r+\alpha\;R\;L\;h_r)^2]-\epsilon\;\theta''_r\;\theta_r-\epsilon\;\theta'^2_r.\end{aligned}$$

It must be noted that Eqs (34)–(36) are linear and decoupled and can thus be solved sequentially to obtain the quantities $f(\eta)$, $h(\eta)$ and $\theta(\eta)$. We opted in this study to use the Chebyshev spectral collocation method to discretize in η and finite differences with central differencing to discretize in ξ. Starting from initial guesses $f_0(\eta)$, $\theta_0(\eta)$ and $\phi_0(\eta)$, Eqs (34)–(36) were solved

iteratively until the approximate solutions converged to within a certain prescribed tolerance level.

Similarly, for the PHF case, Eqs (10), (11) and (32) take the form

$$f'''_{r+1} + a_{1,r} f''_{r+1} + a_{2,r} f'_{r+1} = R_{1,r}, \tag{37}$$

$$h''_{r+1} + b_{1,r} h'_{r+1} + b_{2,r} h_{r+1} = R_{2,r}, \tag{38}$$

$$(1 + \epsilon g_r + Nr) g''_{r+1} + c_{r,1} g'_{r+1} + c_{2,r} g_{r+1} = R_{3,r}, \tag{39}$$

where

$$a_{1,r} = 2f_r - \frac{\beta\,\eta}{2}, a_{2,r} = \beta + M^2 - f'_r,$$
$$R_{1,r} = -[f'^2_r + M^2 + 1 + \beta],$$
$$b_{1,r} = 2f_r - \frac{\beta\,\eta}{2}, \quad b_{2,r} = -[f'_r + M^2 + \beta], \quad R_{2,r} = 0,$$
$$c_{1,r} = 2\epsilon\, g'_r + 2Pr\, f_r - \frac{Pr\beta\,\eta}{2}, \quad c_{2,r} = \epsilon\, g''_r - 2Pr(f'_{r+1} + \alpha R\, L\, h)^2 - \frac{3Pr\,\beta}{2},$$
$$R_{3,r} = Pr\, E_c[(f''_r + \alpha\, R\, L\, h'_r)^2 + M^2(f'_r + \alpha\, R\, L\, h_r)^2] - \epsilon\, g''_r\, g_r - \epsilon\, g'^2_r.$$

5 Results and Discussion

The analysis of the results presented here relate to a decelerating shrinking sheet only (i.e., $\beta \leq 0$) following Fang et al.[30], Rohini et al.[31] and Nandy et al.[32]. We have compared the local skin friction coefficients $f''(0)$ and $h'(0)$ for various values of the parameter α with previously published data (Wang [15], Rahimpour et al. [33] and Mahapatra and Nandy [17]). The comparisons are shown in Table 1 where we observe an very good agreement to the results in the literature thus validating the current numerical results.

The phenomena of heat transfer is studied with respect to the numerical values of the physical parameters namely, (a) the wall temperature gradient $|-\theta'(0)|$ in the PST case and (b) the

Table 1. Comparison table of the values of $f''(0)$ and $h'(0)$ when $M = 0$ with recent literature.

	$f''(0)$				$h'(0)$			
α	Wang [15]	Rahimpour et al. [33]	Mahapatra and Nanday [17]	Present Results	Wang [15]	Rahimpour et al. [33]	Mahapatra and Nanday [17]	Present Results
–0.95	0.9469	0.946815	0.946893	0.946897	0.26845	0.268450	0.268457	0.268458
–0.75	1.35284	1.352850	1.352841	1.352854	–0.22079	–0.220789	–0.220795	-0.220785
–0.50	1.49001	1.490004	1.352841	1.352852	–0.53237	–0.532371	–0.532374	-0.532379
–0.25	1.45664	1.456599	1.456641	1.456648	–0.75639	–0.756390	–0.756380	-0.756376
0.0	1.31193	1.311938	1.311942	1.311950	–0.93873	–0.938732	–0.938731	-0.938745
0.1	1.22911	1.229113	1.229111	1.229117	–1.00400	–1.004026	–1.004031	-1.004032
0.2	1.13374	1.133743	1.133750	1.133757	–1.06590	–1.065933	–1.065951	-1.065946
0.5	0.78032	0.780323	0.780327	0.780332	–1.23550	–1.235451	–1.235460	-1.235454
1.0	0	0	0	0	–1.47930	–1.479337	–1.479341	-1.479332
2.0	–2.13107	–2.131069	–2.131068	-2.131075	–1.88000	–1.879949	–1.879956	-1.879945
5.0	–11.8022	–11.802214	–11.802202	-11.802213	–2.76170	–2.761724	–2.761702	-2.76167

doi:10.1371/journal.pone.0138355.t001

Table 2. Wall temperature gradient $|-\theta'(0)|$ for the PST case taking $Pr = 0.72$, $R = 1$ $\beta = -0.25$, $L = 1$, $E_c = 1$ and $Nr = 2.0$.

ϵ	α	M = 0.0	M = 0.5	M = 1.0
0.0	-0.9	0.470476	0.515791	0.639041
	-0.3	0.469680	0.497224	0.575271
	-0.1	0.389930	0.402194	0.436688
0.1	-0.9	0.435015	0.477871	0.594412
	-0.3	0.434487	0.460699	0.535030
	-0.1	0.358828	0.370508	0.403393
0.2	-0.9	0.403350	0.443995	0.554504
	-0.3	0.403116	0.428120	0.499084
	-0.1	0.331167	0.342317	0.373743

doi:10.1371/journal.pone.0138355.t002

wall temperature $|g(0)|$ in the PHF case. Tables 2 and 3 show that the wall temperature gradient $|-\theta'(0)|$ in the PST case and the wall temperature $|g(0)|$ in the PHF case increases with increasing M when α and ϵ are fixed. The temperature gradient in the PST case and the wall temperature in the PHF case decrease with increases in the thermal conductivity parameter ϵ. We also observe that $|-\theta'(0)|$ and $|g(0)|$ decrease as α increases in both the PST and the PHF cases.

Fig 2 depicts the variation of the skin friction coefficients $f''(0)$ and $h'(0)$ with $\alpha < 0$ (shrinking sheet) and $\alpha > 0$ (stretching sheet) for different values of the magnetic parameter M. Here solid and dashed lines represent the trajectories of $f''(0)$ and $h'(0)$, respectively. Our numerical results reveal that without a magnet (i.e., $M = 0$), Eqs (14) and (15) have unique solutions when $\alpha \geq -1$ and no similarity solution exists for $\alpha < -1$. It is observed that the similarity solution exists up to a critical value $\alpha = \alpha_c (< 0)$, (say) beyond which a solution based on the boundary layer approximations does not exist as the boundary layer separates from the surface. From a physical point of view, a steady solution is not possible unless additional fluid from the stagnation-point is added to the free stream. A steady solution is possible only when ratio of the free stream velocity and shrinking velocity is less than a certain numerical value which again depends on the magnetic field parameter (M). The results show that when M increases, the range of α where similarity solutions exist gradually increases. When $\alpha = 1$, we find that $f''(0) = 0$ because $f(\eta) = \eta$ is the solution of Eq (14) subject to the boundary conditions Eq (16). The results show that when $f''(0) \geq 0$, for a given value of α, $f''(0)$ increases with M. For a shrinking surface, the $h'(0)$ orbits intersect the α-axis but this is not the case for flow over a stretching

Table 3. Wall temperature gradient $|g(0)|$ for the PHF case taking $Pr = 0.72$, $R = 1$ $\beta = -0.25$, $L = 1$, $E_c = 1$ and $Nr = 2.0$.

ϵ	α	M = 0.0	M = 0.5	M = 1.0
0.0	-0.9	0.649572	0.681891	0.764965
	-0.3	0.593890	0.618274	0.686943
	-0.1	0.505823	0.517244	0.549463
0.1	-0.9	0.616233	0.648325	0.731028
	-0.3	0.555240	0.579129	0.646413
	-0.1	0.467061	0.478199	0.509608
0.2	-0.9	0.585066	0.616894	0.699120
	-0.3	0.519071	0.542448	0.608305
	-0.1	0.430932	0.441781	0.472366

doi:10.1371/journal.pone.0138355.t003

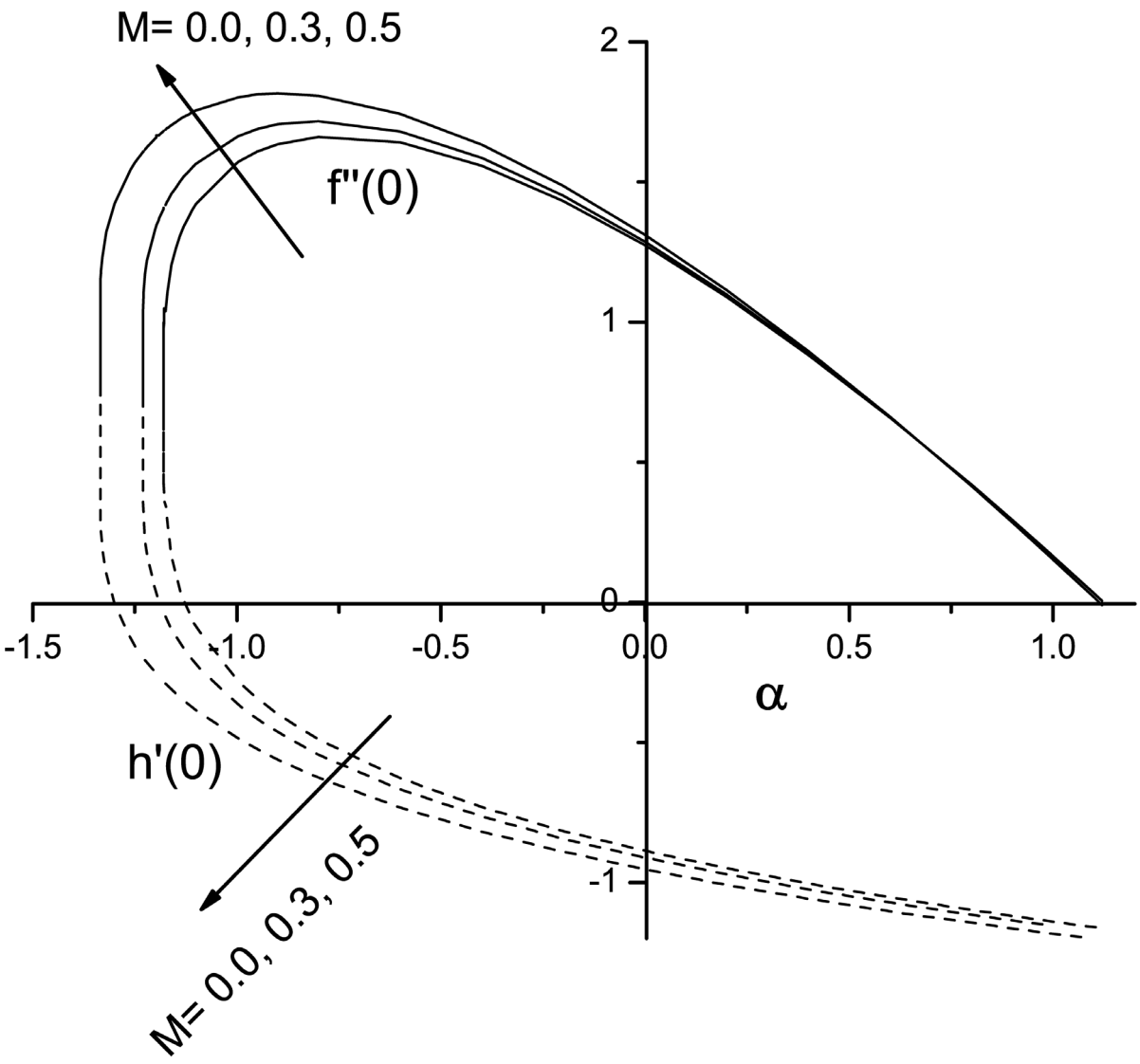

Fig 2. Initial values $F''(0)$ and $h'(0)$ versus α and M.

doi:10.1371/journal.pone.0138355.g002

sheet. For a given value of M, the size of $h'(0)$ decreases with increases in $|\alpha|$. Also, for any given α, $|h'(0)|$ increases with M.

We note that for a stretching sheet α is positive and for a shrinking sheet α is negative while $\alpha = 0$ represents Hiemenz flow. Figs 3 and 4 show the effect of α on the vertical velocity components $f'(\eta)$ and $h(\eta)$. We observe that $f'(\eta)$ increases with increases in α while the value of $h(\eta)$ decreases with increases in the values of α.

Fig 5 displays the effect of α on the temperature profiles $\theta(\eta)$ (for PST case). Here the temperature profiles decrease with an increase in α. Figs 6 and 7 show the effect of M on $f'(\eta)$ and non-alignment variable $h(\eta)$ with respect to η, respectively. It is clear that $f'(\eta)$ increases with increasing values of the magnetic parameter M and $h(\eta)$ decreases with M. We can conclude from the above results is that for shrinking sheet, the effect of non-alignment becomes less pronounced with increasing M.

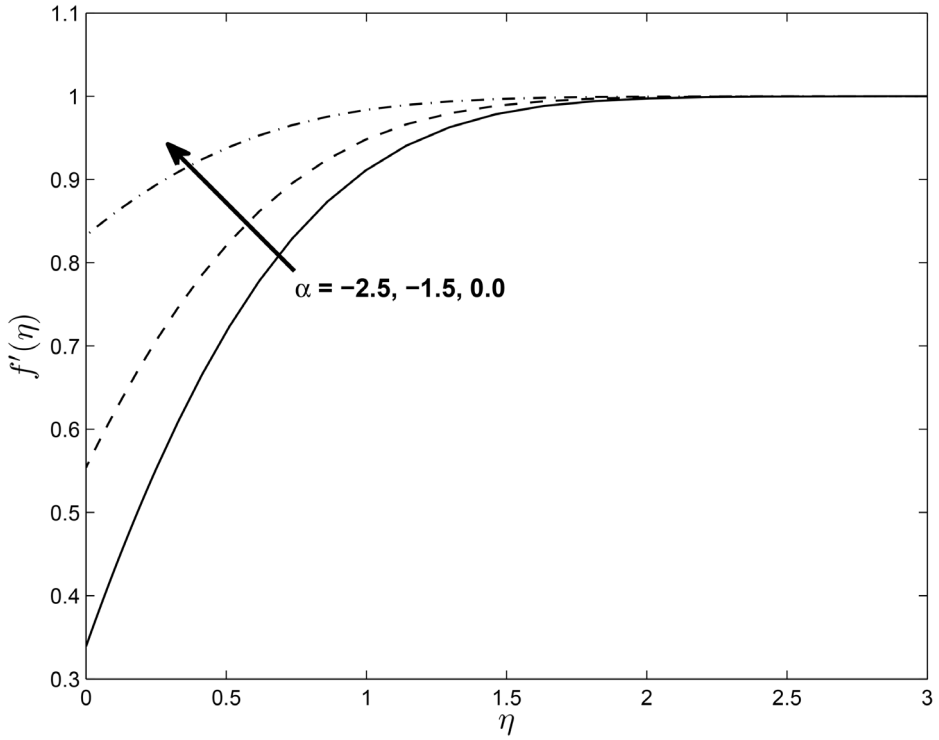

Fig 3. Effect of α on velocity profiles $f'(\eta)$ for $M = 0.1$, $\delta = 0.2$, $\beta = -0.25$, $Pr = 0.72$, $Nr = 0.2$, $Ec = 1.0$, $R = 1.0$ and $\epsilon = 0.5$.

doi:10.1371/journal.pone.0138355.g003

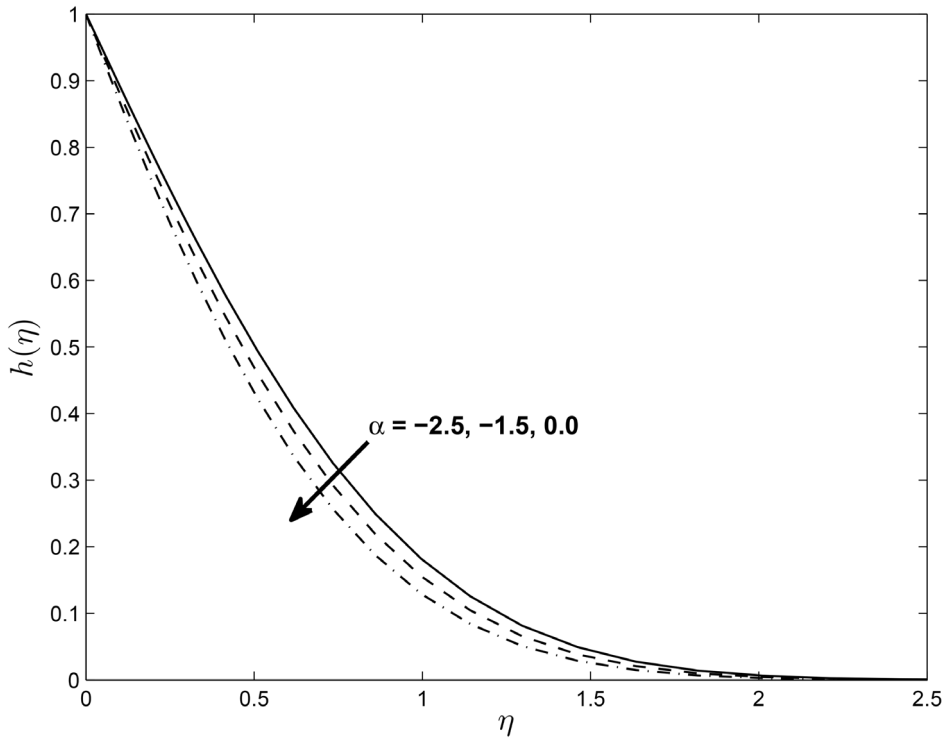

Fig 4. Effect of α on velocity profiles $h(\eta)$ for $M = 0.1$, $\delta = 0.2$, $\beta = -0.25$, $Pr = 0.72$, $Nr = 0.2$, $Ec = 1.0$, $R = 1.0$ and $\epsilon = 0.5$.

doi:10.1371/journal.pone.0138355.g004

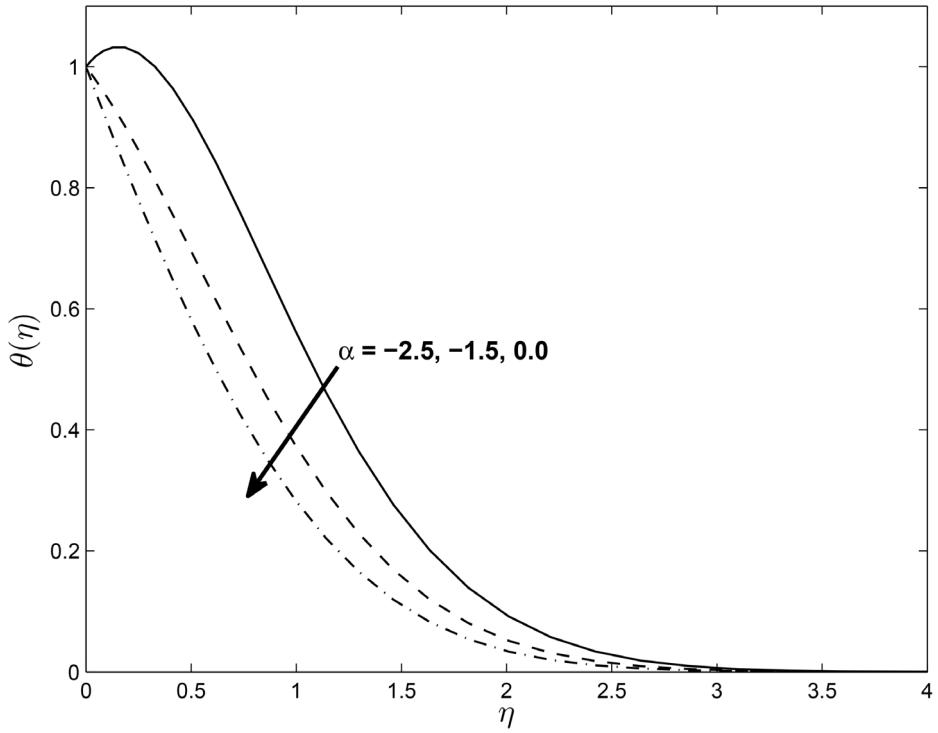

Fig 5. Effect of α on temperature profile for $M = 0.1$, $\delta = 0.2$, $\beta = -0.25$, $Pr = 0.72$, $Nr = 0.2$, $Ec = 1.0$, $R = 1.0$, $L = 1.0$ and $\epsilon = 0.5$.

doi:10.1371/journal.pone.0138355.g005

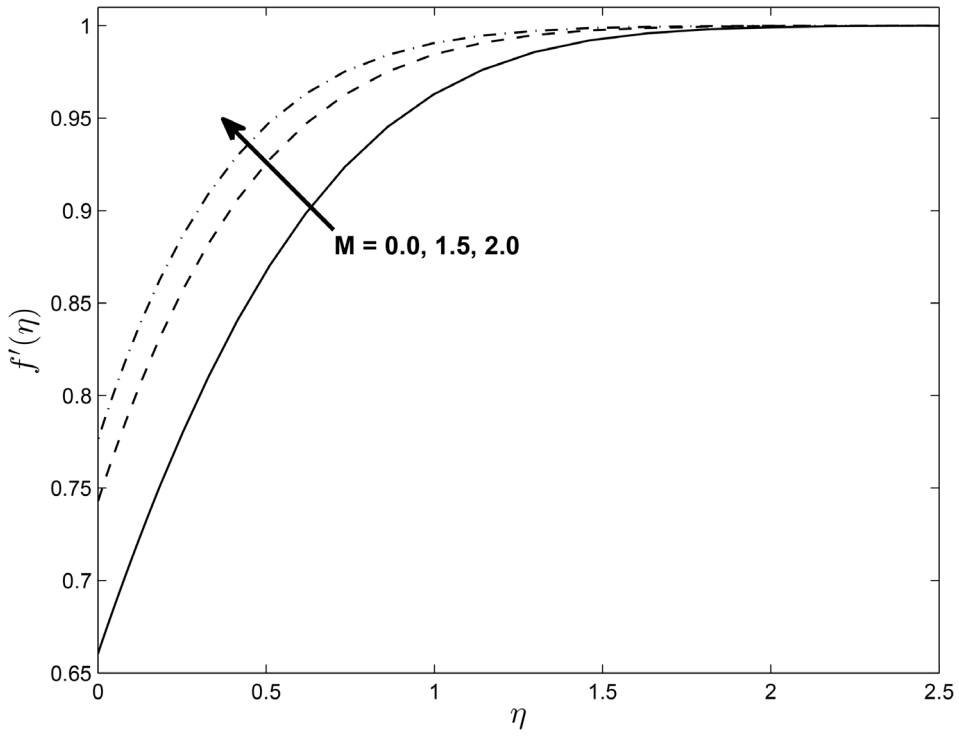

Fig 6. Effect of magnetic parameter M on velocity profiles $f'(\eta)$ for $\delta = 0.2$, $\beta = -0.25$, $\alpha = -0.95$, $Pr = 0.72$, $Nr = 0.2$, $Ec = 1.0$, $R = 1.0$, $L = 1.0$ and $\epsilon = 0.5$.

doi:10.1371/journal.pone.0138355.g006

Figs 8 and 9 show that the temperature profiles decrease monotonically with an increase in the magnetic parameter in both the PST and the PHF cases, respectively. The extent of the reverse circular flow above the sheet decreases with increases in M. This is a consequence of the fact that the temperature field given by Eq (18) is influenced by the advection of the fluid velocity above the sheet. Figs 10 and 11 exhibit the temperature profiles for different values of thermal conductivity parameter ϵ where the other parameters are fixed for both the PST and PHF cases, respectively. The temperature profiles increase with an increase in the thermal conductivity parameter due to increases in the thermal boundary layer thickness in both the PST and PHF cases.

Figs 12 and 13 depict the horizontal velocity profiles $f'(\eta)$ and $h(\eta)$ for different values of the unsteadiness parameter β in the presence of slip at the boundary, respectively. The velocity $f'(\eta)$ decreases with an increase in the unsteadiness parameter β and this implies an accompanying reduction in the thickness of the momentum boundary layer while the opposite trend is observed with $h(\eta)$. We observe that as β increases, the axial boundary layer velocity decreases. In the vicinity of the sheet, the axial fluid velocity decreases while the trend is reversed in the free stream. The parameter β has the effect of reducing the momentum boundary layer thickness for $f'(\eta)$ while enhancing the boundary layer thickness of $h(\eta)$

Figs 14, 15 and 16 show the effect of δ on the velocity components $f'(\eta)$, $h(\eta)$ and temperature profile $\theta(\eta)$ (for PST case), respectively. It is interesting to note that the velocity profile $f'(\eta)$ increases with increase in values of δ while $h(\eta)$ decreases with the increase in the values of δ. The figure also reveals that the temperature profile $\theta(\eta)$ decreases with the increase in the values of δ. This may be explained in the following way; with slip, there is a difference between the flow velocity near the sheet and the shrinking velocity at the surface. As δ increases the slip velocity increases leading to a decrease in the fluid velocity for $h(\eta)$. But the opposite trend is observed for $f'(\eta)$ because momentum boundary layer become thinner due to increasing value of δ. Fig 16 illustrates the fact that the temperature at any given point increases when the slip velocity δ increases.

Figs 17 and 18 depict the effect of Nr on the temperature profile in PST and PHF cases with keeping other parameters fixed, respectively. The temperature profile in two cases increase with increasing in values of Nr, which in turn increases the thermal boundary layer thickness for both PST and PHF cases. This may due to the fact that increases in the value of N_r causes an increase in the interaction with the thermal boundary layer.

Figs 19 and 20 show the variation in the skin friction coefficient $-f''(0)$ with respect to β. We observe that the skin friction coefficients decrease monotonically with increasing values of β and M in Fig 19 while the opposite is true in the Fig 20 for β and δ. The highest value of the skin friction is reached for smaller values of β.

Figs 21 and 22 display the dimensionless wall heat transfer rates $-\theta'(0)$ as a function of β. We observe that the wall heat transfer rate increases with increasing β, M and δ. The maximum value of the dimensionless wall heat transfer rates is achieved for large values of β.

6 Conclusion

An unsteady MHD axisymmetric stagnation-point flow over a shrinking sheet with temperature dependent thermal conductivity and thermal radiation and a Navier slip was investigated in this paper. The surface was assumed to shrink axisymmetrically in its own plane and the flow was permeated by a uniform magnetic field normal to the surface. The temperature profiles in the two cases of prescribed wall temperature and prescribed surface heat flux was shown to increase with the thermal radiation parameter, which in turn increases the thermal boundary layer thickness for both PST and PHF cases. This may be due to the fact that an

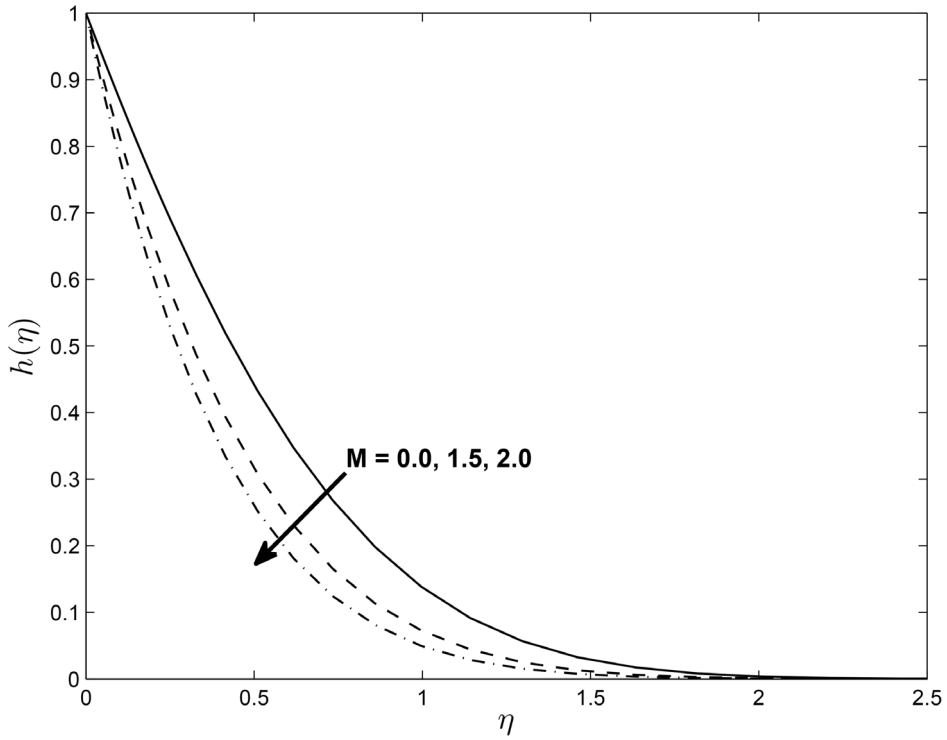

Fig 7. Effect of magnetic parameter *M* on velocity profiles $h(\eta)$ for $\delta = 0.2$, $\beta = -0.25$, $\alpha = -0.95$, $Pr = 0.72$, $Nr = 0.2$, $Ec = 1.0$, $R = 1.0$, $L = 1.0$ and $\epsilon = 0.5$.

doi:10.1371/journal.pone.0138355.g007

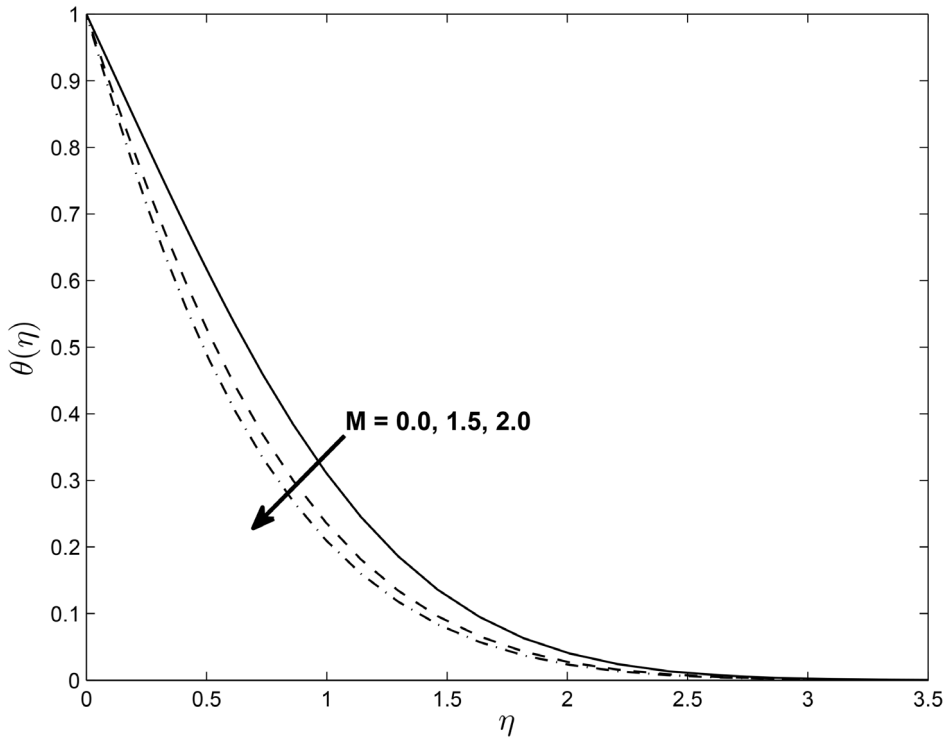

Fig 8. Effects of magnetic parameter *M* on temperature profiles (PST case) for $\delta = 0.2$, $\beta = -0.25$, $\alpha = -0.95$, $Pr = 0.72$, $Nr = 0.2$, $Ec = 1.0$, $R = 1.0$ and $L = 1.0$.

doi:10.1371/journal.pone.0138355.g008

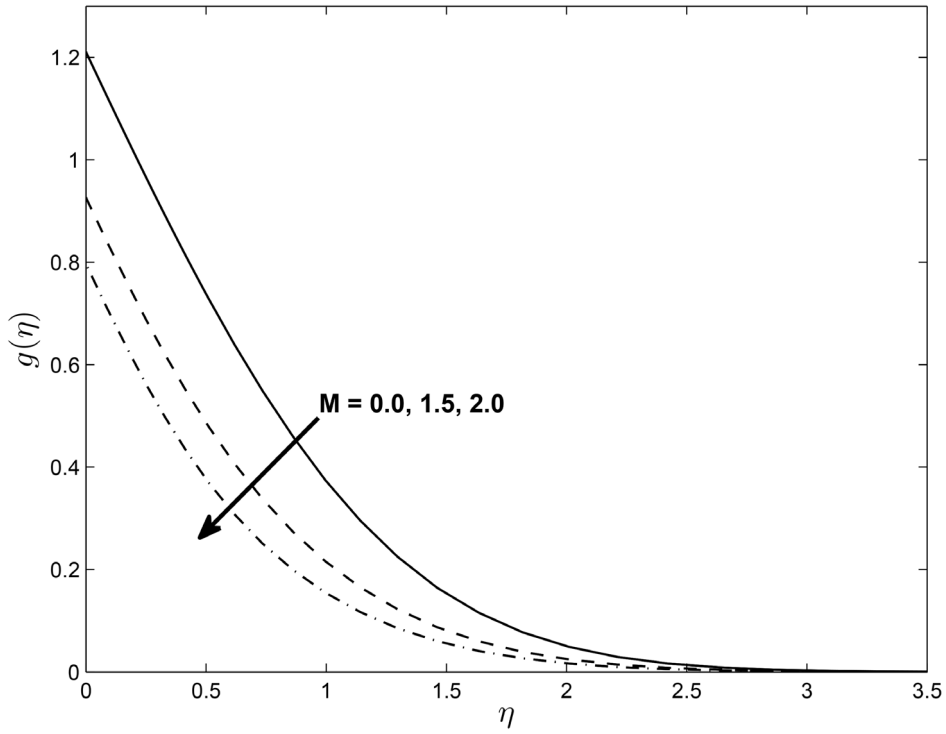

Fig 9. Effects of magnetic parameter *M* on temperature profiles (PHF case) for $\delta = 0.2$, $\beta = -0.25$, $\alpha = -0.95$, $Pr = 0.72$, $Nr = 0.2$, $Ec = 1.0$, $R = 1.0$ and $L = 1.0$.

doi:10.1371/journal.pone.0138355.g009

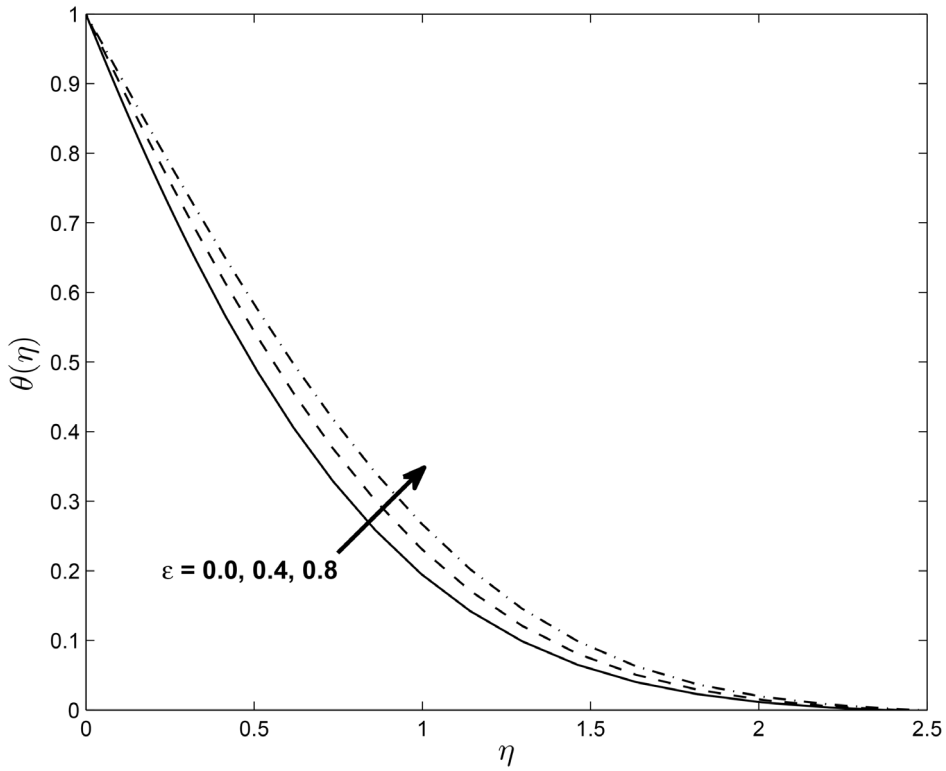

Fig 10. Effects of ϵ on temperature profiles (PST case) for $\delta = 0.2$, $\beta = -0.25$, $\alpha = -0.95$, $Pr = 0.72$, $Nr = 0.2$, $Ec = 1.0$, $R = 1.0$ and $L = 1.0$.

doi:10.1371/journal.pone.0138355.g010

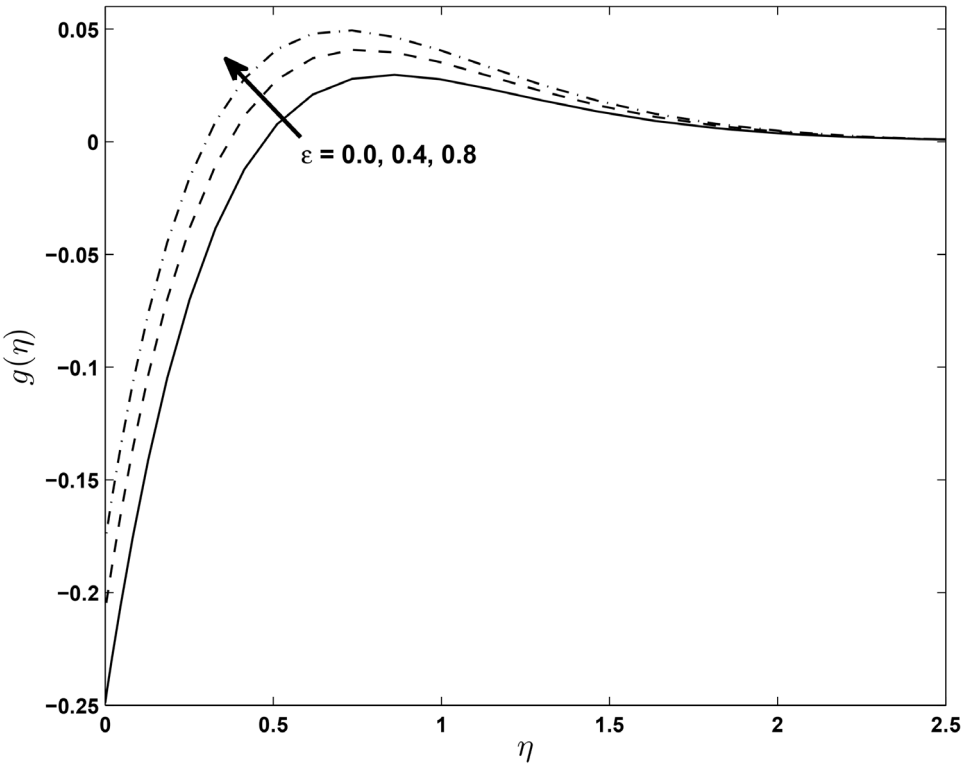

Fig 11. Effects of ϵ on temperature profiles (PHF case) for $\delta = 0.2$, $\beta = -0.25$, $\alpha = -0.95$, $Pr = 0.72$, $Nr = 0.2$, $Ec = 1.0$, $R = 1.0$ and $L = 1.0$.

doi:10.1371/journal.pone.0138355.g011

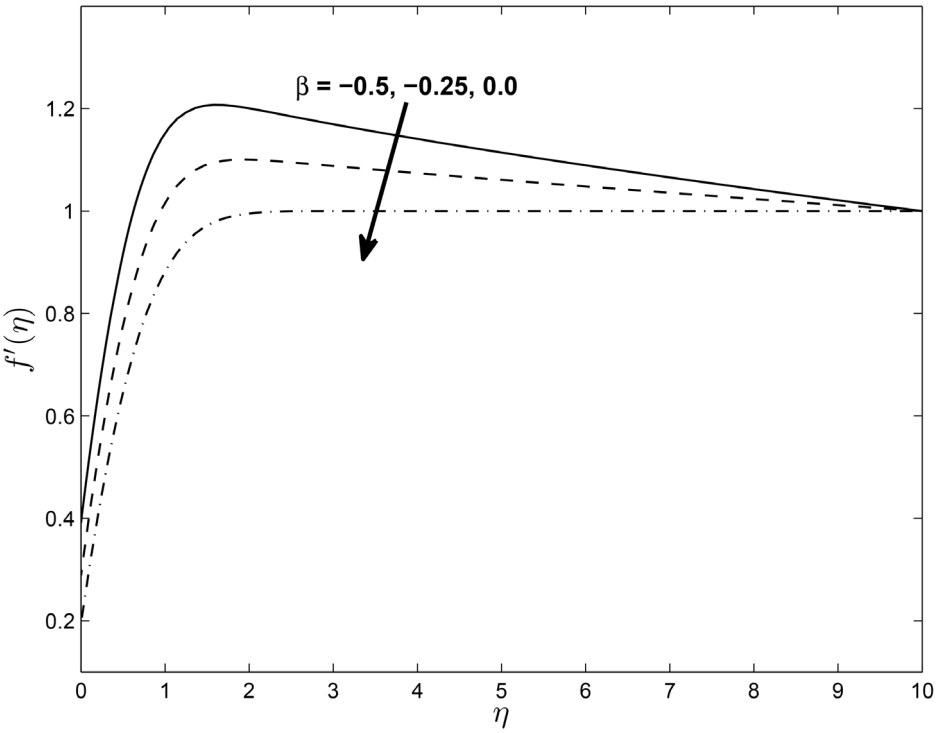

Fig 12. Effect of β on velocity profiles $f'(\eta)$ for $M = 0.1$, $\delta = 0.2$, $\alpha = -0.95$, $Pr = 0.72$, $Nr = 0.2$, $Ec = 1.0$, $R = 1.0$, $L = 1.0$ and $\epsilon = 0.5$.

doi:10.1371/journal.pone.0138355.g012

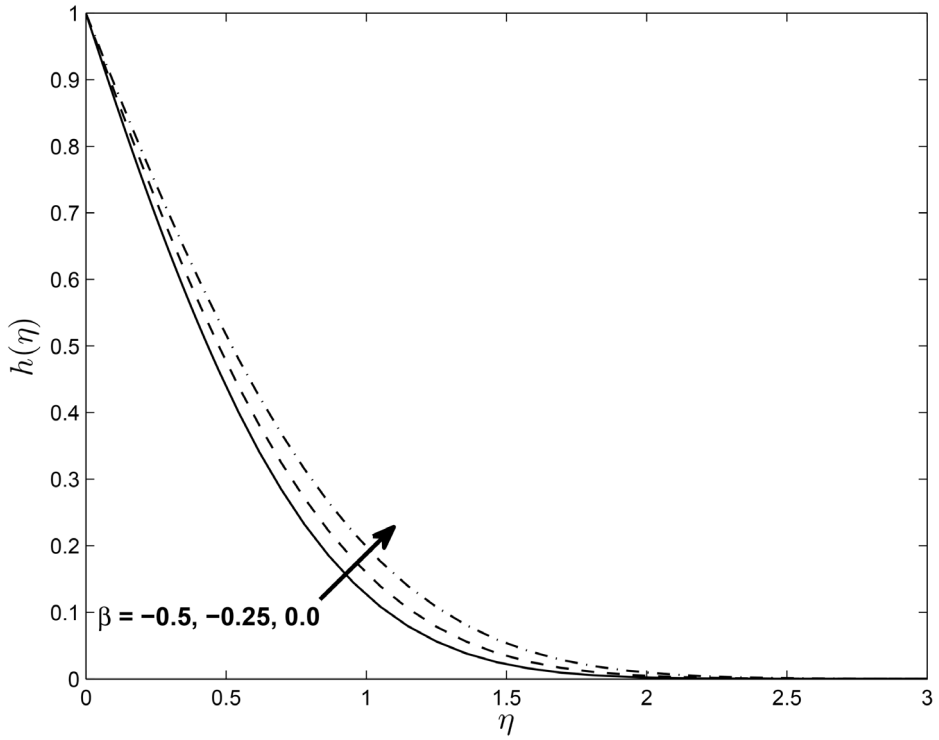

Fig 13. Effect of β on velocity profiles $h(\eta)$ for $M = 0.1$, $\delta = 0.2$, $\alpha = -0.95$, $Pr = 0.72$, $Nr = 0.2$, $Ec = 1.0$, $R = 1.0$, $L = 1.0$ and $\epsilon = 0.5$.

doi:10.1371/journal.pone.0138355.g013

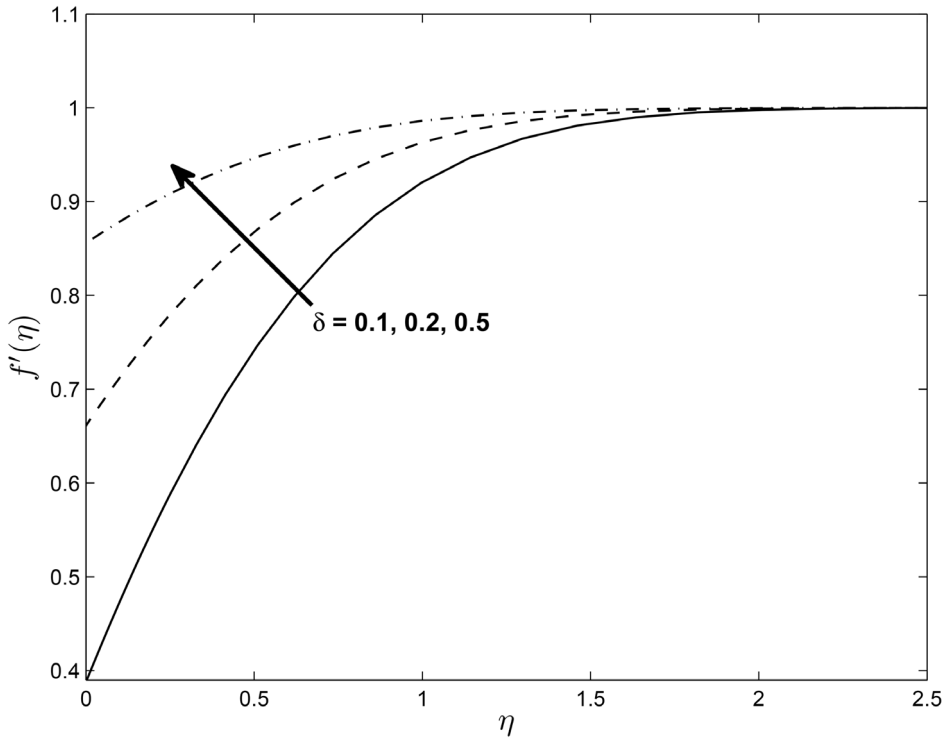

Fig 14. Effect of δ on velocity profiles $f'(\eta)$ for $M = 0.1$, $\beta = -0.25$, $\alpha = -0.95$, $Pr = 0.72$, $Nr = 0.2$, $Ec = 1.0$, $R = 1.0$, $L = 1.0$ and $\epsilon = 0.5$.

doi:10.1371/journal.pone.0138355.g014

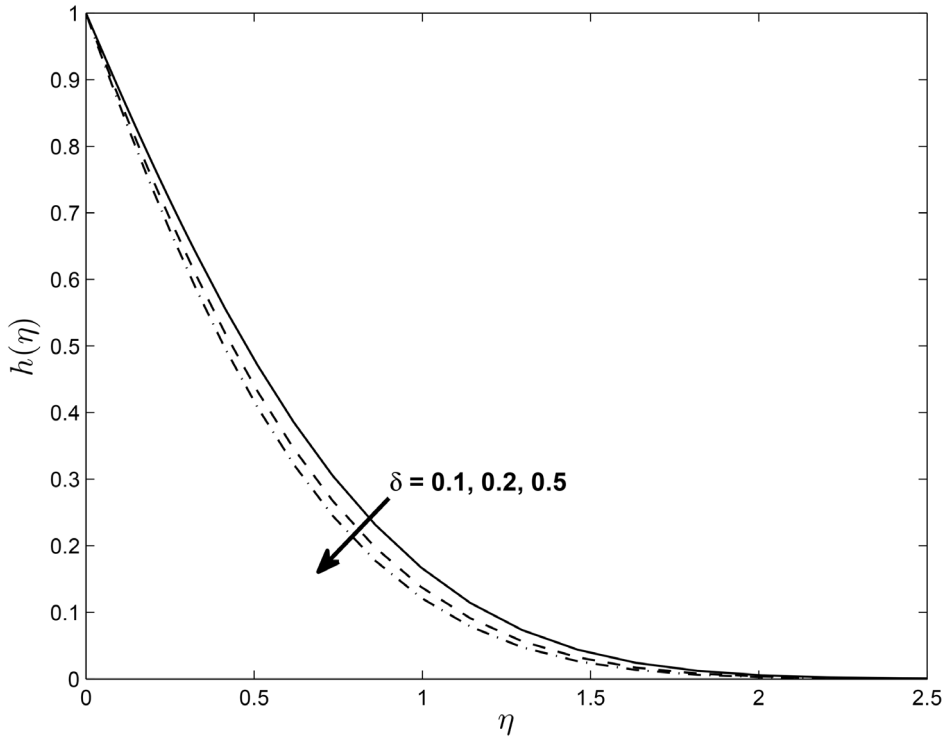

Fig 15. Effect of δ on velocity profiles $h(\eta)$ for $M = 0.1$, $\beta = -0.25$, $\alpha = -0.95$, $Pr = 0.72$, $Nr = 0.2$, $Ec = 1.0$, $R = 1.0$, $L = 1.0$ and $\epsilon = 0.5$.

doi:10.1371/journal.pone.0138355.g015

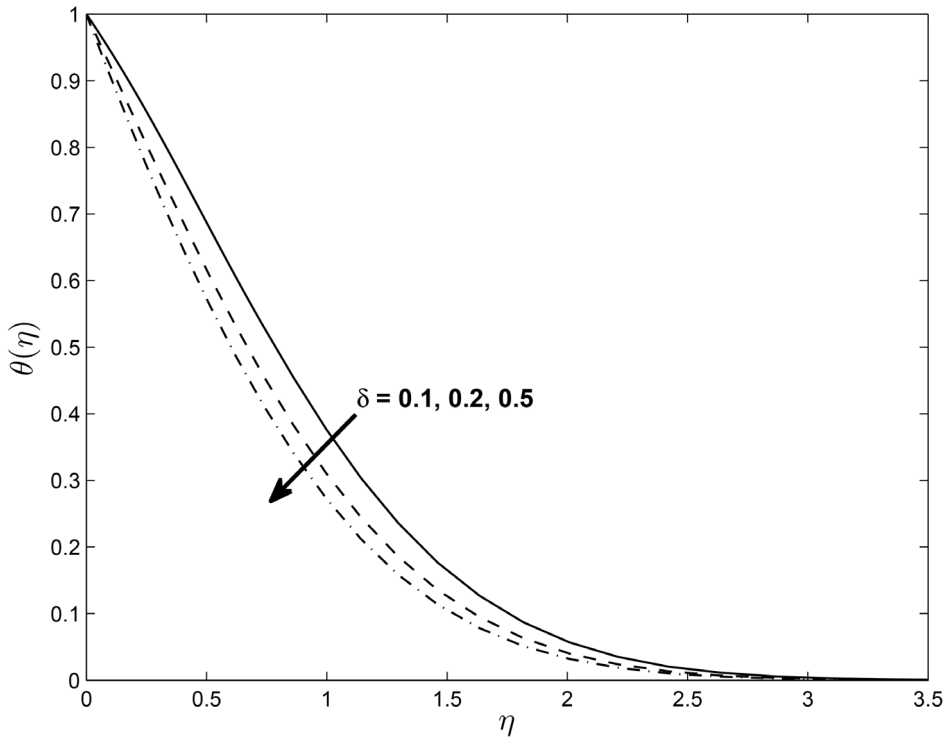

Fig 16. Effect of δ on temperature profile (PST case) for $M = 0.1$, $\beta = -0.25$, $\alpha = -0.95$, $Pr = 0.72$, $Nr = 0.2$, $Ec = 1.0$, $R = 1.0$, $L = 1.0$ and $\epsilon = 0.5$.

doi:10.1371/journal.pone.0138355.g016

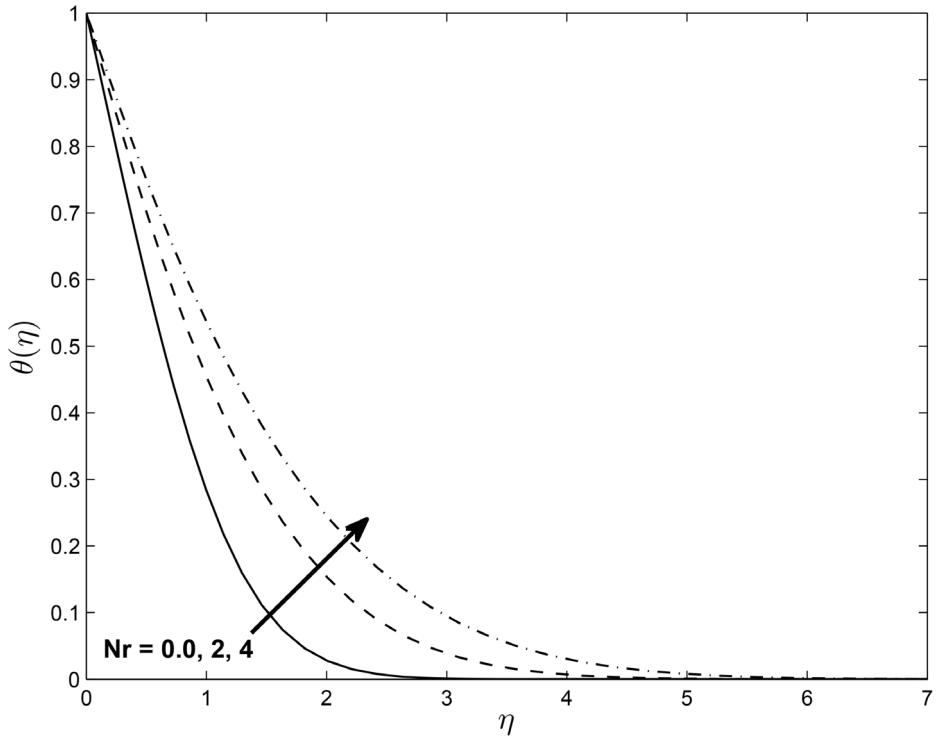

Fig 17. Effects of thermal radiation parameter *Nr* on temperature profiles $\theta(\eta)$ for $\delta = 0.2$, $Pr = 0.72$, $\beta = -0.25$, $Ec = 1.0$, $\alpha = -0.95$, $M = 0.1$, $R = 1.0$ and $L = 1.0$.

doi:10.1371/journal.pone.0138355.g017

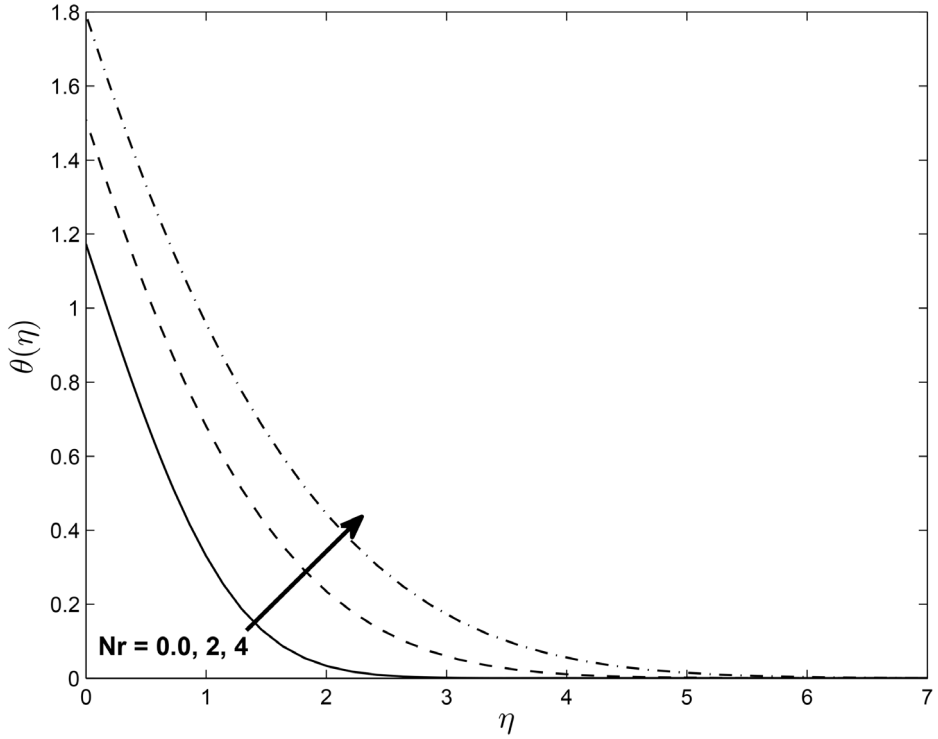

Fig 18. Effects of thermal radiation parameter *Nr* on temperature profiles $g(\eta)$ for $\delta = 0.2$, $Pr = 0.72$, $\beta = -0.25$, $Ec = 1.0$, $\alpha = -0.95$, $M = 0.1$, $R = 1.0$ and $L = 1.0$.

doi:10.1371/journal.pone.0138355.g018

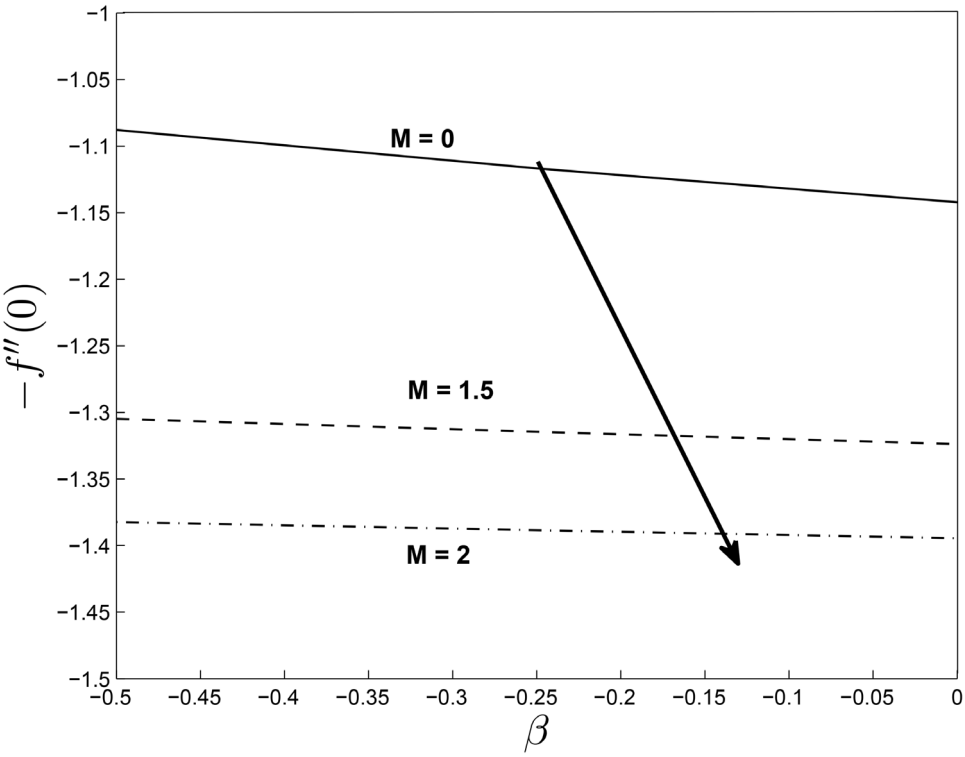

Fig 19. Effect of *M* on Skin friction coefficients for $\alpha = -0.95$, $Pr = 0.72$, $Nr = 0.2$, $Ec = 1.0$, $R = 1.0$, $L = 1.0$ and $\epsilon = 0.5$.

doi:10.1371/journal.pone.0138355.g019

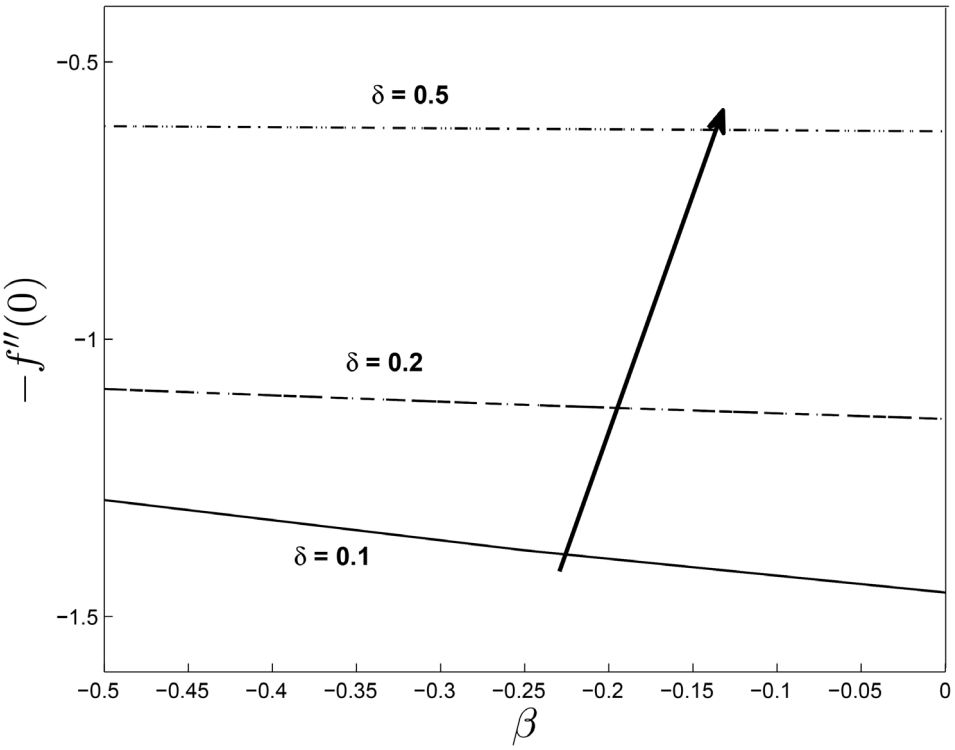

Fig 20. Effect of δ on Skin friction coefficients for $\alpha = -0.95$, $Pr = 0.72$, $Nr = 0.2$, $Ec = 1.0$, $R = 1.0$, $L = 1.0$ and $\epsilon = 0.5$.

doi:10.1371/journal.pone.0138355.g020

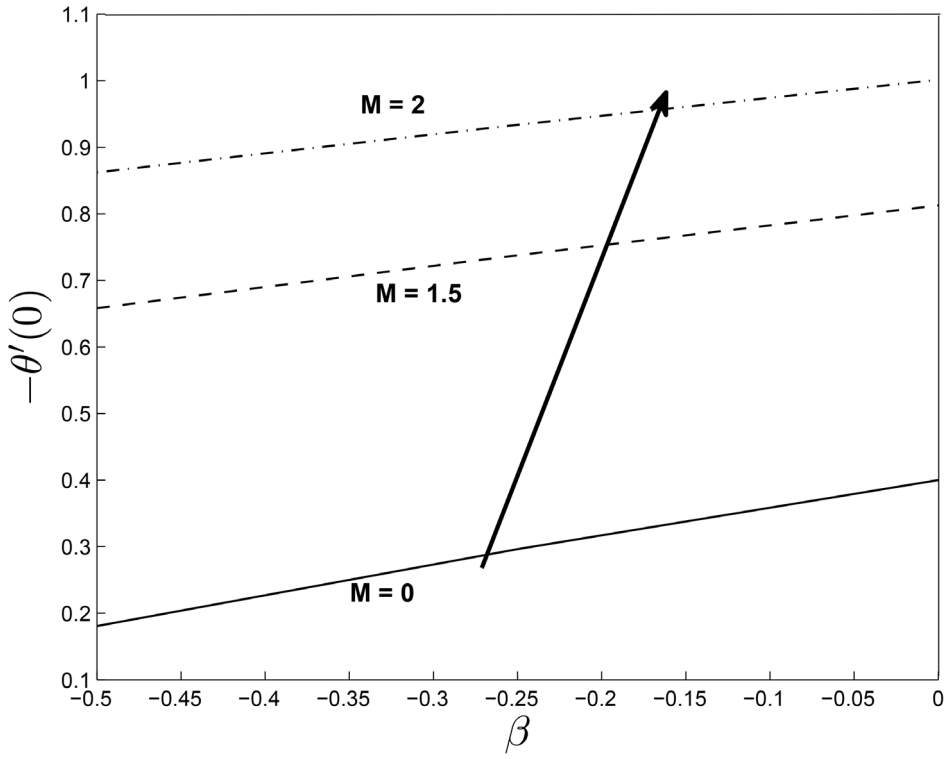

Fig 21. Effect of *M* on heat transfer coefficients for $\alpha = -0.95$, $Pr = 0.72$, $Nr = 0.2$, $Ec = 1.0$, $R = 1.0$, $L = 1.0$ and $\epsilon = 0.5$.

doi:10.1371/journal.pone.0138355.g021

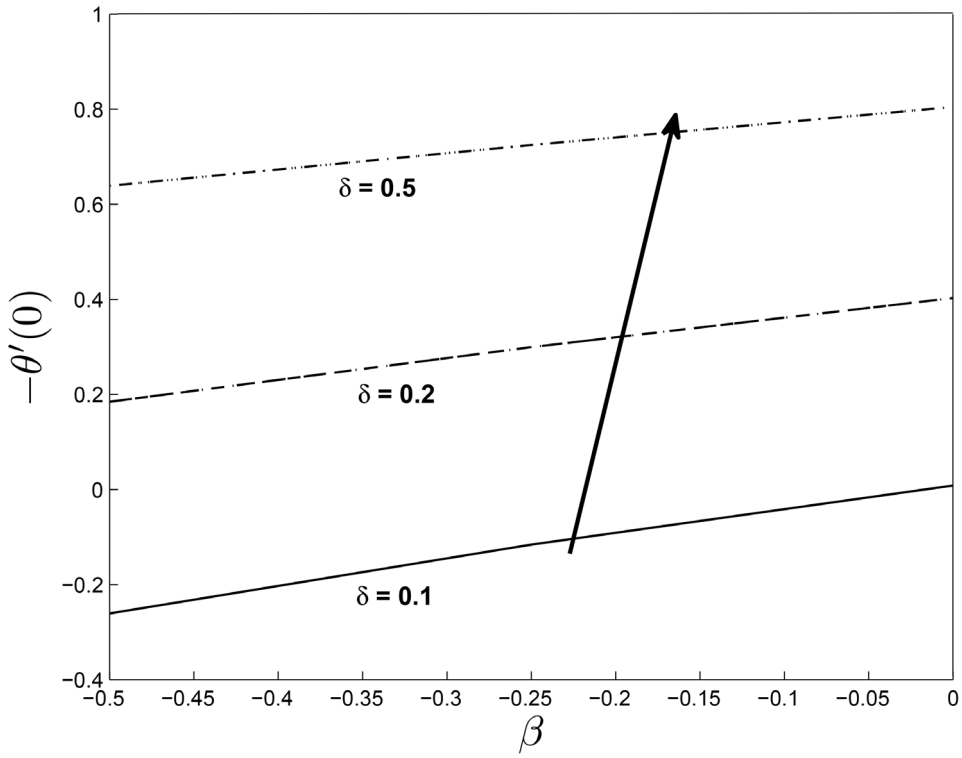

Fig 22. Effect of δ on heat transfer coefficients for $\alpha = -0.95$, $Pr = 0.72$, $Nr = 0.2$, $Ec = 1.0$, $R = 1.0$, $L = 1.0$ and $\epsilon = 0.5$.

doi:10.1371/journal.pone.0138355.g022

increase in N_r induces a significant interaction between the fluid and the thermal boundary layer. It is clear that $f'(\eta)$ increases with increasing magnetic parameter values M while $h(\eta)$ decreases with the magnetic parameter. It can be concluded that for a shrinking sheet, the effect of non-alignment becomes less pronounced with enhanced magnetic parameter values. When slip occurs, the flow velocity near the sheet is no longer equal to the shrinking velocity at the sheet. Then with an increase in δ such slip velocity increases and consequently fluid velocity decreases for $h(\eta)$ under the slip condition at the boundary.

Acknowledgments

Authors wish to thank the referees for their valuable suggestions. Also, authors are thankful to Dr. Samir Kumar Nandy for his valuable suggestions which improve the quality of the paper. The authors are grateful for funding from the University of KwaZulu-Natal.

Author Contributions

Conceived and designed the experiments: SM NH PS. Analyzed the data: SM NH PS. Wrote the paper: SM.

References

1. Gupta AS, Gupta PS (1977) Heat and mass transfer on a stretching sheet with suction and blowing. Canadian Journal of Chemical Engineering 55: 744–746. doi: 10.1002/cjce.5450550619
2. Carragher P, Crane LJ (1982) Heat transfer on a continuous stretching sheet. Zeit. Angew. Math. Mech. 62: 564–565. doi: 10.1002/zamm.19820621009
3. Khan A, Khan I, Ali F, ulhaq S, Shafie S (2014) Effects of wall shear stress on unsteady MHD conjugate flow in a porous medium with ramped wall temperature. PLoS ONE 9(3): e90280. doi: 10.1371/journal.pone.0090280 PMID: 24621775
4. Samiulhaq, Ahmad S, Vieru D, Khan I, Shafie S (2014) Unsteady magnetohydrodynamic free convection flow of a second grade fluid in a porous medium with ramped wall Temperature. PLoS ONE 9(5): e88766. doi: 10.1371/journal.pone.0088766 PMID: 24785147
5. Khalid A, Khan I, Shafie S (2015) Exact solutions for free convection flow of nanofluids with ramped wall temperature. Eur. Phys. J. Plus 130: 57 doi: 10.1140/epjp/i2015-15057-9
6. Wang CY (1984) The three dimensional flow due to a stretching flat surface. Phys. Fluids 27: 1915–1917. doi: 10.1063/1.864868
7. Hussanan A, Ismail Z, Khan I, Hussein AG, Shafie S (2014) Unsteady boundary layer MHD free convection flow in a porous medium with constant mass diffusion and Newtonian heating. Eur. Phys. J. Plus 129: 46. doi: 10.1140/epjp/i2014-14046-x
8. Pavlov KB (1974) Magnetohydrodynamic flow of an incompressible viscous fluid caused by the deformation of a plane surface. Magnitnaya Gidrodinamika 4: 146–147.
9. Mabood F, Khan WA, Ismail AIM (2013) Optimal homotopy asymptotic method for flow and heat transfer of a viscoelastic fluid in an axisymmetric channel with a porous wall. PLoS ONE 8(12): e83581. doi: 10.1371/journal.pone.0083581 PMID: 24376722
10. Homann F (1936) Der Einfluss grosser Zahigkeit bei der stromung um den Zylinder und um die Kugel. Zeit. Angew. Math.Phys. 16: 153–164. doi: 10.1002/zamm.19360160304
11. Chiam TC (1994) Stagnation-point flow towards a stretching plate. J. Phys. Soc. Japan 63: 2443–2444. doi: 10.1143/JPSJ.63.2443
12. Mahapatra TR, Gupta AS (2003) Stagnation-point flow towards a stretching surface, Can. J. Chem. Eng. 81: 258–263.
13. Attia HA (2007) Axisymmetric stagnation point flow towards a stretching surface in the presence of a uniform magnetic field with heat generation. Tam. J. Sci. Eng. 10(1): 11–16.
14. Miklavcic M, Wang CY (2006) Viscous flow due to a shrinking sheet. Quart. Appl. Math. 64(2): 283–290. doi: 10.1090/S0033-569X-06-01002-5
15. Wang CY (2008) Stagnation flow towards a shrinking sheet. Int. J.Nonlinear Mech. 43: 377–382. doi: 10.1016/j.ijnonlinmec.2007.12.021

16. Qasim M, Khan I, Shafie S (2013) Heat transfer in a micropolar fluid over a stretching sheet with Newtonian heating. PLoS ONE 8(4): e59393. doi: 10.1371/journal.pone.0059393 PMID: 23565151

17. Mahapatra TR, Nandy SK (2013) Momentum and heat transfer in MHD axisymmetric stagnation-point flow over a shrinking sheet. Journal of Applied Fluid Mechanics 6 (1): 121–129.

18. Qayyum M, Khan H, Rahim MT, Ullah I (2015) Modeling and analysis of unsteady axisymmetric squeezing fluid flow through porous medium channel with slip boundary. PLoS ONE 10(3): e0117368. doi: 10.1371/journal.pone.0117368 PMID: 25738864

19. Mabood F, Khan WA, Ismail AIM (2015) MHD boundary layer flow and heat transfer of nano fluids over a nonlinear stretching sheet: A numerical study. Journal of Magnetism and Magnetic Materials 374: 569–576. doi: 10.1016/j.jmmm.2014.09.013

20. Mabood F, Khan WA, Uddin MJ, Ismail AIM (2015) Optimal homotopy asymptotic method for MHD slips flow over a radiating stretching sheet. Far East Journal of Applied Mathematics 90(1): 21–40. doi: 10.17654/FJAMJan2015_021_040

21. Mabood F, Khan WA, Ismail AIM (2015) MHD stagnation point flow and heat transfer impinging on stretching sheet with chemical reaction and transpiration. Chemical Engineering Journal 273: 430–437. doi: 10.1016/j.cej.2015.03.037

22. Khan JA, Mustafa M, Hayat T, Alsaedi A (2014) On three-dimensional flow and heat transfer over a non-linearly stretching sheet: analytical and numerical solutions. PLoS ONE 9(9): e107287. doi: 10.1371/journal.pone.0107287 PMID: 25198696

23. Bansal JL (1994) Magnetofluiddynamics of viscous fluid. Jaipur Publishing House, Jaipur, India.

24. Jat RN, Rajotia D (2014) Effects of partial slip on three dimensional MHD viscous flow and heat transfer due to a permeable Axisymmetric shrinking sheet with viscous dissipation and heat source/sink. Thermal Energy and Power Engg. 3(2) 234–244.

25. Chiam TC (1998) Heat transfer in a fluid with variable thermal conductivity over stretching sheet. Acta Mechanica 129: 63–72. doi: 10.1007/BF01379650

26. Shercliff JA (1965) A Textbook of Magnetohydrodynamics. Oxford, Pergamon Press.

27. Motsa SS (2013) A New spectral relaxation method for similarity variable nonlinear boundary layer flow systems. Chemical Engineering Communications 16: 23–57.

28. Motsa SS, Dlamini PG, Khumalo M (2014) Spectral relaxation method and spectral quasilinearization method for Solving Unsteady Boundary Layer Flow Problems. Advances in Mathematical Physics, Article ID 341964, 12: doi: 10.1155/2014/341964

29. Motsa SS, Makukula ZG (2013) On spectral relaxation method approach for steady von Karman flow of a Reiner-Rivlin fluid with Joule heating and viscous dissipation. Central European Journal of Physics 11: 363–374.

30. Fang T, Zhang J, Yao S (2009) Viscous flow over an unsteady shrinking sheet with mass transfer. Chinese Physics Letters 26 (1): 014703. doi: 10.1088/0256-307X/26/1/014703

31. Rohni AM, Ahmad S, Ismail AI, Pop I (2013) Flow and heat transfer over an unsteady shrinking sheet with suction in a nanofluid using Buongiorno's model. International Communications in Heat and Mass Transfer 43: 75–80. doi: 10.1016/j.icheatmasstransfer.2013.02.001

32. Nandy SK, Sumanta S, Mahapatra TR (2014) Unsteady MHD boundary-layer flow and heat transfer of nanofluid over a permeable shrinking sheet in the presence of thermal radiation. Alexandria Engineering Journal 53: 929–937. doi: 10.1016/j.aej.2014.09.001

33. Rahimpour M, Mohebpour SR, Kimiaeifar A, Bagheri GH (2008) On the analytic solution of axisymmetric stagnation flow towards a shrinking sheet. International Journal of Mechanics 1(2): 1–10.

Chapter 7

Conclusions

The primary objective of this thesis was to investigate convection and cross-diffusion effects on nanofluid flow, and heat and mass transfer in boundary layer flow in different geometries and subject to various source terms, and then to apply recent spectral methods to solve the highly non-linear and coupled model equations. Similarity transformations were used to convert non-linear partial differential equations into non-linear coupled ordinary differential equations which were solved numerically using spectral techniques.
The accuracy, convergence and validity of the solutions obtained using the spectral methods were established by careful comparison with solutions for some limiting cases in the published literature, or by use of a different solution method. Graphical and tabulated results have been presented and discussed. The physical results show the significance of different values of parameters on the fluid properties, the skin friction, the heat and mass transfer coefficients.

In summary, the results show that fluid properties such as the velocity, temperature, and solute concentration are appreciably influenced by changes in the fluid and physical parameters for nanofluid flow in porous media. The changes in fluid properties have implications for heat and mass transfer processes. The study has shown that Soret and Dufour effects play a significant role in transport processes and should not be neglected. In terms of the solution methods, the study has shown that SRM and SQLM give accurate solutions for systems of highly non-linear differential equations. The methods have great potential for

use in studies involving complicated non-linear problems in science and engineering.

The main findings and overall results from each chapter are summarized as follows:
Chapter 2:
In this chapter the significance of nanofluids, heat generation or absorption, viscous dissipation, and Soret and Dufour effects on double-diffusive mixed convection MHD due to a stretching/shrinking surface with suction/injection was investigated. The systems of partial differential equations were solved numerically using SRM. The accuracy of the results was tested by comparison with those found in the published literature.
From the numerical simulations the following conclusions could be drawn:

- The velocity profile decreases with an increase in nanoparticle volume fraction, while the opposite is true in the case of temperature.

- The temperature profiles decrease with an increase in suction/injection parameter and the stretching/shrinking parameter.

- The numerical simulations show, *inter alia*, that the skin friction factor increases with both an increase in the nanoparticle volume fraction and the stretching rate and that an increase in the nanoparticle volume fraction leads to a reduction in the wall mass transfer rate. The Soret and Dufour numbers have the opposite effect on thermal and concentration distributions.

- Regarding the stretching/shrinking and suction/injection parameters, we found that the silver-water nanofluid has a lower skin friction coefficient than the copper-water nanofluid.

- A small increase (less than 1%) in the nanoparticle volume fraction leads to a decrease in the wall mass transfer rate. Similarly, the wall mass transfer rate decreases

with an increase in the Hartmann number, suction/injection parameter and a stretching/shrinking parameter.

- The wall heat transfer rate rises with an increase in the Hartmann number, suction/injection parameter and stretching/shrinking parameter, but falls with an increase in the nanoparticle volume fraction.

Chapter 3:

In this chapter we presented an investigation of the effects of thermal-diffusion and chemical reaction parameter on unsteady magnetohydrodynamic nanofluid flow through an impulsively stretching vertical surface. The flow was subject to a heat source, a chemical reaction, Brownian motion and thermophoresis parameters which are assumed to be significant. The model equations that describe the fluid flow were solved using SRM. The findings may be summarized as follows:

- The skin friction decreased with an increase in the nanoparticle volume fraction, while the opposite trend was observed for increasing Hartman numbers.
- The mass transfer coefficient increased with an increase in the nanoparticle volume fraction, chemical reaction parameter, Hartmann number and Brownian motion parameter, while the opposite trend was observed for increasing values of the thermophoresis parameter. The fast flow from the stretching sheet carries with it nanoparticles leading to an increase in the mass volume fraction boundary layer thickness.
- The heat transfer coefficient decreased with increase in the values of the nanoparticle volume fraction, the Hartmann number, thermophoresis and Brownian motion parameters.

Chapter 4:

In this chapter we applied the spectral relaxation method to the problem of unsteady cross-diffusion and couple stress effects with vanishing nanoparticle flux at the wall. The SRM

was used in combination with the SQLM to solve the highly non-linear governing equations. The qualitative and quantitative effects of the dimensionless parameters in the problem such as the couple stress parameter, the Prandtl number, the Brownian motion parameter, the thermophoresis parameter, and the Lewis number on the fluid behavior were determined. Comparison of the results obtained using SRM together with SQLM proved the accuracy and convergence of the SRM. From the numerical investigation, the following conclusions could be drawn:

- The velocity profile decreased with increasing values of the couple stress parameter until back flow was obtained in the range $2 \leq \eta \leq 8$.
- The unsteadiness parameter slowed the motion of fluid within the boundary layer.
- The stronger couple stress parameter reduced the nanofluid velocity, as well as increasing the thickness of both the thermal and mass volume fraction boundary layers.

Chapter 5:

In this chapter we used the SRM to solve the problem of cross-diffusion, double-diffusion, and hydromantic effects, on convection fluid flow, over a vertical surface saturated with a nanofluid. The systems of partial differential equations subject to boundary conditions, were solved numerically using SRM and there was a strong correlation between our results and those found in the literature, reinforcing the accuracy of our obtained results. From the numerical investigation, we determined the influence of the physical parameters, and found the following:

- The values of skin friction increase with increase in the values of the nanoparticle volume fraction and magnetic parameter.
- The temperature and concentration profiles increase with increasing values of the nanoparticle volume fraction and thermophoresis parameter while the opposite trend

is observed for the concentration profile with increasing the values of the Brownian motion parameter.

- The thermal conductivity of the nanofluid increases with increasing in the nanoparticle volume fraction, which reduces the thermal boundary layer thickness and the temperature gradient at the wall. The axial velocity of a silver-water nanofluid is comparatively less than that of a copper-water nanofluid.

Chapter 6:

Here we studied the effects of thermal radiation on unsteady MHD axisymmetric stagnation-point flow with Navier slip conduction. We considered temperature dependent thermal conductivity and viscous dissipation. The flow was due to a surface that is shrunk axisymmetrically in its own plane with a linear velocity. The model equations that describe the fluid flow were solved using SRM to provide numerical solutions. We discussed two different types of surface heating, namely a prescribed surface temperature (PST) and a prescribed surface heat flux (PHF). The results are summarized as follows:

- The temperature profiles in the two cases of prescribed wall temperature and prescribed surface heat flux were shown to increase with the thermal radiation parameter, which in turn increased the thermal boundary layer thickness for both prescribed wall temperature and prescribed surface heat flux cases. This may be due to the fact that an increase in the value of the thermal radiation parameter causes an increase in the interaction with the thermal boundary layer.

- Near the sheet, flow reversal was observed, and the region of reverse cellular flow decreased with an increase in the magnetic parameter.

- The skin friction coefficients decreased monotonically with increasing unsteadiness and magnetic parameter, while the opposite was true for velocity slip parameter.

- The temperature profiles increased with increasing thermal radiation for both the prescribed surface temperature (PST) and the prescribed wall heat flux (PHF) cases.

Future extensions and limitations of the research work

Our understanding of the potential applications of nanofluids is as yet, incomplete. Nanofluid research could lead to major breakthroughs in the development of the next generation of heat transfer fluids for engineering applications.

From an experimental point of view, more work is needed to understand the fundamental physics of energy transport in nanofluids, and to determine the nature and structure of nanoparticles that offer the most efficiency at minimum cost. Theoretical predictions using mathematical modelling would compliment and validate the experimental findings. There is a compelling argument in favour of nanofluids, because of their energy efficiency, but it needs to be proved that they are ethical. We face public and safety concerns, both in the production and in the use of nanofluids in terms of their impact on the environment. For these reasons, there is great potential for further basic and applied research on the productions and application of nanofluids in the sciences.

Limitation

We have presented various studies on the flow of nanofluids, and have investigated heat and mass transfer processes in porous media. Some useful insights have been gained on the influence and significance of various fluid and physical parameters on the transport properties. We have further shown the accuracy and reliability of certain spectral techniques in determining solutions of highly non-linear and coupled equations such as those that describe fluid flow, energy and mass transport. Nonetheless, certain limitations can readily be identified in the work presented here. For instance the SRM becomes less accurate for problems with complex geometries, and problems involving many parameters and derivatives in the boundary conditions. According to Lele [141], the use of some spectral methods in turbulent fluid flows is limited to flows in simple domains and simple boundary conditions. The values of various physical parameters that we considered were chosen from

previously published literature and in some cases, these values may not be experimentally determined.

References

[1] Z. Chen and R. Ewing. Fluid flow and transport in porous media: mathematical and numerical treatment. *American Mathematical Society, Rhode Island*, 2002.

[2] J. Bear and Y. Bachmat. Introduction to modeling of transport phenomena in porous media. *Kluwer Academic Publishers, Dordrecht, Netherlands*, 17:555, 1990.

[3] D. Ingham and I. Pop. Transport phenomena in porous media. *London, England, 450*, 2005.

[4] T. Corey. Mechanics of inmmiscible fluids in porous media. *Water Resources, USA, 252*, 1994.

[5] J. Vazquez. The porous medium equations. *Clinical Microbiology Reviews*, 471–495, 2007.

[6] J. H. Strange and J. B. W. Webber. Multidimensionally resolved pore size distributions. *Applied Magnetic Resonance*, 12:231–245, 1997.

[7] D. Nield and A. Bejan. Convection in porous media. *Springer Verlag, 654*, 1999.

[8] M. Kaviany. Principles of heat transfer in porous media. *Springer*, 1995.

[9] J. H. Lethr and J. K. Lethr. Standard handbook in environmental science, health and technology. *McGraw-HILL, New York, 1600*, 2000.

[10] M. V. Bruschke and S. G. Advani. A finite element/control volume approach to mold filling in anisotropic porous media. *Polymer Composities*, 11:398–405, 1990.

[11] P. S. Gupta and A. S. Gupta. Heat and mass transfer on a stretching sheet with suction or blowing. *Canadian Journal of Chemical Engineering*, 55:744–746, 1977.

[12] H. Mondal and D. Pal. Non-darcian buoyancy driven heat and mass transfer over a stretching sheet in a porous medium with radiation and ohmic heating. *International Journal of Nonlinear Science*, 14:115–123, 2012.

[13] H. Darcy. Les fontaines publiques de la ville de Dijon. *Paris Victor Dalmont*, 1856.

[14] K. Vafai. Handbook of porous media. *CRC Press, New York*, 2005.

[15] M. Benzeghiba, A. Campo, and S. Chikh. Thermosolutal convection in a partly porous vertical annular cavity. *Journal of Heat Transfer*, 125:703–715, 2003.

[16] L. Zheng, C. Zhang, X. Zhang, and J. Zhang. Flow and radiation heat transfer of nanofluid over a stretching sheet with velocity slip and temperature jump in porous medium. *Journal of the Franklin Institute*, 350:990–1007, 2013.

[17] P. Ranganatha and R. Viskanta. Mixed convection boundary layer flow along a vertical surface in a porous medium. *Numerical Heat Transfer*, 7:305–317, 1984.

[18] D. A. Nield and A. V. Kuznetsov. The cheng-minkowycz problem for natural convection boundary layer flow in a porous medium saturated by a nanofluid. *International Journal of Heat and Mass Transfer*, 52:5792–5795, 2009.

[19] M. Kumari and G. Nath. Natural convection from vertical cone in a porous medium due to the combined effects of heat and mass diffusion with non-uniform wall temperature/concentration or heat/mass flux and suction/injection. *International Journal of Heat and Mass Transfer*, 52:3064–3069, 2009.

[20] B. Amin and H. Azarkish. Samples of theoretical investigations in convective heat transfer of nanofluids. *University Sistan and Baluchestan*, 7:141–150, 2009.

[21] J. P. Holman. Heat transfer. *Mcgraw-Hill Series in Mechanical Engineering, Mishawaka*, 1986.

[22] L. Burmeister. Convection heat transfer. *John Wiley and Sons, Canada*, 1993.

[23] S. Thirumale. Fundamentals of heat and mass transfer. *Dorling Kindersley, India*, 2006.

[24] D. A. Nield and A. V. Kuznetsov. Thermal instability in a porous medium layer saturated by a nanofluid. *International Journal of Heat and Mass Transfer*, 52: 5796–5801, 2009.

[25] J. Welty, C. Wicks, and R. Wilson. Fundamentals of momentum heat and mass transfer. *Mcgraw-Hill Series in Mechanical Engineering*, 1984.

[26] Y. Jaluria. Natural convection heat and transfer. *Pregamon Press, Oxford*, 1980.

[27] W. Kays and M. Crawford. Convective heat and mass transfer. *McGraw-HILL, New York*, 1993.

[28] R. S. R. Gorla and A. Zinolabedini. Free convection from a vertical plate with non-uniform surface temperature and embedded in a porous medium. *Transactions of ASME, Journal Energy Resources Technology*, 109:26–30, 1987.

[29] R. S. R. Gorla and A. Tornabene. Free convection from a vertical plate with non-uniform surface heat flux and embedded in a porous medium. *Transport in Porous Media Journal*, 3:95–106, 1988.

[30] B. Gebhart, Y. Jaluria, R. Mahajan, and B. Sammakia. Buoyancy-induced flows and transport springer. *Springer, USA, 971*, 1988.

[31] M. M. Rathore and R. Kapuno. Engineering heat transfer. *Jones and Bartllet, Canada*, 1:7637–7752, 2010.

[32] Y. Jaluria and B. Gebhart. Stability and transition of buoyancy induced flows in a stratified medium. *Journal of Fluid Mechanics*, 12:593–612, 1974.

[33] P. Cheng and W. J. Minkowycz. Free convection about a vertical flat plate embedded in a porous medium with application to heat transfer from a dike. *Journal of Geophysical Research*, 82:2040–2044, 1977.

[34] Y. Jaluria and K. Himasekhar. Buoyancy induced two dimensional vertical flows in a thermally stratified enviroment. *Computers and Fluids*, 11:39–49, 1983.

[35] R. Rudramoorthy and K. Mayilsamy. Heat and mass transfer. *Dorling Kindersley, India*, 2011.

[36] R. Wooding. Rayleigh instability of a thermal boundary layer in flow through a porous medium. *Journal of Fluid Mechanics*, 9:183–192, 1960.

[37] F. Lai. Coupled heat and mass transfer by natural convection from a horizontal line source in saturated porous medium. *International Communications in Heat and Mass Transfer*, 17:489–499, 1990.

[38] J. Lioyd and M. Sparrow. Combined force and free convection flow on vertical surfaces. *International Journal of Heat and Mass Transfer*, 13:434–438, 1970.

[39] E. W. Mureithi and D.P. Mason. On the stability of a forced free boundary layer flow with viscous heating. *Fluid Dynamics Research*, 31:65–78, 2002.

[40] W. Siegmann and L. Rubenfeld. A nonlinear model for double diffusive convection. *Journal on Applied Mathematics*, 29:540–557, 1975.

[41] C. H. Hsia, T. Ma, and S. Wang. Bifurcation and stability of two-dimensional double-diffusive convection. *International Journal of Heat and Mass Transfer*, 53: 3030–3034, 2010.

[42] M. Bourich, M. Hasnaoui, and A. Amahmid. Double diffusive natural convection in porous enclosure partially heated from below and differentially salted. *International Journal of Heat and Fluid Flow*, 25:1034–1046, 2004.

[43] A. Mojtabi and M. C. C. Mojtabi. Double diffusive convection in porous media. *Handbook Porous Media*, 7:269–320, 2005.

[44] B. B. Beya and T. Lilia. Oscillatory double diffusive mixed convection in a two-dimensional ventilated enclosure. *International Journal of Heat and Mass Transfer*, 50:4540–4553, 2007.

[45] M. Mamou. Stability analysis of double diffusive convection in porous enclosures. *Institute for Aerospace Research, National Research Council, Canada*, 11:113–154, 2002.

[46] A. Akbarzadeh and P. Manins. Convection layers generated by side walls in solar ponds. *Solar Energy*, 41:521–529, 1988.

[47] P. A. L. Narayana and P. Sibanda. Soret and Dufour effects on free convection along a vertical wavy surface in a fluid saturated Darcy porous medium. *Communications on Pure and Applied Analysis*, 7:23–48, 2008.

[48] D. Nield. Onset of thermohaline convection in a porous medium. *Water Resources Research*, 4:553–560, 1968.

[49] P. G. Baines and A. E. Gill. On thermohaline convection with linear gradients. *Journal of Fluid Mechanics*, 37:289–306, 1969.

[50] D. Gershuni, E. Zhukhovisskii, and D. Lyubimov. Thermal concentration instability of a mixture in a porous medium. *Sovling Physic Dokl*, 21:375–377, 1976.

[51] A. A. Khan and A. Zebib. Double diffusive instability in a vertical layer of a porous medium. *Journal of Heat Transfer*, 103:179–181, 1981.

[52] A. Raptis, G. Tzivanidis, and N. Kafousias. Free convection and mass transfer flow through a porous medium bounded by infinite vertical limiting surface with constant suction. *Letters in Heat and Mass Transfer*, 8:417–424, 1981.

[53] N. Rudraiah, P. K. Srimani, and R. Friedrich. Finite amplitude convection in a two component fluid saturated porous layer. *International Journal of Heat and Mass Transfer*, 25:715–722, 1982.

[54] D. A. Nield, D. M. Manole, and J. L. Lage. Convection induced by inclined thermal and solutal gradients in a shallow horizontal layer of a porous medium. *Journal of Fluid Mechanics*, 257:559–574, 1993.

[55] A. Amahmid, M. Hasnaoui, and P. Vasseur. On the transition between aiding and opposing double diffusive flows in a vertical porous matrix. *Solar Energy*, 3:123–137, 2000.

[56] Z. Alloui, P. Vasseur, L. Robillard, and A. Bahloul. Onset double-diffusive convection in a horizontal Brinkmann cavity. *Chemical Engineering Communications*, 197: 387–399, 2010.

[57] P. R. Patil, C. P. Parvathy, and K. S. Venkatakrishnan. Thermohaline instability in a rotating anisotropic porous medium. *Applied Scientific Research*, 46:73–88, 1989.

[58] M. S. Malashetty and D. Basavaraja. Effect of thermal modulation on the onset of double diffusive convection in a horizontal fluid layer. *International Journal of Thermal Sciences*, 44:323–332, 2005.

[59] Y.S. Li, Z. W. Chen, and J. M. Zhan. Double-diffusive Marangoni convection in a rectangular cavity: Transition to chaos. *International Journal of Heat and Mass Transfer*, 53:5223–5231, 2010.

[60] T. Okedayo, Gideon, and S. O. Abah. Plane stagnation double-diffusive magnetohydromagnetic convective flow with convective boundary condition in a porous media. *American Journal of Computational Mathematics*, 2:223–227, 2012.

[61] C. RamReddy, P. V. S. N. Murthy, A. J. Chamkha, and A. M. Rashad. Influence of viscous dissipation on free convection in a non-Darcy porous medium saturated with nanofluid in the presence of magnetic field. *The Open Transport Phenomena Journal*, 5:20–29, 2013.

[62] Y. Xuan and Q. Li. Heat transfer enhancement of nanofluids. *International Journal of Heat and Fluid Flow*, 21:58–64, 2000.

[63] J. A. Eastman, S. U. S. Choi, S. Li, W. Yu, and L. J. Thompson. Anomalously increased effective thermal conductivities containing copper nanoparticles. *Applied Physics Letters*, 78:718–720, 2001.

[64] P. K. Kameswaran, P. Sibanda, and A. S. N. Murti. Nanofluid flow over a permeable surface with convective boundary conditions and radiative heat transfer. *Mathematical Problems in Engineering*, 2013:ID201219, 11, 2013.doi:10.1155/2013/201219.

[65] S. Zeinali Heris, M. Nasr Esfahany, and S. Gh. Etemad. Numerical investigation of nanofluid laminar convective heat transfer through circular tube. *Numerical Heat Transfer, Part A: Applications*, 52:1043–1058, 2007.

[66] S. U. S. Choi, Z. G. Zhang, W. Yu, F. E. Lockwood, and E. A. Grulke. Anomalous thermal conductivity enhancement on nanotube suspensions. *Applied Physics Letters*, 79:2252–2254, 2001.

[67] P. Vassallo, R. Kumar, and S. D. Amico. Pool boiling heat transfer experiments in silica-water nanofluids. *International Journal of Heat and Mass Transfer*, 47: 407–411, 2004.

[68] S.M. You, J. H. Kim, and K. H. Kim. Effect of nanoparticles on critical heat flux of water in pool boiling heat transfer. *Applied Physics Letters*, 83:3374–3376, 2003.

[69] J. Routbort. Argonne national lab. *Michellin North America*, 2009.

[70] F. Awad, N. A. H. Haroun, P. Sibanda, and M. Khumalo. On couple stress effects on unsteady nanofluid flow over stretching surfaces with vanishing nanoparticle flux at the wall. *Journal of Applied Fluid Mechanics*, 9:1937–1944, 2016.

[71] P. K. Kameswaran and P. Sibanda. Thermal dispersion effects on convective heat and mass transfer in an Ostwald de Waele nanofluid flow in porous media. *Boundary Value Problems*, (2013):2013:243, doi:10.1186/1687–2770–2013–243.

[72] K. V. Wong and O. de Leon. Applications of nanofluids current and future. *Advances in Mechanical Engineering*, 2010:11, ID:519659, 2010.

[73] J. Boungiorno, H. Lin-Wen, S. J. Kim, H. Ryan, T. Bao, and F. Eric. Nanofluids for enhanced economics and safety of nuclear reactors. An evaluation of the potential features, issues and research gaps. *Nuclear Technology*, 162:80–91, 2008.

[74] K. B. Pavlov. Magnetohydromagnetic flow of an incompressible viscous fluid caused by defor-mation of a surface. *Magnitnaya Gidrodinamika*, 4:507–510, 1974.

[75] K. Jafar, R. Nazar, A. Ishak, and I. Pop. MHD flow and heat transfer over stretching/ shrinking sheets with external magnetic field, viscous dissipation and joule effects. *Canadian Journal on Chemical Engineering*, 99:1–11, 1974.

[76] N.A.H Haroun, P. Sibanda, S. Mondal, and S. S. Motsa. On unsteady MHD mixed convection in a nanofluid due to a stretching/shrinking surface with suction/injection using the spectral relaxation method. *Boundary Value Problems*, (2015):2015:24, doi:10.1186/s13661–015–0289–5.

[77] A. J. Chamkha. MHD flow of a uniformly stretched vertical permeable surface in the presence of heat generation/absorption and a chemical reaction. *International Communications in Heat and Mass Transfer*, 30:413–422, 2003.

[78] R. Kandasamy and P. G. Palanimani. Effects of chemical reactions, heat, and mass transfer on nonlinear magnetohydrodynamic boundary layer flow over a wedge with a porous medium in the presence of ohmic heating and viscous dissipation. *Journal of Porous Media*, 10:489–502, 2007.

[79] D. S. P. Anjali and M. Thiyagarajan. Effects of chemical reactions, heat, and mass transfer on nonlinear magnetohydrodynamic boundary layer flow over a wedge with a porous medium in the presence of ohmic heating and viscous dissipation. *Heat and Mass Transfer*, 42:671–677, 2006.

[80] A. Postelnicu. Influence of chemical reaction on heat and mass transfer by natural convection from vertical surfaces in porous media considering Soret and Dufour effects. *Heat and Mass Transfer*, 43:595–602, 2007.

[81] P. Vadasz. Heat conduction in nanofluid suspensions. *Journal of Heat Transfer*, 128: 465–477, 2006.

[82] R. W. Griffiths. Layered double-diffusive convection in porous media. *Journal Fluid Mechanic*, 102:221–248, 1981.

[83] B. J. Murray and C. F. Chen. Double-diffusive convection in a porous medium. *Journal of Applied Fluid Mechanics*, 201:147–166, 1989.

[84] S. Webb, D. Reneta, P. Suhas, and H. J. S. Fernando. Double-diffusive convection in narrow aspect cylinders experimental data and cfd simulations. *American Physical Society, Annual Meeting of the APS Division of Fluid Dynamics*, 11, 2009.

[85] B. Bai, L. Zhang, L. Zhang, and H. Li. Experimental study on double-diffusive convection during solidification of $NH_4CL - H_2O$ hypereutectic in cylindrical cavity. *Heat Transfer Conference, collocated with the Fluids Engineering, Energy Sustainability, and 3rd Energy Nanotechnology Conference, Heat Transfer: Jacksonville, Florida, ASME*, 1:713–718, 2008.

[86] N. Barman and P. Dutta. Studies on macrosegregation and double-diffusive convection during directional solidification of binary mixture. *Materials Science and Technology*, 24:1230–1237, 2008.

[87] S. Mergui, S. Geoffroy, and C. Benard. Ice block melting into a binary solution, coupling of the interfacial equilibrium and the flow structures. *Journal of Heat Transfer*, 124:1147–1157, 2002.

[88] B. Gebhart and L. Pera. The nature of vertical natural convection flow resulting from the combined buoyancy effects of thermal and mass diffusion. *International Journal of Heat and Mass Transfer*, 14:2025–2050, 1971.

[89] W. J. Minkowycz, P. Cheng, and F. Moalem. The effect of surface mass transfer on buoyancy induced Darcian flow adjacent to a horizontal heated surface. *International Journal of Heat and Mass Transfer*, 12:55–65, 1985.

[90] A. J. Chamkha and S. M. M. El-Kabeir. Unsteady heat and mass transfer by MHD mixed convection flow over an impulsively stretched vertical surface with chemical reaction and Soret and Dufour effects. *Chemical Engineering Communications*, 200: 1220–1236, 2013.

[91] F. C. Lai. Coupled heat and mass transfer by mixed convection from a vertical plate in a saturated porous medium. *International Communications in Heat and Mass Transfer*, 18:93–106, 1991.

[92] K. A. Yih. Coupled heat and mass transfer in mixed convection over a wedge with variable wall temperature and concentration in porous media. *International Communications in Heat and Mass Transfer*, 25:1145–1158, 1998.

[93] C. Cheng. Transient heat and mass transfer by natural convection from vertical surface in porous media. *Journal physics and Applied Physics*, 33:1425–1430, 2000.

[94] Md. S. Khan, I. Karim, L. E. Ali, and A. Islam. Unsteady MHD free convection boundary-layer flow of a nanofluid along a stretching sheet with thermal radiation and viscous dissipation effects. *International Nano Letters*, doi:10.1186/2228–5326–2–24, 2012.

[95] A. Mahdy. Unsteady mixed convection boundary layer flow and heat transfer of nanofluids due to stretching sheet. *Nuclear Engineering and Design*, 249:248–255, 2012.

[96] T. Chen, C. Yuh, and A. Moutsoglou. Combined heat and mass transfer in mixed convection along vertical and inclined plates. *International Journal of Heat and Mass Transfer*, 23:527–537, 1980.

[97] M. A. Hossain. Viscous and joule heating effects on mhd-free convection flow with variable plate temperature. *International Journal of Heat and Mass Transfer*, 35: 3485–3487, 1992.

[98] M. Acharya, G. C. Dash, and L. P. Singh. Magnetic field effects on the free convection and mass transfer flow through porous medium with constant suction and constant heat flux. *Indian Journal Pure Applied Mathematics*, 31:1–18, 1999.

[99] A. Ishak, R. Nazar, and I. Pop. Heat transfer over an unsteady stretching permeable surface with prescribed wall temperature. *Nonlinear Analysis: Real World Applications*, 10:2909–2913, 2009.

[100] N. Joshi, M. Kumar, and S. K. Budhani. Numerical solution of heat and mass transfer with thermal radiation and MHD boundary layer flow over a stretching surface with suction/injection. *International Journal of Computational Engineering Research*, 2: 2250–3005, 2012.

[101] S. Manjunatha, B. Gireesha, and C. Bagewadi. Effect of thermal radiation on boundary layer flow and heat transfer of dusty fluid over an unsteady stretching sheet. *International Journal of Engineering, Science and Technology*, 4:36–48, 2012.

[102] K. Bhattacharyya, S. Mukhopadhyay, and G. C. Layek. Unsteady mhd boundary layer flow with diffusion and first order chemical reaction over a permeable stretching sheet with suction or blowing. *Chemical Engineering Communications*, 200: 379–397, 2013.

[103] P. K. Kameswaran, M. Narayana, P. Sibanda, and P. V. S. N. Murthy. Hydromagnetic nanofluid flow due to a stretching or shrinking sheet with viscous dissipation and chemical reaction effects. *International Journal of Heat and Mass Transfer*, 55: 7587–7595, 2012.

[104] K. L. Hsiao and B. M. Lee. Conjugate heat and mass transfer for MHD mixed convection with viscous dissipation and radiation effect for viscoelastic fluid past a stretching sheet. *Engineering and Technology*, 62:318–325, 2010.

[105] T. Hayat, M. Qasim, and Z. Abbas. Homotopy solution for the unsteady three dimensional MHD flow and mass transfer in a porous space. *Communications in Nonlinear Science and Numerical Simulation*, 9:2375–2387, 2010.

[106] A. A. Joneidi, G. Domairry, and M. Babaelahi. Analytical treatment of MHD free convective flow and mass transfer over a stretching sheet with chemical reaction. *Journal of the Taiwan Institute of Chemical Engineers*, 41:35–43, 2010.

[107] C. Y. Cheng. Double diffusion from a horizontal cylinder of elliptic cross section with uniform wall heat and mass fluxes in a porous medium. *International Communications in Heat and Mass Transfer*, 38:1201–1205, 2011.

[108] D. R. Simitev. Double-diffusive convection in a rotating cylindrical annulus with conical caps. *Physics of the Earth and Planetary Interiors*, 186:183–190, 2011.

[109] A. V. Kuznetsov and D. A. Nield. Anatural convective boundary-layer flow of a nanofluid past a vertical plate: A revised model. *International Journal of Thermal Sciences*, 77:126–129, 2014.

[110] M. Narayana, P. Sibanda, S. S. Motsa, and P. G. Siddheshwar. On double diffusive convection and cross diffusion effects on a horizontal wavy surface in a porous medium. *Boundary Value Problems*, (2012)::88, doi:10.1186/1687–2770–2012–88.

[111] D. A. Nield and A. Bejan. Convection in porous media, electronic resource, third edition. *New York, Springer Science and Business Media*, 2006.

[112] L. B. Benamo-Mellya, J. P. Caltagirone, B. Faissat, F. Montel, and P. Costeseque. Unsteady mixed convection boundary layer flow due to a stretching vertical surface. *International Journal of Heat and Mass Transfer*, 44:1285–1297, 2001.

[113] S. Vincent, J. P. Caltagirone, P. Lubin, and T. N. Randrianarivelo. An adaptative augmented lagrangian method for three dimensional multimaterial flows. *Computers and Fluids*, 33:1273–1289, 2004.

[114] Md. S. Alam and Md. S. H. Mollah. Influence of chemical reaction and heat generation/absorption on MHD free convective heat and mass transfer flow along an inclined stretching sheet considering Dufour and Soret effects. *Asian Transactions on Basic and Applied Sciences*, 2:2221–4291, 2012.

[115] S. P. Anjalidevi and R. U. Devi. Soret and Dufour effects on MHD slip flow with thermal radiation over a porous rotating infnite disk. *Communications in Nonlinear Science and Numerical Simulation*, 16:1917–930, 2011.

[116] E. R. G. Eckert and R. M. Drake. Analysis of heat and mass transfer. *McGraw-Hill Education, New York*, 1995.

[117] N. G. Kafoussias and E. W. Williams. Thermal-diffusion and diffusion-thermo effects on mixed free-forced convective nad mass transfer boundary layer flow with temperature dependent viscosity. *International Journal Engineering Science*, 33: 1369–1384, 1995.

[118] R. G. Mortimer and H. Eyring. Elementary transition state theory of the Soret and Dufour effects. *In Proceedings of the National Academy of Sciences, Chemistry, USA*, 77:1728–1731, 1980.

[119] L. Onsager. Reciprocal relations in irreversible processes. *Journal of Physical Review Letters*, 37:405–426, 1931.

[120] M. S. Alam, M. M. Rahman, M. A. Maleque, and M. Ferdows. Dufour and Soret effects on steady MHD combined free-forced convective and mass transfer flow past a semi-infinite vertical plate. *Thammasat International Journal of Science and Technology*, 11:1–12, 2006.

[121] M. A. Mansour, N. F. El-Anssary, and A. M. Aly. Effects of chemical reaction and thermal stratification on MHD free convective heat and mass transfer over a vertical stretching surface embedded in a porous media considering Soret and Dufour numbers. *Chemical Engineering Journal*, 145:340–345, 2008.

[122] P. A. L. Narayana and P. Sibanda. Soret and Dufour effects on free convection along a vertical wavy surface in a fluid saturated Darcy porous medium. *International Journal of Heat and Mass Transfer*, 53:3030–3034, 2010.

[123] F. G. Awad, P. Sibanda, S. S. Motsa, and O. D. Makinde. Convection from an inverted cone in a porous medium with cross-diffusion effects. *Computers and Mathematics with Applications*, 61:1431–1441, 2011.

[124] N. A. H. Haroun, P. Sibanda, S. Mondal, and S. S. Motsa. Heat and mass transfer of nanofluid through an impulsively vertical stretching surface using the spectral relaxation method. *Boundary Value Problems*, (2015):2015:161, doi:10.1186/s13661–015–0424–3.

[125] G. Adomian. A review of the decomposition method and some recent results for nonlinear equation. *Mathematical and Computer Modelling: International Journal*, 7:17–43, 1990.

[126] J. C. Williams and T. B. Rhyne. Boundary layer development on a wedge impulsively set into motion. *SIAM Journal On Applied Mathematics*, 38:215–224, 1980.

[127] S. S. Motsa, P. Dlamini, and M. Khumalo. Solving hyperchaotic systems using the spectral relaxation method. *Mathematical Problems in Engineering*, 2012:(2012), ID 203461, 18, doi:10.1155/2012/203461.

[128] S. S. Motsa, P. G. Dlamini, and M. Khumalo. Spectral relaxation method and spectral quasilinearization method for solving unsteady boundary layer flow problems. *Advances in Mathematical Physics*, 2014:ID:341964, 12, doi:10.1155/2014/341964.

[129] S. Shateyi and G. T. Marewo. A new numerical approach of MHD flow with heat and mass transfer for the UCM fluid over a stretching surface in the presence of thermal radiation. *Mathematical Problems in Engineering*, (2013):2013:196, doi:10.1186/1687–2770–2013–196.

[130] S. S. Motsa. New iterative methods for solving nonlinear boundary value problems. *Fifth Annual Workshop on Computational Applied Mathematics and Mathematical Modelling in Fluid Flow, UKZN, South Africa*, 3:1–63, 2012.

[131] S. S. Motsa. A new spectral relaxation method for similarity variable nonlinear boundary layer flow systems. *Chemical Engineering Communications*, 201:241–256, 2014.

[132] P. Sibanda, S. S. Motsa, and Z. Makukula. A spectral-homotopy analysis method for heat transfer flow of a third grade fluid between parallel plates. *International Journal of Numerical Methods for Heat and Fluid Flow*, 22:4–23, 2012.

[133] S. S. Motsa and Z. G. Makukula. On spectral relaxation method approach for steady von *Kármán* flow of a Rreiner-Rivlin fluid with joule heating, viscous dissipation and suction/injection. *Central European Journal Physics*, 78:718–720, 2013.

[134] S. Shateyi. A new numerical approach to MHD flow of a Maxwell fluid past a vertical stretching sheet in the presence of thermophoresis and chemical reaction. *Boundary Value Problems*, 2013:1–14, 2013:196.

[135] S. Shateyi and O. D. Makinde. Hydromagnetic stagnation-point flow towards a radially stretching convectively heated disk. *Mathematical Problems in Engineering*, 2013:(2013), ID 616947, 8, doi:10.1155/2013/616947.

[136] S. S. Motsa and S. Shateyi. Successive linearisation analysis of unsteady heat and mass transfer from a stretching surface embedded in a porous medium with suction/injection and thermal radiation effects. *Canadian Journal of Chemical Engineering*, DOI 10.1002/cjce.20640:1323–1335, 2012.

[137] R. E. Bellman and R. E. Kalaba. Quasilinearization and nonlinear boundary-value problems. *Elsevier, New York*, 215, 1965.

[138] P. Dlamini, S. S. Motsa, and M. Khumalo. On the comparison between compact finite difference and pseudospectral approaches for solving similarity boundary layer problems. *Mathematical Problems in Engineering*, 2013:(2013), ID 746489, 15, doi:10.1155/2013/746489.

[139] S. S. Motsa and P. Sibanda. On extending the quasilinearization method to higher order convergent hybrid schemes using the spectral homotopy analysis method. *Journal of Applied Mathematics*, 2013:(2013), ID 879195, 9, doi:10.1155/2013/879195.

[140] S. S. Motsa and P. Sibanda. Spectral method based numerical solutions of partial differenial equations. *Sixth Annual Workshop on Computational Applied Mathematis and Mathematical Modelling in Fluid flow, UKZN, PMB, South Africa*, 7:1–7, 2013.

[141] S. K. Lele. Compact finite difference schemes with spectral-like resolution. *Journal of Computalional Physics*, 103:16–42, 1992.